

# **Finite element advancements to improve performance of cementless hip implants**

**Maria Tarata**

*Finite element advancements  
to improve performance  
of cementless hip implants*

*Maria Tarata*

**Copyright**

© 2012, Maria Tarata

All rights reserved. No parts of this book can be reproduced in any form without written permission from the author.

**ISBN**

978-90-6464-590-7

**Layout and printing**

GVO drukkers & vormgevers B.V., Ede

**Cover design**

Paolo Soro

The research described in this thesis was performed at the Orthopaedic Research Laboratory (Radboud University Nijmegen Medical centre, Nijmegen, The Netherlands) and is part of the Nijmegen Centre for Evidence Based Practice (NCEBP)

# Finite element advancements to improve performance of cementless hip implants

Proefschrift  
ter verkrijging van de graad van doctor  
aan de Radboud Universiteit Nijmegen  
op gezag van de rector magnificus prof. mr. S.C.J.J. Kortmann,  
volgens besluit van het college van decanen  
in het openbaar te verdedigen op

dinsdag 6 november 2012 om 13.30 uur precies

door

Maria Tarata

geboren op 11 oktober 1982  
te Rzeszów (Polen)



**Promotor**

Prof. dr. ir. N. Verdonschot (Universiteit Twente)

**Copromotor**

Dr. ir. D. Janssen

**Manuscriptcommissie**

Prof. dr. W.J.G. Oyen

Prof. dr. W.B. van den Berg

Prof. dr. ir. H.F.J.M. Koopman (Universiteit Twente)

# Contents

<b>Chapter 1:</b>	Introduction	<b>7</b>
<b>Chapter 2:</b>	Experimental versus computational analysis of micromotions at the implant-bone interface	<b>19</b>
<b>Chapter 3:</b>	Improving peri-prosthetic bone adaptations around cementless hip stems; a clinical and Finite Element study	<b>35</b>
<b>Chapter 4:</b>	Balancing incompatible endoprosthetic design goals. A combined ingrowth and bone remodeling simulation	<b>59</b>
<b>Chapter 5:</b>	Effect of intra-operative impaction force on the primary stability and probability of bone damage in cementless reconstructions of varied bone quality	<b>77</b>
<b>Chapter 6:</b>	Towards a method to simulate the process of bone ingrowth in cementless THA using Finite Element Method	<b>91</b>
<b>Chapter 7:</b>	Towards a more realistic prediction of peri-prosthetic micromotions	<b>107</b>
<b>Chapter 8:</b>	The effect of bone ingrowth depth on the tensile and shear strength of the implant-bone E-beam produced interface	<b>123</b>
<b>Chapter 9:</b>	The effect of bone ingrowth depth on the tensile and shear strength of implant-bone interface. Comparison between a geometrically ordered and random EBM and laser produced structure	<b>139</b>
<b>Chapter 10:</b>	General discussion	<b>153</b>
<b>Chapter 11:</b>	Summary	<b>161</b>
<b>Chapter 12:</b>	Samenvatting	<b>171</b>
	Acknowledgements	<b>181</b>
	Curriculum Vitae	<b>187</b>



# Chapter

---

# 1

## *Introduction*

The hip joint, one of the body's largest weight bearing joints, consists of the femur and acetabulum of the pelvis. In a healthy hip joint, the femoral head and acetabulum are covered with articular cartilage. Almost frictionless contact between both parts is achieved thanks to synovial fluid released by the synovium. Damage to articular cartilage causes pain and reduction in hip mobility <sup>1,2</sup>. Hip joint degeneration (osteoarthritis) can be a result of mechanical instabilities <sup>3,4</sup>, aging changes <sup>5,6</sup> or complications after traumatic hip dislocation <sup>7</sup>. If the extent of pain, joint deformity and functional restrictions due to osteoarthritis cannot be treated conservatively, total hip arthroplasty (THA) is recommended <sup>8</sup>. THA is a successful surgical procedure <sup>9</sup> which restores normal anatomy of the hip and improves health-related quality of patient's life <sup>10</sup>. Frequent indications for THA include also fractures of the femoral neck <sup>11</sup>.

In THA, the reconstructed hip joint consists of two basic components: the femoral implant (made of metal alloys, such as stainless steel, cobalt, chrome or titanium) and the acetabular cup (made of polyethylene, ceramics or metal). The method of implant fixation in THA can be either cemented or uncemented (Fig. 1). In the cemented procedure, surgical cement is used to fill the gap between the prosthesis and bone in order to assure implant fixation. In the uncemented procedure, implants are press-fitted into the intramedullary canal. In the past decades, the most common method of fixation in THA was acrylic bone cement. However, as reported by the Swedish Hip Arthroplasty Register, the proportion of all-cemented and hybrid prostheses in the recent years are reduced in favor of totally uncemented, reversed hybrids and resurfacing prostheses <sup>9</sup>. This thesis focuses on femoral implants of uncemented THA.

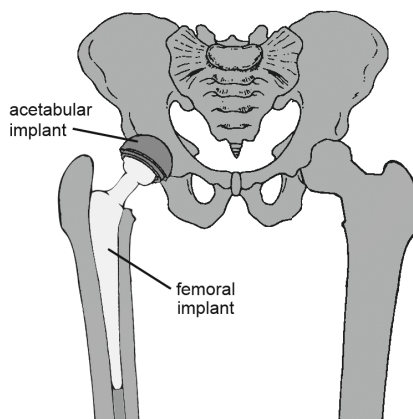


*Fig. 1 Healthy human hip joint (right) and a hip joint after uncemented total hip arthroplasty THA (left).*

Uncemented THA is commonly used in younger, more active patients with good bone stock. According to the Finnish arthroplasty register <sup>12</sup> modern uncemented stems seem to have better resistance to aseptic loosening than cemented stems in younger patients.

Given that the life expectancy of young patient is high, it is important to assure long term survival of these cementless components.

Failure of uncemented THA can be caused by poor primary or secondary stability of an implant (meaning relative large motion between the implant and bone), or by extensive bone resorption (Fig. 2). Implant primary stability is defined during the surgical procedure. Surgeons are advised to stabilize the prosthesis by impaction, causing the implant to be clamped within the femoral canal. Good primary stability is achieved when post-operative mechanical stability of an implant assures low magnitudes of interface micromotions<sup>13</sup>. However, excessive impaction can lead to bone fissures<sup>14</sup> during rasping or insertion of the stem. Hence, a balance should be found between achieving an adequate stability by stem impaction and preventing bone damage.

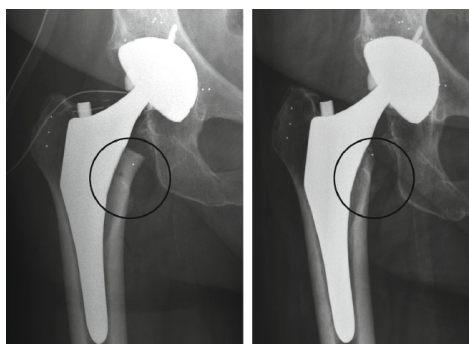


*Fig. 2 An example of bone loss in Gruen zone 7 after cementless THA. An ABG II hip prosthesis postoperatively (left) and 24 months (right). (from Alm et al., 2009<sup>15</sup>)*

Implant primary stability has a considerable effect on implant secondary stability. If implant-bone interface micromotions are high, no bone but fibrous tissue is created at the interface (Fig. 3) leading to poor secondary stability<sup>16</sup>. Besides the magnitude of interface micromotions, there are also other factors (implant or patient-related) influencing secondary stability. For instance, interface characteristics, such as pore size<sup>17</sup>, porosity<sup>18,19</sup> and surface roughness<sup>20,21</sup>, are known to have a great effect on bone ingrowth, especially on metal-bone interface strength<sup>22</sup>. Bone ingrowth can be enhanced by applying an additional surface coating to improve surface bioactivity and osteoconductivity<sup>23</sup>. Coating materials can improve the area of bone ingrowth, the bone-to-implant contact fraction<sup>19,24</sup> and the implant-bone interface strength<sup>25</sup>.

Even though a good primary and secondary stability of cementless implant is assured, it may not be sufficient for long term implant survival. After THA, due to the changes in load distribution, bone tissue will be stress-shielded and will adapt to the new mechanical conditions<sup>26</sup>. Hence, another cause of failure of uncemented THA is implant loosening due to reduced proximal bone loading, resulting in proximal bone resorption (Fig. 2). The extent of bone remodeling is affected by many factors, amongst which implant stiffness,

implant design<sup>27</sup> and extent of interface coating<sup>28,29</sup> play a considerable role. Stiffer implants tend to cause more bone resorption than composite ones<sup>30</sup>. On the other hand, composite implants evoke higher micromotions than stiffer implants, jeopardizing bone ingrowth<sup>31</sup>. Implants with only a proximal coating (to enhance bone ingrowth) have been reported to cause less bone resorption than fully coated designs<sup>27,29,32</sup>. Given that bone ingrowth and bone remodeling are coexisting processes, a good balance between both processes would be the key to a long term survival of cementless femoral components.

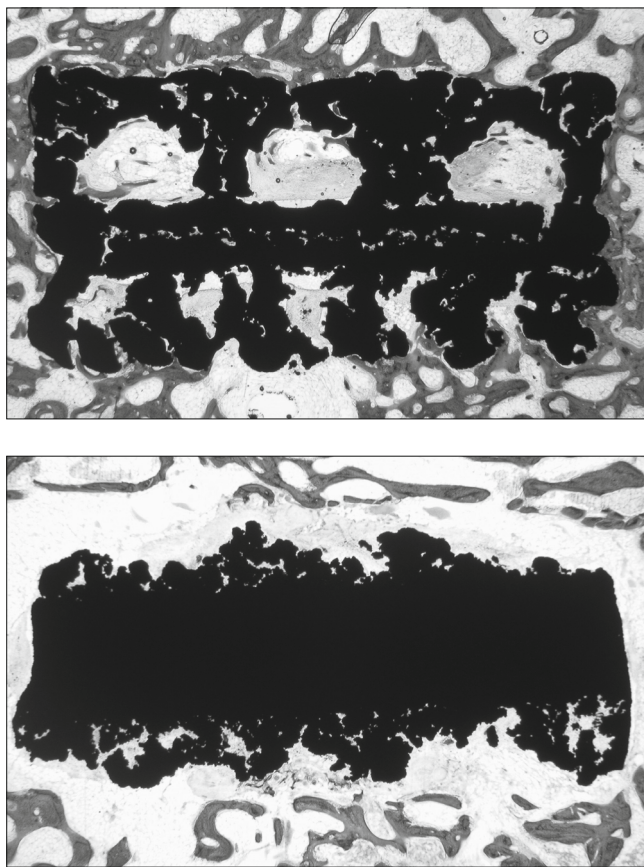


*Fig. 3 Histology images of metal (black)-bone (grey) interface. Bone ingrowth and ongrowth into porous structures (top). Fibrous tissue, rather than bone created at the metal-bone interface (bottom).*

Survival of cementless implants is commonly assessed in pre-clinical experimental and animal studies. For instance, *in vitro* studies judge implant stability based on the magnitude of interface micromotions<sup>33-35</sup> or migration<sup>36</sup>. In these studies, using various sensors attached to the bone and implant, interface micromotions are measured in a few locations around the implant, providing information on mechanical stability. New metal surfaces for

cementless implants are commonly tested in animal studies to assess bone ingrowth<sup>37</sup> and interface strength<sup>38,39</sup>. Pre-clinical experimental animal studies have some limitations, for instance, inaccuracies of measurement sensors or high costs of animal experiment.

Some of limitations can be overcome by performing pre-clinical assessment of implant stability using computational methods, such as finite element modeling (FEM). FEM models allow to assess implant stability by analyzing the magnitudes of interface micromotions<sup>40-42</sup>. Several FEM studies tested the effects of surgical factors on implant stability, looking at the effect of implant malalignment<sup>43</sup>, implant-bone interface gaps, bone properties<sup>44</sup>, interference fit<sup>41</sup> and loading conditions<sup>40</sup>. Besides implant stability, also bone remodeling after THA and interface strength of complex morphologies<sup>45,46</sup> can be simulated. Naturally, also FEM has limitations, mainly in simplifications of physical conditions. However, given increasing capabilities of FEM, it can well complement pre-clinical experimental and animal studies.

This thesis addresses many aspects concerning the stability of cementless THA reconstructions. The effect of numerous surgical and implant-related factors, which may affect implant survival, was studied on a macro and micro scale. The main goal of this thesis was to develop and improve upon FEM simulations to ultimately improve functioning of cementless implants.

## The relation between FEM and clinical and experimental research

**Chapters 2 and 3** evaluate the value of FEM as compared to experimental and clinical studies, respectively.

### Experimental versus FEM implant-bone micromotions (Chapter 2)

Implant stability in *in vitro* studies is measured using special micromotion sensors attached to the bone and implant. Given the size of these sensors and their attachment location, micromotions are often measured not at the vicinity of the actual interface. Large jigs supporting the sensors require multiple attachment points to the bone, with the assumption that bone is rigid. However, as bone and implants undergo elastic deformation, such assumption may lead to the miscalculation of interface micromotions and an incorrect prediction of implant stability. Using FEM, we tested the effect of elastic deformation of bone on measured micromotions. In a case-specific FEM model, micromotions at the actual metal-bone interface were compared with micromotions computed mimicking an experimental approach. It was hypothesized that because of elastic deformation of the bone, the magnitudes of both measurements will differ.



### **Periprosthetic bone remodeling: Clinical versus FEM prediction (Chapter 3)**

Based on shape adaptation of an Omnifit® stem (a clinically well performing design<sup>47,48</sup>), the Symax™ hip stem was developed. Both stems, built of the same alloy, are proximally coated and distally uncoated. The main difference is in the implant shape and the type, porosity and thickness of interface coating. The Symax™ stem is also distally treated with a surface process, which is meant to reduce the adherence of osteoblasts and suppress the subsequent bone growth onto the implant. These special features in the Symax™ design were implemented to enhance proximal loading of bone and therefore reduce bone stress shielding in that area<sup>49</sup>.

**Chapter 3** compares clinical data and FE bone remodeling prediction for both designs. The goal was to investigate whether improvements in implant design can be predicted in an FEM remodeling study.

### **Surgical and implant-related parameters to improve implant stability**

FEM can be used to investigate the potential effects of surgical and implant-related parameters, without requiring a large patient population or numerous experimental tests. In **Chapter 4**, the implant stiffness was varied in order to balance incompatible design goals. Whereas in **Chapter 5**, the balance between impaction force and implant stability was assessed.

### **Balancing incompatible implant design goals (Chapter 4)**

Another aspect that was investigated in this thesis concerned incompatible goals<sup>50</sup> when designing a prosthetic component. Stiff implants are known to cause more bone resorption than composite ones<sup>30</sup>. On the other hand, stiff implants cause lower interface micromotions, while composite stems are likely to evoke high micromotions proximally<sup>31</sup>. Given the aforementioned, by changing the implant stiffness one should be able to find a balance between acceptable interface micromotions and bone resorption. New materials, such as trabecular metal allow adapting the implant stiffness such that the incompatible design goals are well balanced. In **Chapter 4** an FEM methodology is proposed which combines ingrowth and remodeling simulation to improve implant design.

### **Balancing implant stability and risk of intra-operative bone damage (Chapter 5)**

An inadequate post-operative fit between the implant and host bone may jeopardize bone ingrowth. During the surgery, the cementless prosthesis is stabilized by impaction, which is causing the implant to be clamped within the femoral canal. However, too high

impaction force could cause fissures and fractures in the bone, likely leading to failure of the complete reconstruction. The effect of intra-operative impaction on implant stability and the accompanying risk of bone damage was studied in **Chapter 5**. The effect of intra-operative impaction force on implant primary stability at various levels of bone quality and on bone at risk of damage was analyzed.

## **Towards a more realistic simulation of ingrowth and micromotions predictions**

**Chapters 6 and 7** study possible improvements to the current FEM simulations of implant survival. An FEM simulation of bone ingrowth progression was proposed in **Chapter 6**. In **Chapter 7**, the effect of more detailed and realistic loading and boundary condition on bone-implant interface micromotions was studied.

### **Bone ingrowth simulation (Chapter 6)**

Previous FEM studies simulated the mechanical implication of bone ingrowth by specifying a zero relative displacement between bone and implant nodes<sup>51</sup> or by changing the implant-bone contact definition from frictional to bonded<sup>52,53</sup>.

The occurrence of ingrowth is governed by the magnitudes of interface micromotions and gaps. The effects of these two interface-related factors have been shown clearly in the literature<sup>13,54</sup>. However, there are also other factors playing a role in the bone ingrowth process, such as the time after implantation<sup>38,55</sup> and bone type and quality<sup>56,57</sup>, have been shown to play a role in bone ingrowth as well. The study presented in **Chapter 6** aimed to build further on the earlier FEM ingrowth simulations and proposes a bone ingrowth progression simulation that includes the effect of gradual bone maturation in time and the effect of bone quality on osseointegration.

### **The effect of more realistic loading configuration on micromotions (Chapter 7)**

Interface micromotions in FEM studies are commonly defined as a relative displacement between adjacent bone and stem nodes. An activity (e.g. walking) under which this motion occurs is often simulated by instantaneous loading (when maximum hip joint forces are acting on the femur). Micromotions occurring during the activity are then computed between the unloaded and loaded state. It is therefore unknown how the direction and magnitude of micromotions develop during the complete activity. Besides simplified loading conditions, FEM studies assume also certain simplifications to physiological boundary conditions. THA reconstructions are either diaphyseally (condyles not modeled) or distally constrained (complete femur model)<sup>58</sup> with often only the hip joint contact and abductor

forces acting on the femur<sup>59</sup>. However, it has been shown that physiological deflections of the femoral head are only obtained when physiological constraints with all muscle forces were applied to the reconstruction<sup>60</sup>. **Chapter 7** discusses the pattern of interface micro-motions throughout the complete activity of normal walking and assesses the effect of simplified boundary conditions in FEM on implant stability prediction.

## Detailed implant-bone interface micro-mechanics

On a macroscopic level, FEM simulations are not capable to assess the effect of different surface structures on metal-bone interface strength. Thus, another aspect presented in this thesis concerns the interface mechanics, on a microscopic scale.

### Theoretical prediction of interface strength (Chapter 8-9)

**Chapters 8 and 9** concern theoretical prediction of the metal-bone interface strength based on the magnitude of histomorphometric parameters of ingrown bone. New techniques allow manufacturing interface structures with any desired characteristics. These new surfaces are commonly tested in animal experiments<sup>37</sup>, where interface strength<sup>38</sup> or histomorphometric data (bone-implant contact area, ingrowth depth) at defined time points after implantation can be assessed. A few histological studies showed a good correlation between interface strength and ingrowth depth at varied time points<sup>39,61,62</sup>. One could therefore assume that increasing bone ingrowth depth causes an increase in interface strength. The FEA study presented in **Chapter 8** tests this hypothesis using FE micro-models of a metal-bone interface with varying bone ingrowth depths. In **Chapter 9**, we tested whether magnitudes of histomorphometric parameters, such as bone ingrown volume, area of metal-bone interlock or total bone contact area, can be discriminative when theoretically predicting interface strength of a surface structure.

In summary, this thesis shows a broad spectrum of issues in THA related to loosening of cementless implants. Studies presented in this thesis focus on designing FEM tools or show the capability of existing simulations to support and strengthen pre-clinical prediction of implant survival.

## Reference List

- 1 **Stone AA, Broderick JE, Porter LS, Kaell AT.** The experience of rheumatoid arthritis pain and fatigue: examining momentary reports and correlates over one week. *Arthritis Care Res* 1997;10(3):185-93.
- 2 **Bijlsma JW, Knahr K.** Strategies for the prevention and management of osteoarthritis of the hip and knee. *Best Pract Res Clin Rheumatol* 2007;21(1):59-76.
- 3 **Beck M, Kalhor M, Leunig M, Ganz R.** Hip morphology influences the pattern of damage to the acetabular cartilage: femoroacetabular impingement as a cause of early osteoarthritis of the hip. *J Bone Joint Surg Br* 2005;87(7):1012-8.
- 4 **Kim YJ, Bixby S, Mamisch TC, Clohisy JC, Carlisle JC.** Imaging structural abnormalities in the hip joint: instability and impingement as a cause of osteoarthritis. *Semin Musculoskelet Radiol* 2008;12(4):334-45.
- 5 **Buckwalter JA, Mankin HJ, Grodzinsky AJ.** Articular cartilage and osteoarthritis. *Instr Course Lect* 2005;54:465-80.
- 6 **Martin JA, Buckwalter JA.** Roles of articular cartilage aging and chondrocyte senescence in the pathogenesis of osteoarthritis. *Iowa Orthop J* 2001;21:1-7.
- 7 **Sahin V, Karakas ES, Aksu S, Atlihan D, Turk CY, Halici M.** Traumatic dislocation and fracture-dislocation of the hip: a long-term follow-up study. *J Trauma* 2003;54(3):520-9.
- 8 **Harris WH.** Traumatic arthritis of the hip after dislocation and acetabular fractures: treatment by mold arthroplasty. An end-result study using a new method of result evaluation. *J Bone Joint Surg Am* 1969;51(4):737-55.
- 9 **Garelick G, Kärrholm J, Rogmark C, Herberts P.** Swedish Hip Arthroplasty Register. Annual Report 2008.2009;
- 10 **Ethgen O, Bruyere O, Richy F, Dardennes C, Reginster JY.** Health-related quality of life in total hip and total knee arthroplasty. A qualitative and systematic review of the literature. *J Bone Joint Surg Am* 2004;86-A(5):963-74.
- 11 **Schmidt AH, Leighton R, Parvizi J, Sems A, Berry DJ.** Optimal arthroplasty for femoral neck fractures: is total hip arthroplasty the answer? *J Orthop Trauma* 2009;23(6):428-33.
- 12 **Eskelinen A, Remes V, Helenius I, Pulkkinen P, Nevalainen J, Paavolainen P.** Total hip arthroplasty for primary osteoarthritis in younger patients in the Finnish arthroplasty register. 4,661 primary replacements followed for 0-22 years. *Acta Orthop* 2005;76(1):28-41.
- 13 **Jasty M, Bragdon C, Burke D, O'Connor D, Lowenstein J, Harris WH.** In vivo skeletal responses to porous-surfaced implants subjected to small induced motions. *J Bone Joint Surg Am* 1997;79(5):707-14.
- 14 **Lindahl H.** Epidemiology of periprosthetic femur fracture around a total hip arthroplasty. *Injury* 2007;38(6):651-4.
- 15 **Alm JJ, Mäkinen TJ, Lankinen P, Moritz N, Vahlberg T, Aro HT.** Female patients with low systemic BMD are prone to bone loss in Gruen zone 7 after cementless total hip arthroplasty. *Acta Orthop* 2009;80(5):531-7.
- 16 **Søballe K, Hansen ES, Rasmussen H, Jørgensen PH, Bünger C.** Tissue ingrowth into titanium and hydroxyapatite-coated implants during stable and unstable mechanical conditions. *J Orthop Res* 1992;10(2):285-99.
- 17 **Itälä AI, Ylänen HO, Ekholm C, Karlsson KH, Aro HT.** Pore diameter of more than 100 microm is not requisite for bone ingrowth in rabbits. *J Biomed Mater Res* 2001;58(6):679-83.
- 18 **Kujala S, Ryhanen J, Danilov A, Tuukkanen J.** Effect of porosity on the osteointegration and bone ingrowth of a weight-bearing nickel-titanium bone graft substitute. *Biomaterials* 2003;24(25):4691-7.
- 19 **Wazen RM, Lefebvre LP, Baril E, Nanci A.** Initial evaluation of bone ingrowth into a novel porous titanium coating. *J Biomed Mater Res B Appl Biomater* 2010;94(1):64-71.
- 20 **Brentel AS, de Vasconcellos LM, Oliveira MV, Graça ML, de Vasconcellos LG, Cairo CA, Carvalho YR.** Histomorphometric analysis of pure titanium implants with porous surface versus rough surface. *J Appl Oral Sci* 2006;14(3):213-8.
- 21 **Vasconcellos LM, Oliveira MV, Graça ML, Vasconcellos LG, Cairo CA, Carvalho YR.** Design of dental implants, influence on the osteogenesis and fixation. *J Mater Sci Mater Med* 2008;19(8):2851-7.

- 22 **Buser D, Nydegger T, Oxland T, Cochran DL, Schenk RK, Hirt HP, Snétivy D, Nolte LP.** Interface shear strength of titanium implants with a sandblasted and acid-etched surface: a biomechanical study in the maxilla of miniature pigs. *J Biomed Mater Res* 1999;45(2):75-83.
- 23 **Zhang E, Zou C.** Porous titanium and silicon-substituted hydroxyapatite biomodification prepared by a biomimetic process: characterization and in vivo evaluation. *Acta Biomater* 2009;5(5):1732-41.
- 24 **Nguyen HQ, Deporter DA, Pilliar RM, Valiquette N, Yakubovich R.** The effect of sol-gel-formed calcium phosphate coatings on bone ingrowth and osteoconductivity of porous-surfaced Ti alloy implants. *Biomaterials* 2004;25(5):865-76.
- 25 **Søballe K, Hansen ES, Brockstedt-Rasmussen H, Hjortdal VE, Juhl GI, Pedersen CM, Hvid I, Bunger C.** Gap healing enhanced by hydroxyapatite coating in dogs. *Clin Orthop Relat Res* 1991;(272):300-7.
- 26 **Huiskes R, Weinans H, van Rietbergen B.** The relationship between stress shielding and bone resorption around total hip stems and the effects of flexible materials. *Clin Orthop Relat Res* 1992;(274):124-34.
- 27 **Engh CA, Bobyn JD.** The influence of stem size and extent of porous coating on femoral bone resorption after primary cementless hip arthroplasty. *Clin Orthop Relat Res* 1988;(231):7-28.
- 28 **Turner TM, Sumner DR, Urban RM, Rivero DP, Galante JO.** A comparative study of porous coatings in a weight-bearing total hip-arthroplasty model. *J Bone Joint Surg Am* 1986;68(9):1396-409.
- 29 **Skinner HB, Kim AS, Keyak JH, Mote CD, Jr.** Femoral prosthesis implantation induces changes in bone stress that depend on the extent of porous coating. *J Orthop Res* 1994;12(4):553-63.
- 30 **Bobyn JD, Glassman AH, Goto H, Krygier JJ, Miller JE, Brooks CE.** The effect of stem stiffness on femoral bone resorption after canine porous-coated total hip arthroplasty. *Clin Orthop Relat Res* 1990;(261):196-213.
- 31 **Otani T, Whiteside LA, White SE, McCarthy DS.** Effects of femoral component material properties on cementless fixation in total hip arthroplasty. A comparison study between carbon composite, titanium alloy, and stainless steel. *J Arthroplasty* 1993;8(1):67-74.
- 32 **Bobyn JD, Mortimer ES, Glassman AH, Engh CA, Miller JE, Brooks CE.** Producing and avoiding stress shielding. Laboratory and clinical observations of noncemented total hip arthroplasty. *Clin Orthop Relat Res* 1992;(274):79-96.
- 33 **Bühler DW, Berlemann U, Lippuner K, Jaeger P, Nolte LP.** Three-dimensional primary stability of cementless femoral stems. *Clin Biomech (Bristol , Avon)* 1997;12(2):75-86.
- 34 **Bühler DW, Oxland TR, Nolte LP.** Design and evaluation of a device for measuring three-dimensional micro-motions of press-fit femoral stem prostheses. *Med Eng Phys* 1997;19(2):187-99.
- 35 **Monti L, Cristofolini L, Viceconti M.** Methods for quantitative analysis of the primary stability in uncemented hip prostheses. *Artif Organs* 1999;23(9):851-9.
- 36 **Westphal FM, Bishop N, Honl M, Hille E, Puschel K, Morlock MM.** Migration and cyclic motion of a new short-stemmed hip prosthesis--a biomechanical in vitro study. *Clin Biomech (Bristol , Avon)* 2006;21(8):834-40.
- 37 **Biamond JE, Hannink G, Jurrius A, Verdonchot N, Buma P.** In vivo assessment of bone ingrowth potential of 3-dimensional E-beam produced implant surfaces and the effect of additional treatment by acid-etching and hydroxyapatite coating. *Journal of Biomaterials Applications* 2010;
- 38 **Bobyn JD, Stackpool GJ, Hacking SA, Tanzer M, Krygier JJ.** Characteristics of bone ingrowth and interface mechanics of a new porous tantalum biomaterial. *J Bone Joint Surg Br* 1999;81(5):907-14.
- 39 **Oh S, Tobin E, Yang Y, Carnes DL, Jr., Ong JL.** In vivo evaluation of hydroxyapatite coatings of different crystallinities. *Int J Oral Maxillofac Implants* 2005;20(5):726-31.
- 40 **Pancanti A, Bernakiewicz M, Viceconti M.** The primary stability of a cementless stem varies between subjects as much as between activities. *J Biomech* 2003;36(6):777-85.
- 41 **Abdul-Kadir MR, Hansen U, Klabunde R, Lucas D, Amis A.** Finite element modelling of primary hip stem stability: the effect of interference fit. *J Biomech* 2008;41(3):587-94.
- 42 **Pettersen SH, Wik TS, Skallerud B.** Subject specific finite element analysis of implant stability for a cementless femoral stem. *Clin Biomech (Bristol , Avon)* 2009;24(6):480-7.
- 43 **Abdul-Kadir M, Hansen U, Klabunde R, Amis A.** The effect of malalignment and undersizing on primary stability of cementless stems. *J Biomech* 2006;39(Supplement 1):S514.

- 44 **Abdul-Kadir M, Kamsah N.** The effect of bone properties due to skeletal diseases on stability of cementless hip stems. *American Journal of Applied Sciences* 2009;6(12):1988-94.
- 45 **Stolk J, Verdonchot N, Murphy BP, Prendergast PJ, Huiskes R.** Finite element simulation of anisotropic damage accumulation and creep in acrylic bone cement. *Eng Fract Mech* 2004;71:513-28.
- 46 **Waanders D, Janssen D, Mann KA, Verdonchot N.** The mechanical effects of different levels of cement penetration at the cement-bone interface. *J Biomech* 19-4-2010;43(6):1167-75.
- 47 **Epinette JA, Manley MT.** Uncemented stems in hip replacement--hydroxyapatite or plain porous: does it matter? Based on a prospective study of HA Omnifit stems at 15-years minimum follow-up. *Hip Int* 2008;18(2):69-74.
- 48 **Hsieh PH, Shih CH, Lee PC, Yang WE, Lee ZL.** Cementless total hip arthroplasty using the omnifit system: An 8.2 year follow-up study of 166 hips. *J Orthop Surg (Hong Kong)* 2000;8(2):45-51.
- 49 **Ten Broeke RH, Alves A, Baumann A, Arts JJ, Geesink RG.** Bone reaction to a biomimetic third-generation hydroxyapatite coating and new surface treatment for the Symax hip stem. *J Bone Joint Surg Br* 2011;93(6):760-8.
- 50 **Huiskes R.** Failed innovation in total hip replacement. Diagnosis and proposals for a cure. *Acta Orthop Scand* 1993;64(6):699-716.
- 51 **Spears IR, Pfeleiderer M, Schneider E, Hille E, Bergmann G, Morlock MM.** Interfacial conditions between a press-fit acetabular cup and bone during daily activities: implications for achieving bone in-growth. *J Biomech* 2000;33(11):1471-7.
- 52 **Fernandes PR, Folgado J, Jacobs C, Pellegrini V.** A contact model with ingrowth control for bone remodelling around cementless stems. *J Biomech* 2002;35(2):167-76.
- 53 **Folgado J, Fernandes PR, Jacobs CR, Pellegrini VD, Jr.** Influence of femoral stem geometry, material and extent of porous coating on bone ingrowth and atrophy in cementless total hip arthroplasty: an iterative finite element model. *Comput Methods Biomech Biomed Engin* 2009;12(2):135-45.
- 54 **Engh CA, O'Connor D, Jasty M, McGovern TF, Bobyn JD, Harris WH.** Quantification of implant micromotion, strain shielding, and bone resorption with porous-coated anatomic medullary locking femoral prostheses. *Clin Orthop Relat Res* 1992;(285):13-29.
- 55 **Hofmann AA, Bloebaum RD, Bachus KN.** Progression of human bone ingrowth into porous-coated implants. Rate of bone ingrowth in humans. *Acta Orthop Scand* 1997;68(2):161-6.
- 56 **Fini M, Giavaresi G, Rimondini L, Giardino R.** Titanium alloy osseointegration in cancellous and cortical bone of ovariectomized animals: histomorphometric and bone hardness measurements. *Int J Oral Maxillofac Implants* 2002;17(1):28-37.
- 57 **Shih LY, Shih HN, Chen TH.** The effects of sex and estrogen therapy on bone ingrowth into porous coated implant. *Journal of Orthopaedic Research* 2003;21(6):1033-40.
- 58 **Kleemann RU, Heller MO, Stoeckle U, Taylor WR, Duda GN.** THA loading arising from increased femoral anteversion and offset may lead to critical cement stresses. *J Orthop Res* 2003;21(5):767-74.
- 59 **Lengsfeld M, Burchard R, Günther D, Pressel T, Schmitt J, Leppke R, Griss P.** Femoral strain changes after total hip arthroplasty--patient-specific finite element analyses 12 years after operation. *Med Eng Phys* 2005;27(8):649-54.
- 60 **Speirs AD, Heller MO, Duda GN, Taylor WR.** Physiologically based boundary conditions in finite element modelling. *J Biomech* 2007;40(10):2318-23.
- 61 **Johansson CB, Han CH, Wennerberg A, Albrektsson T.** A quantitative comparison of machined commercially pure titanium and titanium-aluminum-vanadium implants in rabbit bone. *Int J Oral Maxillofac Implants* 1998;13(3):315-21.
- 62 **Castellani C, Lindtner RA, Hausbrandt P, Tschegg E, Stanzl-Tschegg SE, Zanoni G, Beck S, Weinberg AM.** Bone-implant interface strength and osseointegration: Biodegradable magnesium alloy versus standard titanium control. *Acta Biomater* 2011;7(1):432-40.



## *Experimental versus computational analysis of micromotions at the implant-bone interface*



## Abstract

*In total hip arthroplasty micromotions at the implant-bone interface influence the long term survival of the prosthesis. These micromotions are often measured using sensors that are fixed to the implant and bone at points which are remote from the interface. Given that the implant-bone system is not rigid, errors may be introduced. It is not possible to assess the magnitude of these errors with the currently available experimental methods. However, this problem can be investigated using finite element method (FEM).*

*The hypothesis, that the actual interface micromotions differ from measured in the experimental manner, was tested using a case-specific FE model, validated against deflection experiments. The FE model was used to simulate an 'experimental' method to measure micromotions. This 'experimental' method was performed by mimicking the distance between the measurement points; the implant point was selected at the interface while the bony point at the outer surface of bone.*

*No correlation was found between the micromotions computed at the interface and when using remote reference points. Moreover, the magnitudes of micromotions computed with the latter method were considerably greater. By reducing the distance between the reference points the error decreased, but correlation stayed unchanged. Care needs to be taken when interpreting the results of the micromotion measurement systems that use bony reference points at a distance from the actual interface.*

## Introduction

In cementless total hip arthroplasty (THA) the primary stability of prosthetic components is important for the long-term survival, as excessive micromotions at the implant-bone interface may postpone or even prevent osseointegration of the component <sup>1,2</sup>. Interfacial micromotions can be measured in pre-clinical experimental set-ups, using linear variable differential transducers (LVDT's) <sup>3-6</sup>, optoelectronic tracking devices <sup>7-9</sup>, or video systems with retroflective markers <sup>10</sup>. None of these experimental methods allow for micromotion measurement at the actual implant-bone interface. Furthermore, some of them require a relatively large frame to be attached to the reconstruction, and for all methods holes have to be made in the femoral bone for access to the implant surface <sup>11</sup>. This poses limitations for extensive investigations of parametric variations of reconstructions with cementless implants.

Given that bone undergoes elastic deformation when subjected to load, it can considerably affect the measurement if the recording is not performed at the actual interface. For instance, a single LVDT implant-bone relative motion measurement system <sup>3,4</sup> is mounted transcortically by means of an anchorage set-up; the motion is measured between the pin connected to the stem and the LVDT support attached to the bone surface. When taking a point on the prosthesis and a point at the external bone surface, the deformation of the bone can affect the measurement of implant-bone relative displacement. The effect of the strain across the cortical bone on the relative implant-bone motion measurement was investigated in an experimental study by Monti et al. (1999). They reported that measuring the relative motion between points in proximity of the interface causes an error of several microns, which was considered unacceptable for precise micromotion measurements. The effect of bone elastic deformation is likely even greater when a six-degrees-of-freedom (6DOF) LVDT system is used. Such a system measures the motion of a point at the surface of the prosthesis relative to the motion of a reference point on the frame that is anchored to the bone <sup>11</sup>. The frame is attached to the bone at several points, which entails that the reference bony point is a virtual, averaged point of these attachment locations. This LVDT set-up is based on the assumption that the averaged frame attachment point adequately represents the bony point at the interface, while actually the distance between the reference point and the actual interface may be several millimetres, sometimes even centimetres. Although the frame is rigid, the bone surrounding the implant is not, which means bone deformations may affect the measurements. The rigid frame may amplify bone deformations, leading to the measurement of a certain micromotion value even when there is no relative displacement at the implant-bone interface at all. In summary, it is unclear how experimental micromotion measurements are related to the actual motions at the stem-bone interface.

This problem can be investigated using finite element method (FEM) models of reconstructions with cementless stems. The FEM allows for quantification of the micromotions

by tracing the relative motion of points at the actual implant-bone interface<sup>12-14</sup>. Mechanical validation of the models can be done by mimicking laboratory experiments, in a case-specific manner<sup>15-17</sup>. FEM models allow for high accuracy micromotion calculations at multiple locations simultaneously, but can also simulate experimental methods by using more remote bony points, allowing for the quantification of potential experimental measurement errors.

In the present study the validity of common experimental methods to measure interface micromotions was investigated using FEM models. The hypothesis was that the points, between which motion is measured using experimental methods, are too far away from the implant-bone interface to accurately measure the actual interface motion. In addition, it was investigated whether reducing the distance between the measurement points would reduce the error. To test the hypothesis the authors performed an FEM study in which micromotions were computed at the actual interface (node-to-surface method) and between an implant point at the interface and a point at the outer bone surface ('experimental' method).

## Materials and Methods

The FEM models used in the current study were validated against lab experiments, in which the deflection of the implant and bone was measured during mechanical tests. These tests were simulated in six case-specific FEM simulations. Validation was performed by comparing the experimental and simulated deflections of implant and bone for each of the six reconstructions.

### Creation and validation of the FEM models

Six cadaveric femurs (4 donors; one female, age 77 and three males, age 74, 81 and 82) were used for the experiments. The femurs were implanted with two different cementless prostheses (3 bones for each design): the CLS Spotorno (Zimmer, GmbH, Winterthur, Switzerland) (sizes 10, 11.25) and the VerSys Epoch FullCoat (Zimmer, Inc., Warsaw, IN, USA) (sizes 13,15,16 (outer diameter of the distal part of stem in mm)). The CLS is a proximally fixed Ti alloy prosthesis, the ribs in its proximal region assure primary and rotational stability. The Epoch is a low stiffness composite prosthesis consisting of the inner CoCrMo core, middle PEEK layer (thickness 1.3 mm) and outer layer of Ti fibre metal (thickness 1.65 mm). Pre-operative planning was performed by two experienced surgeons who also conducted the implantations. After marking the position of the implants in the femur, the stems were removed. For deflection measurement purposes, holes (d=10 mm) were drilled through the intramedullary canal at six locations (proximal, mid and distal region, both medially and laterally) (Fig. 1). Subsequently, tantalum markers were attached to the femur at all

six locations, for Roentgen Stereophotogrammetric Analysis (RSA) in a later stage (Fig. 1).

Next, the femurs with the implants removed were scanned using Computed Tomography (CT). The femurs were scanned in a water basin, along with a hydroxyapatite calibration phantom (solid, 0, 50, 100, 200 mg/ml calcium hydroxyapatite, Image Analysis, Columbia, KY, USA). Finally, the implants were re-inserted in the femurs to the position that was previously marked. Plastic tracers (Fig. 1) were glued to the implant surface at the six locations in order to track implant movement. The femurs were cut distally and fixed within a cylindrical metal sleeve using polymethylmethacrylate (PMMA).

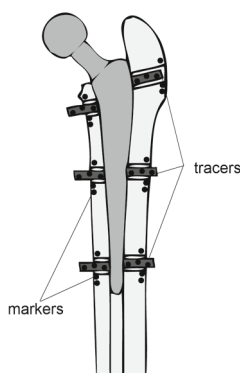


*Fig. 1 RSA technique: 18 bone markers and 18 stem markers, distributed over six locations (three markers at each location for bone and stem). Around each of the six holes, three markers with a diameter  $d$  of 0.8 mm were inserted in the femurs, plastic tracers (each with 3 tantalum markers ( $d=0.5$  mm)) were glued to the prosthesis surface.*

The reconstructions were tested under relatively simple loading conditions. The CLS reconstructions were oriented in an upright position, while the Epoch reconstructions were positioned in an anatomical position. In order to maximize the deflection, all reconstructions were loaded dynamically in the axial direction (MTS 458.2 MicroConsole, Minneapolis, MN, USA), while increasing the load amplitude in a step-wise fashion until failure of the reconstruction. Deflection of implant and femur was measured just prior to failure for the CLS reconstruction (1900 N, 2000 N, 2500 N) and at 1500 N for the Epoch reconstructions. Using RSA (precision  $40\text{ }\mu\text{m}^{18}$ ), deflection of implant and bone was measured by comparing the averaged marker positions of implant and bone in the unloaded and loaded situation, at each of the six locations.

The CT data was used to generate six subject-specific FEM models of femoral bones using medical imaging software (MIMICS 11.0, Materialise, Leuven, Belgium). The FEM models of the CLS Spotorno stem and VerSys EPOCH FullCoat stem were constructed from three-dimensional models obtained from the manufacturer using an FEA pre-processor (Patran, MSC Software Corporation, Santa Ana, CA, USA). The solid models of the implants were subsequently imported into the bone surface models using an FEM software package

(MSC.MARC-Mentat 2007r1, MSC Software Corporation, Santa Ana, CA, USA). The position of the tantalum markers in both bone and stem as measured using RSA provided information that allowed to precisely position the stem in the bone model. Cavities at the implant-bone interface that represent the natural irregular contours of the inside femoral surface were recreated using an in-house algorithm<sup>19</sup> (Fig. 2). The FEM models were created from four-noded tetrahedral elements (average of 52,033 elements for each model). The isotropic properties of cortical and trabecular bone were derived from the calibrated CT data<sup>20</sup>. Bone material properties were assigned based on the local ash density<sup>21</sup>. The holes in bones were represented in the models as low-stiffness elements. The material properties for the stems were obtained from the manufacturer (Table 1).

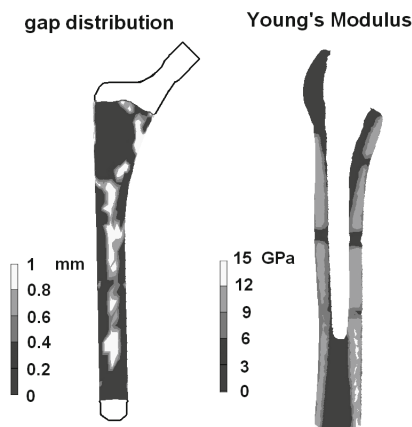


Fig. 2 An example of a realistic gap distribution projected onto a stem model (left) and a Young's modulus distribution in a bone model (right).

Table 1 List of the material properties used.

IMPLANT	MATERIAL	YOUNG'S MODULUS [GPa]	POISSON'S RATIO
CLS	TiAlV	105	0.3
EPOCH	CoCrMo core	240	0.3
	PEEK (middle layer)	3.4	0.3
	Fibre mesh (outer layer)	6.9	0.3

Frictional contact was simulated at the implant-bone interface using a node-to-surface contact algorithm (MSC.MARC 2007r1, MSC Software Corporation, Santa Ana, CA, USA) (not to confuse with the node-to-surface micromotion calculation manner). A friction coefficient of 0.3 was assumed for the CLS<sup>12</sup>, and 0.5 for the EPOCH reconstructions<sup>22</sup>. To validate the models the experimental loading conditions were mimicked. Model validation was performed by means of regression analysis that was performed between the experimental (RSA) and FEM model deflection measurements.

### Interfacial micromotions

Two methods to calculate micromotions were applied to all six case-specific FEM models of cementless hip reconstructions. The calculations were performed under normal walking loading conditions<sup>23</sup>, including a hip contact force only, as often is the case in *in-vitro* tests<sup>7,10</sup>.

On average eight micromotion measurement points per model were used (distributed around the implant surface), assuring that they were not in proximity of the low stiffness elements representing the holes. In the first method (node-to-surface) micromotions were computed by projecting the displacement of an implant node onto the local endosteal surface of the bone (Fig. 3). This method did also take into account the local deformation of the bone surface. Furthermore, it allowed for decomposition of the total relative displacement into actual micromotions and normal displacements ('gapping' of the interface). For the current study, only micromotions parallel to the bone surface were included for the node-to-surface method. In the second 'experimental' method (Fig. 3) micromotions were computed by comparing the relative displacements of a node located at the implant surface and of a node at the exterior bone surface. The authors did not choose a specific experimental methodology to simulate the 'experimental' approach, only the experimental distance between the measurement points was simulated. Similarly, to what one would observe in a real experimental set-up the distance between the measurement points ranged from 3.75 mm to 16.26 mm (on average 9.9 mm).

The hypothesis was tested using regression analyses; the micromotions predicted by the node-to-surface method were compared with the micromotions predicted by the 'experimental' method. Additional micromotion computations, in which a bony reference point was selected at halfway between the interface and the outer bone surface (the node-in-between-node method), were performed (Fig. 3). This method allowed to investigate whether the correlation with the actual micromotions improves when the distance between the reference points is reduced, i.e. the 'bone node' is moved closer to the actual interface. Furthermore, the correlation between the measurement error and the distance between the reference point and the actual interface was quantified.

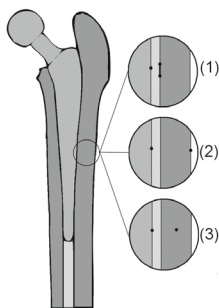


Fig. 3 Methods to calculate micromotions: (1) node-to-surface, (2), 'experimental', (3) node-to-in-between-node.

## Results

### FEM model validation - deflection

The FEM and experimental data of deflection in X, Y and Z directions at the six locations (Fig. 4) was grouped for the CLS and EPOCH reconstructions. The CLS reconstructions showed an excellent correlation with experimental measurements when grouped for all directions (slope=0.95,  $r^2=0.96$ , P-value<<0.05). The EPOCH models showed a good correlation with the experimental measurements, although the structural stiffness was somewhat overestimated (slope=0.62,  $r^2=0.88$ , P-value<<0.05). The correlations of the deflection of all marker points in the X, Y and Z directions were  $r^2= 0.72, 0.73, 0.90$  for the EPOCH, and  $r^2= 0.84, 0.94, 0.91$  for the CLS, respectively.

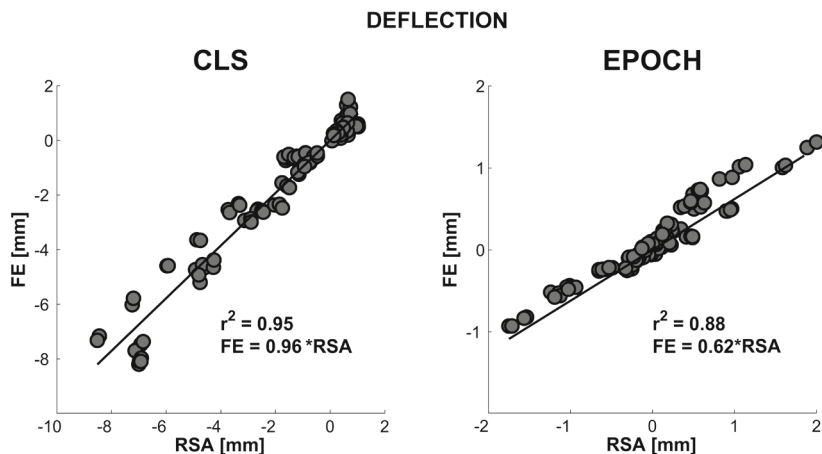


Fig. 4 FEM models validation against experimental results. Deflection results were grouped in X, Y and Z direction for reconstructions with the CLS and EPOCH stem.

## Micromotion analysis

When comparing the two different micromotion measurement methods, virtually no correlation was found between the node-to-surface and the 'experimental' methods (slope = 1.51,  $r^2 = 0.05$ ; Fig. 5). The 'experimental' method considerably overestimated the actual interfacial micromotions, as calculated by the node-to-surface method.

The results showed that the micromotion error becomes smaller when reducing the distance of the bone reference point to the actual implant-bone interface (Fig. 6). When the distance between the reference points was reduced by 50 per cent, the error decreased correspondingly ((Fig. 7); slope=0.47,  $r^2=0.82$ , P-value<<0.05). However, the correlation with the actual micromotions was still very poor (slope=0.81,  $r^2=0.05$ ).

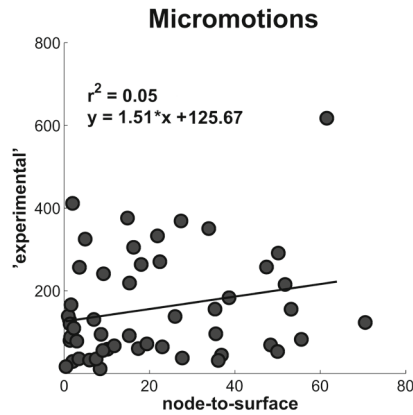


Fig. 5 Results of node-to-surface versus 'experimental' micromotion calculation manner.

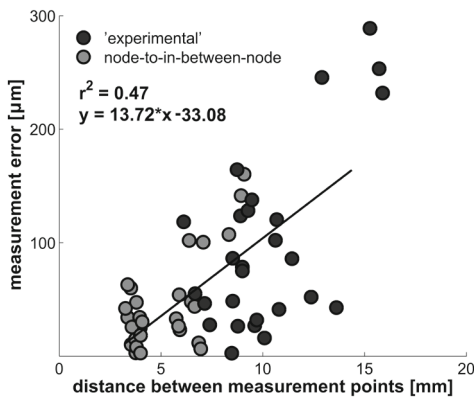


Fig. 6 Micromotions measurement error vs. distance between measurement reference points for the EPOCH reconstructions.

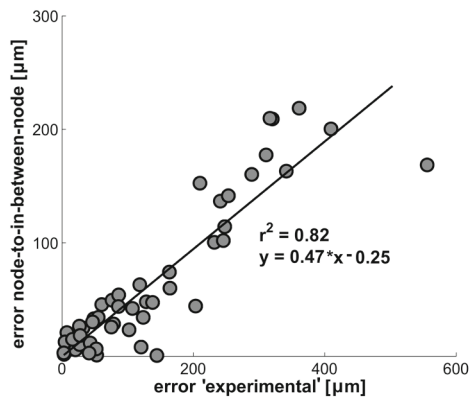


Fig. 7 Regression analysis between errors when micromotions measured in the 'experimental' and node-to-in-between-node manner.



## Discussion

In the current study the hypothesis about the inferior capacity of the experimental methods to accurately measure implant-bone micromotions at the interface was tested. The authors hypothesized that micromotions measured experimentally differ considerably from actual implant-bone motion at the interface. FEM is the best suitable available tool to test such a hypothesis as no experimental method exists that can measure implant-bone motion at the actual interface. In the present study validated case-specific FEM models allowed for computing micromotion at the actual interface, but also for simulating an experimental set-up. The results proved the hypothesis: the micromotions computed at the interface were considerably different from the 'experimental' micromotions. The simulations indicated that elastic deformation of bone causes large micromotion measurement errors. Furthermore, there was no correlation between the two measurements. By reducing the distance between the reference points in the 'experimental' methods one can proportionally reduce the error, although the correlation with the actual interface motions is not improved. The current study shows that it is important to choose a bony reference point as close as possible to the actual interface. Evidently this is very difficult to attain in experimental conditions.

The results of the current study indicated that the measurement errors of the 'experimental' method are caused by bone deformation. The effect of elastic bone deformation was measured in the experimental study by Monti et al., (1999). In that study an LVDT was glued to the external surface of bone, while a pin attached to that LVDT sensed the shear motions corresponding to the elastic strain at three controlled depths in bone (0.5 mm above the external surface, 0.5 mm above the implant-bone interface and midway between these two levels). The mean shear motion recorded varied depending on the location of the reference point, increasing with increasing distance between the reference points. Subsequently, they compared their experimental findings with the FEM prediction and found slightly larger values predicted by the FEM model, but with the same distribution across the cortical bone. They did not compare the micromotions measured experimentally with actual motions at the interface as predicted by their FEM model. In the present study such a comparison was performed, which allowed the authors to quantify the error made in the experimental measurements. To the authors' knowledge this is the first FEM study where the effect of bone elastic deformation on measured micromotions was investigated by mimicking an experimental method and computing micromotions at the interface.

The magnitudes of the interface motions (up to 80  $\mu\text{m}$ ) predicted by the node-to-surface method were in the range of micromotions reported in other FEM studies<sup>13,14</sup>. Abdul-Kadir et al., (2008) calculated micromotions up to 150  $\mu\text{m}$  under stair climbing loading condition, while Pettersen et al., (2009), reported micromotions in the range of 40  $\mu\text{m}$ . Similarly, in the present study the majority of the implant-bone relative motion at the interface was below 40  $\mu\text{m}$ . The magnitude of micromotions computed when simulating an experimental

approach was considerably greater than micromotions measured experimentally using the LVDT<sup>3</sup> or optoelectronic tracking device<sup>7</sup> systems. The maximal values computed in the present study in the 'experimental' method were mainly below 400  $\mu\text{m}$ , while the micromotions reported in the study of Buhler et al., (1997a) were on average 96  $\mu\text{m}$  for the CLS stem. It is possible that other localization of the measurement system in that experimental study (medial or lateral site instead of anterior or posterior (study of Buhler et al., 1997a)) would lead to greater micromotion values. Additionally, the error caused by the elastic deformation of bone is likely to depend on bone quality and loading conditions. Moreover, the presence of holes in the current FEM models could have an effect on the magnitudes of measured motions, particularly in the 'experimental' approach. Given that bone with holes is subjected to more bending more elastic deformation will occur.

The threshold value of micromotions below which stable bone ingrowth will occur has been reported in the literature to be in the range of 40  $\mu\text{m}$ . Jasty et al., 1997<sup>24</sup> reported micromotions below 40  $\mu\text{m}$  to assure complete or partial ingrowth of bone into porous-coated implants. In this study an in-vivo loading device was used to apply a fixed amount of oscillatory rotational motion to cylindrical porous-coated implants placed in the lateral femoral condyles. Another study, regarding post-mortem tests on canine limbs<sup>1</sup>, reported a relative motions between implant and bone smaller than 28 $\mu\text{m}$  to allow bone to grow into the pores, while micromotions beyond 150 $\mu\text{m}$  were found to prevent bone formation. Given that the threshold for osseointegration is very low and analyzing the outcome of the present study it needs to be mentioned that the experimental predictions of bone ingrowth based on measured micromotions can be effected by an error if the measurements are not performed at the actual interface.

The current results suggest that when simulating the experiment, in order to validate an FEM model, one needs to simulate the experiment exactly, considering that the interfacial micromotions differ from those measured at a proximity to the interface. For instance, to validate an FEM model based on the measurements of the 6DOF LVDTs system one should ideally simulate the frame and its attachment location accurately to allow direct comparisons between experimental and FEM data. The present study demonstrates that the factors like localization of the reference points, their relative distance and distance from the interface should be taken into consideration when validating FEM models.

The models used in the present study to test the hypothesis were closely reproducing the post-operative situation. Similarly to recent FEM studies<sup>6,13,16,25</sup> that measured implant stability by analyzing micromotions at the interface, the models used here were validated against the experimental data and were case-specific. The presence of gaps is known to have an effect on interfacial micromotions<sup>6</sup>. Therefore a realistic gap distribution at the implant-bone interface was simulated. Furthermore, the stems were positioned accurately using the RSA markers, that allowed for reproduction of the actual postoperative situation. All this resulted in a good agreement between the FEM and experimental results when correlating deflection of the reconstructions.

The study was limited with respect to the fact that only six reconstructions were analyzed. Furthermore, the reconstructions were subjected to a rather simple loading configuration where muscle forces were excluded. However, these forces are often also absent in the experimental measurements. Another limitation is the presence of holes in the bones, which may have altered the mechanical behaviour of the femur. However, given that same models were used to compare the two methods for micromotions measurement, the presence of holes does not undermine our study. Additionally, care was taken that the measurement points were not in proximity of the holes.

In conclusion, the present study showed that care needs to be taken when interpreting the results of *in vitro* micromotions measurement systems which are based on bony reference points remote from the interface. The measurements may be considerably affected by deformation of the reconstruction and may have little to no correlation with the actual micromotions at the interface. To facilitate accurate measurement of micromotions of cementless implants, the distance between the measurement reference point and the actual interface should be minimized.

## **Acknowledgements**

This study was funded in part by Zimmer, Inc., Warsaw, IN, USA.

## Reference List

- 1 **Pilliar RM, Lee JM, Maniopoulos C.** Observations on the effect of movement on bone ingrowth into porous-surfaced implants. *Clin Orthop Relat Res* 1986;(208):108-13.
- 2 **Engh CA, O'Connor D, Jasty M, McGovern TF, Bobyn JD, Harris WH.** Quantification of implant micromotion, strain shielding, and bone resorption with porous-coated anatomic medullary locking femoral prostheses. *Clin Orthop Relat Res* 1992;(285):13-29.
- 3 **Monti L, Cristofolini L, Viceconti M.** Methods for quantitative analysis of the primary stability in uncemented hip prostheses. *Artif Organs* 1999;23(9):851-9.
- 4 **Baleani M, Cristofolini L, Toni A.** Initial stability of a new hybrid fixation hip stem: experimental measurement of implant-bone micromotion under torsional load in comparison with cemented and cementless stems. *J Biomed Mater Res* 15-6-2000;50(4):605-15.
- 5 **Chareancholvanich K, Bourgeault CA, Schmidt AH, Gustilo RB, Lew WD.** In vitro stability of cemented and cementless femoral stems with compaction. *Clin Orthop Relat Res* 2002;(394):290-302.
- 6 **Viceconti M, Brusi G, Pancanti A, Cristofolini L.** Primary stability of an anatomical cementless hip stem: a statistical analysis. *J Biomech* 2006;39(7):1169-79.
- 7 **Bühler DW, Berlemann U, Lippuner K, Jaeger P, Nolte LP.** Three-dimensional primary stability of cementless femoral stems. *Clin Biomech (Bristol , Avon )* 1997;12(2):75-86.
- 8 **Bühler DW, Oxland TR, Nolte LP.** Design and evaluation of a device for measuring three-dimensional micro-motions of press-fit femoral stem prostheses. *Med Eng Phys* 1997;19(2):187-99.
- 9 **Speirs AD, Slomczykowski MA, Orr TE, Siebenrock K, Nolte LP.** Three-dimensional measurement of cemented femoral stem stability: an in vitro cadaver study. *Clin Biomech (Bristol , Avon )* 2000;15(4):248-55.
- 10 **Westphal FM, Bishop N, Honl M, Hille E, Puschel K, Morlock MM.** Migration and cyclic motion of a new short-stemmed hip prosthesis--a biomechanical in vitro study. *Clin Biomech (Bristol , Avon)* 2006;21(8):834-40.
- 11 **Berzins A, Sumner DR, Andriacchi TP, Galante JO.** Stem curvature and load angle influence the initial relative bone-implant motion of cementless femoral stems. *J Orthop Res* 1993;11(5):758-69.
- 12 **Pancanti A, Bernakiewicz M, Viceconti M.** The primary stability of a cementless stem varies between subjects as much as between activities. *J Biomech* 2003;36(6):777-85.
- 13 **Abdul-Kadir MR, Hansen U, Klabunde R, Lucas D, Amis A.** Finite element modelling of primary hip stem stability: the effect of interference fit. *J Biomech* 2008;41(3):587-94.
- 14 **Pettersen SH, Wik TS, Skallerud B.** Subject specific finite element analysis of implant stability for a cementless femoral stem. *Clin Biomech (Bristol , Avon )* 2009;24(6):480-7.
- 15 **Trabelsi N, Yosibash Z, Milgrom C.** Validation of subject-specific automated p-FE analysis of the proximal femur. *J Biomech* 9-2-2009;42(3):234-41.
- 16 **Reggiani B, Cristofolini L, Varini E, Viceconti M.** Predicting the subject-specific primary stability of cementless implants during pre-operative planning: preliminary validation of subject-specific finite-element models. *J Biomech* 2007;40(11):2552-8.
- 17 **Taddei F, Pancanti A, Viceconti M.** An improved method for the automatic mapping of computed tomography numbers onto finite element models. *Med Eng Phys* 2004;26(1):61-9.
- 18 **Verdonschot N, Barink M, Stolk J, Gardeniers JW, Schreurs BW.** Do unloading periods affect migration characteristics of cemented femoral components? An in vitro evaluation with the Exeter stem. *Acta Orthop Belg* 2002;68(4):348-55.
- 19 **Waanders D, Janssen D, Miller MA, Mann KA, Verdonschot N.** Fatigue creep damage at the cement-bone interface: An experimental and a micro-mechanical finite element study. *J Biomech* 12-8-2009;
- 20 **Keyak JH, Kaneko TS, Tehranzadeh J, Skinner HB.** Predicting proximal femoral strength using structural engineering models. *Clin Orthop Relat Res* 2005;(437):219-28.
- 21 **Keyak JH, Falkinstein Y.** Comparison of in situ and in vitro CT scan-based finite element model predictions of proximal femoral fracture load. *Med Eng Phys* 2003;25(9):781-7.

- 22 **Rancourt D, Shirazi-Adl A, Drouin G, Paiement G.** Friction properties of the interface between porous-surfaced metals and tibial cancellous bone. *J Biomed Mater Res* 1990;24(11):1503-19.
- 23 **Heller MO, Bergmann G, Deuretzbacher G, Durselen L, Pohl M, Claes L, Haas NP, Duda GN.** Musculo-skeletal loading conditions at the hip during walking and stair climbing. *J Biomech* 2001;34(7):883-93.
- 24 **Jasty M, Bragdon C, Burke D, O'Connor D, Lowenstein J, Harris WH.** In vivo skeletal responses to porous-surfaced implants subjected to small induced motions. *J Bone Joint Surg Am* 1997;79(5):707-14.
- 25 **Chong DY, Hansen UN, Amis AA.** Analysis of bone-prosthesis interface micromotion for cementless tibial prosthesis fixation and the influence of loading conditions. *J Biomech* 19-4-2010;43(6):1074-80.





# Chapter

---

# 3

***Improving Peri-Prosthetic  
Bone Adaptations  
around Cementless Hip Stems;  
a Clinical and Finite Element Study***

ten Broeke RH, Tarala M, Arts JJ, Janssen D, Verdonchot N and Geesink RG  
Submitted to Medical Engineering and Physics



## Abstract

*In this study we assessed whether the Symax<sup>TM</sup> implant which is a further optimization of the Omnifit<sup>®</sup> stem would yield improved results in terms of peri-prosthetic bone remodeling in a clinical and a computer Finite Element (FE) simulation study. Relative to the Omnifit<sup>®</sup> the Symax<sup>TM</sup> implant is altered in shape and surface treatment. Proximally the implant has a BONIT<sup>®</sup>-HA coating which should stimulate bone ingrowth; distally the surface is treated to prevent bone ingrowth and reduce distal load-transfer.*

*In a randomized clinical trial, 2 year DEXA measurements between the uncemented Symax<sup>TM</sup> and Omnifit<sup>®</sup> stem (n=25 for each group) showed bone mineral density (BMD) loss in Gruen zone 7 of 14% and 20%, respectively ( $p < 0.05$ ). The FE models predicted a 26% bone loss in Gruen zone 7 for the Omnifit<sup>®</sup>. In contrast to the clinical study, a similar amount of bone loss (28%) was found around the Symax<sup>TM</sup>. When the distal treatment to the Symax<sup>TM</sup> was ignored in the model, a bone loss of 35% was predicted, supporting the benefit of this surface treatment to improve proximal bone maintenance.*

*The theoretical concept for improved proximal bone loading by the Symax<sup>TM</sup> was supported by the DEXA-results, but was not reproduced by FE-remodeling. This was probably caused by insufficient knowledge about the biological and subsequent mechanical effects of the new coating and surface treatment. These aspects should be investigated to a more detailed level before FE models can be used reliably to predict biological aspects of these types of coating changes to the peri-prosthetic bone remodeling process.*

## Introduction

Successful biologic fixation of uncemented total hip prostheses is inevitably associated with resorptive bone remodeling, because of load sharing and stress protection of bone by the implant. This has been a concern in the early generations of stems where proximal femoral bone loss up to 62 % was detected, both experimentally as well as clinically <sup>1-3</sup>. Theoretically this bone resorption, secondary to femoral stress shielding, may in the long term compromise implant support, and cause debonding, implant subsidence and periprosthetic bone fracture. Therefore in the development of new designs for total hip arthroplasty, a need is felt for diagnostic tools that can discriminate between superior and inferior implants. Such tools should be able to predict unacceptable clinical outcome like excessive bone loss, high risk of loosening and revision, in an early postoperative or even preoperative stage.

For this purpose Finite Element Analysis (FEA) has often been used to estimate loads and stresses in periprosthetic bone and interfaces <sup>4-6</sup>. Through the process of Numerical Shape Optimization (NSO) the optimal geometry and material of an implant were calculated, based on predefined goals in terms of maximally acceptable strains and stresses in the bone and interfaces <sup>7</sup>. With growing knowledge on failure scenarios of hip implants, computer simulation of processes like interface debonding could be performed <sup>8</sup>, and predictions for aseptic loosening were formulated of particular designs under specific loading conditions <sup>9</sup>.

The major limitations of these FE techniques is that it remains a computer model that predefines several assumptions on implant material properties, bone properties <sup>10</sup>, implant-bone interface conditions (bonded or debonded circumstances, surface percentage of osseointegration), and loading-boundary conditions (interface loading forces during daily activities, hip contact-forces and muscle forces) <sup>11,12</sup>. Furthermore, reconstructions differ from patient to patient and not all failure mechanisms can be simulated with required detail. It is obvious that because of all these assumptions and limitations, the extent to which FE-models can realistically simulate failure mechanisms, is uncertain. This explains the discrepancy between clinical results of (failed) hip reconstructions and FE calculations, and therefore these retrospective studies can only partially validate the technique <sup>10</sup>.

Despite these limitations, it is generally assumed that FEA can adequately predict bone remodeling around implants as these FEA are suitable to address the relationship between mechanical stimuli and bone remodeling, as illustrated by the strain adaptive bone remodeling theory <sup>13</sup>. Bone remodeling is often expressed as the postoperative change in periprosthetic bone mineral density (BMD) as measured by dual energy x-ray absorptiometry (DEXA). In recent years several studies have been performed to retrospectively correlate 2-D and 3-D FEA predictions with the effects on bone density <sup>14-16</sup>. Attempts were focused on finding a quantitative relationship between absolute values of

stress in the bone at implantation, and subsequent remodeling changes in terms of BMD-values. By analyzing bone remodeling around a known implant one can propose changes to its design in order to improve the load transfer between implant and bone and reduce bone resorption. These changes can concern implant's shape, material composition or implant-bone interface properties.

As an example the Symax<sup>TM</sup> stem has been developed from the Omnifit<sup>®</sup> design in order to improve the press fit characteristics of the proximal stem geometry. At the same time a more bioactive biomimetic BONIT<sup>®</sup>-HA coating, applied to the proximal part of the stem, should result in faster, deeper and more extensive bone-implant contact, as could be confirmed from a human retrieval study <sup>17</sup>, and from experimental studies in animals <sup>18,19</sup>. In earlier studies it has been shown that osteoconductive coatings like hydroxyapatite may be used to promote proximal stress transfer, diminishing effects of stress shielding <sup>1,20,21</sup>. Furthermore the Dotize<sup>®</sup> treatment on the distal part of the stem was used to prevent bone apposition in that area, and guarantee selective loading of the proximal femur <sup>17</sup>.

In this study we hypothesized that by application of the combined change in shape and surface treatment the Symax<sup>TM</sup> stem will better preserve periprosthetic bone stock than the Omnifit<sup>®</sup>. This hypothesis was tested in a prospective RCT comparing the Symax<sup>TM</sup> with the Omnifit<sup>®</sup> and it was assessed whether the result of the clinical trial could have been predicted by FE simulations.

## Material and Methods

### Implants

The Omnifit<sup>®</sup> HA stem (Stryker<sup>®</sup>, Mahwah, New Jersey, USA) is forged from Ti6Al4V alloy, has a macrotextured surface and a plasmaspray HA-coating on the proximal 40 % of the stem (Fig. 1). The HA coating has a thickness of 50 µm (45 to 65) with a porosity of < 3 %. The HA after spraying has a relatively high crystalline phase of 65 %, explaining the slow resorbability. Until now the implant is one of the most successful and best documented uncemented HA-coated stems <sup>22-24</sup>.

The uncemented Symax<sup>TM</sup> hip stem (Stryker<sup>®</sup> EMEA, Montreux, Switzerland) was based on shape optimization of the Omnifit<sup>®</sup> stem. Preclinical design studies consisted of CT-investigations combined with finite element analyses to optimize fit and fill with even stress distribution without peak stresses in the bone and at the interface. The Symax<sup>TM</sup> stem is made of the same alloy as the Omnifit<sup>®</sup>. It features a proximal plasma-sprayed CP Titanium coating with an open porosity of 20-40 % to enhance initial stem fixation, and a biomimetic electrochemically deposited BONIT<sup>®</sup> HA coating with a high porosity of 60 %, and 10-20 µm thick (proprietary to DOT GmbH, Rostock, Germany) (Fig. 2). The crystalline structure of the

coating is - contrary to plasma sprayed coatings – not monolithic, but fine crystalline, and the CaP crystallites are fixed to the implant surface in the shape of platelets or pins nearly in vertical alignment <sup>19</sup>. The adhesion strength of both HA-coatings is comparable and about 65 MPa.

Distally the Symax<sup>TM</sup> stem is treated with the Dotize<sup>®</sup> surface process, an electrolytic conversion of titanium surfaces in which the thin native oxide film is replaced by a thicker oxidised surface layer that reduces protein adsorption and consequently distal bone apposition and osseointegration <sup>25</sup>.



*Fig. 1 The HA Omnifit<sup>®</sup> hip stem, geometrically a straight double wedge design, is made of Ti-alloy, has a macro-textured surface of which the proximal 40 % is plasma sprayed HA-coated, and has a distal matte finish, all aimed at proximal fixation. The HA-coating is highly crystalline (65%) explaining slow resorbability.*



*Fig. 2 Illustrations of the Symax<sup>TM</sup> stem in AP (left) and lateral (right) view, showing a straight stem with the neck in an anteverted position. It features a proximal plasma-sprayed CP Titanium layer, with a biomimetic electrochemically deposited BONIT<sup>®</sup> HA coating of very high porosity of 60 %, and only 10-20 µm thick. Distally the stem is treated with the Dotize<sup>®</sup> surface process, which reduces distal bone apposition and osseointegration.*

## **Clinical Trial Study**

### **Design and Patient selection**

A prospective, individually randomized, two group, parallel comparative trial was performed between the uncemented Symax™ (n=25) and the Omnifit®-HA stems (n=25). The diagnosis and indication for total hip arthroplasty (THA) was in all cases osteoarthritis (OA) of the hip. Exclusion criteria were a history of hormonal therapy, any medication or illness known to affect bone metabolism, and a Quetelet index (BMI) higher than 35. After signing the appropriate informed consent forms, patients were allocated at random to one of either group in a 1:1 randomization ratio for either the Symax™ or the Omnifit® stem. The allocation sequence was generated by an independent trial bureau and concealed from the operating surgeon. Participants were enrolled from sequentially numbered, identical, opaque, sealed envelopes just before the operation, being unaware of the content and sequence of the envelopes (allocation concealment). Both groups were comparable in terms of patient demographics (see Table 1). The study was approved by the local Medical Ethics Committee prior to the start of the study (registration nr.: 02-072), and was carried out in line with the Seoul amendment (2008) of the Helsinki declaration.

### **Surgical protocol and Postoperative management**

All operations were performed randomly by the same 2 staff surgeons (R.t.B. or R.G.) according to completely identical and standardized orthopaedic procedures using the postero-lateral approach. Patients were treated with 24 hours intravenous antibiotic prophylaxis (Augmentin®), DVT prophylaxis with a small molecular heparin (Fraxiparin®) during 6 weeks and prophylaxis against heterotopic ossifications with an NSAID (Indocid®) for 14 days. Patients were allowed to full weightbearing from day 1.

### **DEXA protocol**

In the first postoperative week the baseline BMD measurement was performed with the fan-beam Hologic QDR 4500A densitometer (Hologic Inc., Waltham, MA, USA) according to the protocol, including exact positioning of the leg with stabilizing rotation using standard knee and foot support devices. Quality control of the densitometer was executed through daily automatic self-calibration, not showing any significant drift during the study period. Considering a difference in length of HA-coating between the stem-designs, the periprosthetic regions of interest (ROI) were placed around the stem according to adapted Gruen zones in such a way that ROI 1 and 7 covered comparable bone areas, and ROIs 2 to 6 were equally divided around the rest of the stem (Fig. 3). The overall BMD was summarized in a net average value <sup>26</sup>. DEXA scans were taken from the

AP-lumbar spine in the first postoperative week as well, serving as a baseline measurement for comparison to referenced normals. This was repeated at 24 months follow-up to monitor any systemic changes in bone, not related to the effect of the THA. All DEXA-scans were done by the same independent analyst.

Follow up evaluations were performed at 6 weeks, 3 months, 6 months, 1 year and 2 years, and analysis of all raw scans was independently done by one member of the research staff (R.H.) without involvement of the operating surgeon.

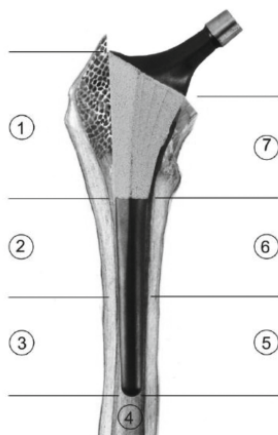


*Fig. 3 Drawing showing delineation of Gruen zones 1 to 7 in the AP view around the Symax™ stem.*

### Statistics of the clinical trial

Longitudinal BMD results (in g/cm<sup>2</sup>) per Gruen zone and as a net average are expressed as relative values with the immediate postoperative DEXA measurement of the operated femur being the reference value, set at 100 %. Absolute and relative BMD values are described by mean and standard deviation, demographic parameters by mean and range. Since no deviations from normal distribution could be observed, comparing the Symax™ and Omnifit® group in any of the ROIs, the one-sample t-test in cases of paired data (comparisons within a group) and the two-sample t-test in cases of unpaired data (comparisons between groups) was used.

The statistically required sample size is based on a power-analysis performed on the minimally to detect mean difference of BMD-results between stem designs ( $\delta$ ). Based on earlier studies we assumed this difference to be 25 %. By convention, an  $\alpha$ -error rate of 0.05 was adopted, and the  $\beta$ -error was set at 0.20 (power  $1 - \beta = 80\%$ ). We were planning a study of a continuous response variable from independent control and experimental subjects with 1 control(s) per experimental subject. In a previous study the response

within each subject group was normally distributed with standard deviation 25 %. If the true difference in the experimental and control means was 20 %, we would need to study 25 subjects in the Symax™ arm and 25 subjects in the Omnifit® arm to be able to reject the null hypothesis that the population means of these groups were equal with probability (power) 0.8. The type I error probability associated with the test of this null hypothesis was 0.05.

Microsoft Office Excel 2003 (Microsoft Corporation, Redmond, Washington, USA) and SPSS software 15.0 for Windows (SPSS Inc., Chicago, Illinois, USA) was used for data analysis.

## **Finite Element Bone Remodeling Study**

### **Finite element model**

We created an FEM model of a bone from CT data of a human femur (81 year-old male, left femur). The bone was CT scanned along with a calibration phantom (solid, 0, 50, 100, 200 mg/ml calcium hydroxyapatite, Image Analysis, Columbia, KY, USA). The data was processed using a medical imaging software package (MIMICS 11.0). Subsequently, we created two uncemented THA reconstructions implanted with the Omnifit® and the Symax™ stem. The stems were positioned in the virtual bone by an experienced surgeon (R.t.B.), using in-house software (DCMTK MFC 10.8), which allows manipulation of a solid (stem) model within the visualized CT-data of the femur<sup>27</sup>. The models of the reconstructions were solid meshed using an FEA preprocessor (Mentat 2007r1, MSC Software), and they consisted of ~97.000 and ~18.000 linear four-noded tetrahedral elements for the bones and stems, respectively. The isotropic properties of cortical and trabecular bone were derived from the calibrated CT data. The calibration phantom was used to convert Hounsfield Units (HU) to calcium equivalent densities ( $\rho\text{CHA}$ ). An in-house software package was used to assign a calcium equivalent density ( $\rho\text{CHA}$ ) to each element, based on the average  $\rho\text{CHA}$  value of all pixels in the element volume. The ash density was computed using relationships specific to the type of phantom used ( $\rho_{\text{ash}} = 0.0633 + 0.887 \rho\text{CHA}$ ). The elastic modulus ( $E$ , MPa) was computed for each element from ash density ( $\rho_{\text{ash}}$ ) using correlations for trabecular and cortical bone<sup>28</sup>. The elastic modulus of the stems was set to 105 GPa. The Poisson's ratio for the bone and implant was set to 0.3. The reconstructions were fixed distally and subjected to an alternating loading history of normal walking and stair climbing (Fig. 4)<sup>29</sup>.

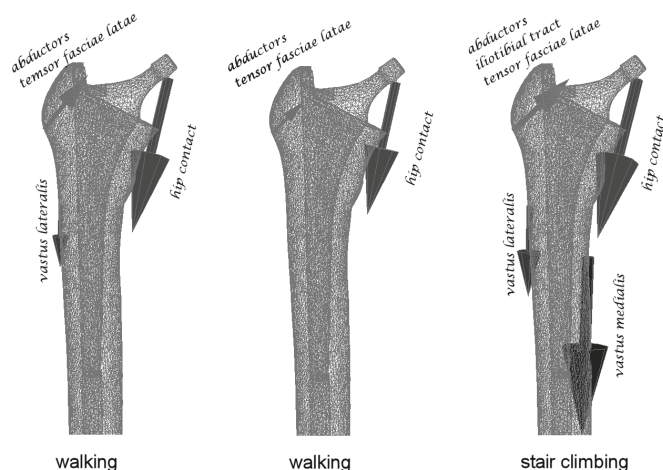


Fig. 4 The reconstruction was subjected to the loading condition of normal walking and stair climbing.

### Bone remodeling and DEXA simulation

We used the strain adaptive remodeling theory to simulate changes in bone mineral density in time ( $dp/dt$ )<sup>30</sup>. The size of 'dead zone' and computer time unit were determined in our previous remodeling study in which we utilized the same bone model as here<sup>45</sup>. In that study the FE remodeling prediction around the EPOCH FullCoat stem was fitted to 2 year clinical DEXA data in order to define the adequate 'dead zone' and to determine the time unit in the simulation<sup>31</sup>. The best fit was obtained for dead zone value 0.35 and time unit 60 (meaning that 60 computer time units correspond to 2 year clinical reality). A further description of the remodeling theory used is given in our previous remodeling study<sup>27</sup>. These previously determined values of 'dead zone' and time unit were used here when performing the remodeling prediction in the reconstructions with the Omnifit® and Symax™ stems. To allow for clinically relevant interpretation of the remodeling results, we used an in-house software package (DCMTK MFC 10.8) to project the FE results of bone remodeling onto 2D virtual DEXA images. In short, this in-house algorithm maps a 3D voxel mesh onto the FE reconstruction. Each pixel in 2D DEXA image has a calcium equivalent value corresponding to the summation of the calcium equivalent values of 3D voxels along the chosen DEXA scan axis. Detailed description of the in-house algorithm used here is also given in our previous study<sup>27</sup>.

We defined the seven Gruen zones according with the guidelines<sup>32</sup>, adapted for uncemented stems with proximal coating, and computed bone density (BMD) (g/cm<sup>2</sup>) and local bone mineral content (BMC) (g) at one and two years postoperatively for each implant composition. The bone loss predicted by our simulations was defined as a percentage of the pre-operative bone mass.



## Cases Analyzed

The design changes of Symax™ relative to the Omnifit® stem concerned three aspects: the shape, proximal coating and treatment of distal stem with Dotize® surface process. Two of these changes were modeled in our FE study. The differences between proximal coatings of both stems were not simulated as both stems were assumed to be bonded to the bone at the coated locations. The difference in shape between both stems was modeled based on data provided by the manufacturers. The radiography findings in the reconstruction with Symax™ reveal reactive lines around the anodized surface of the stem (Fig. 5). However, the actual effect of the distal surface treatment of the Symax™ stem would be difficult to predict pre-clinically. Therefore, we simulated two extreme cases for the Symax™ stem (with a gap of 0.5mm around the distal part of the stem and without a gap assuming a frictional contact ( $\mu=0.3$ ) between implant and bone distally). While, in the reconstruction with Omnifit® stem the distal implant-bone interface was modeled by assuming a frictional contact ( $\mu=0.3$ ) between implant and bone<sup>33</sup>. Hence, we simulated one case for the Omnifit® stem and two cases for the Symax™ stem (either with or without a distal gap).

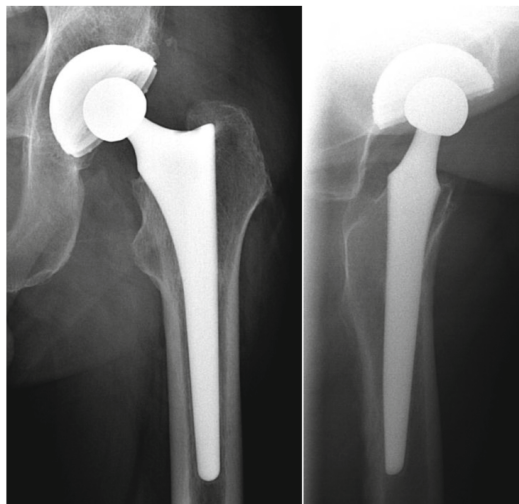


*Fig. 5 X-rays showing reactive lines in Gruen zone 2 up to and including zone 6 (AP view, left), and zone 9 up to and including zone 13 (lateral view, right) around a Symax™ stem. This is a sign of absence of bone attachment in the distal anodized part of the stem.*

## Results

### Clinical DEXA results

There was no statistical difference in the demographic details and initial bone quality between patients in either group, confirming that preoperative conditions between the two

groups were comparable (Table 1). There was one patient (Omnifit®) withdrawn from the study because of protocol violation, no further patients were lost to follow-up. There was no difference in physical activity among patients postoperatively, as assessed with the activity score from the Harris Hip Score.

All patients had all their scans performed during the entire follow-up and within the pre-defined timeframe. At one year follow-up all stems showed radiological evidence of stable bone ingrowth according to the classification of Engh<sup>34</sup>. At one and two years the lumbar spine BMD did not show significant difference between the implant groups, nor between  $t_0$  and  $t_2$  years values. This illustrates that differences in bone remodeling could not be explained by metabolic bone disease in one or either group, nor by activity or age-related differences in bone density between the groups.

Evolution of BMD in both implant groups is shown in Table 2 and represented graphically in Fig. 6. A decrease in BMD was detected with both stems in all Gruen zones except zone 4, at 3 months after surgery, varying between -1.9 % and -9.5 % for the Symax™ prosthesis and between -1.0 % and -13.0 % for the Omnifit® prosthesis. Starting between 3 and 6 months postoperatively, complete recovery of bone loss was initiated in zones 2, 3, 5 and 6. The same pattern was seen for the 'net average'. In zone 1 and, particularly zone 7, however, there was additional bone loss that seemed to stabilize between 1 and 2 years follow-up. The maximal loss in zone 7 for the Omnifit® is -20.3 %, and for the Symax™ -14 %. Only in zone 7 the difference in bone loss between the two stem designs was statistically significant during the entire follow-up, starting from 6 weeks and in favor of the Symax™ stem, with a p-values of 0.05 (at 1 year) and even 0.01 (at 2 years). In all other zones (1 – 6) there was no statistically significant difference in remodeling, although BMD values were consequently higher in the Symax™ group.

*Table 1 Patient characteristics and baseline demographic data*

	Omnifit®	Symax™
Mean age at operation in years (range)	60.4 (39-71)	60.2 (46-72)
Weight in kg (range)	78.5 (60-96)	82.2 (54-105)
Body Mass Index (range)	27.2 (22-32)	27.8 (22-37)
Male/Female	15/9	12/13
Normal start BMD	16	17
Osteopenic/osteoporotic start BMD	7/1	7/1

*Table 2 Periprosthetic BMD around Omnifit® (n=24) and Symax™ (n=25) stem during 2 year prospective follow-up; presenting absolute values per ROI, with standard deviation, and expressed as percentage of direct postoperative value (= baseline reference). 'Average' representing the average of the net sum of all ROIs.*

BMD	post-op	6 wks	3mnth	6mnths	1yr	2yrs
<b>Omnifit®</b>						
ROI 1	0.887 ± 0.167	0.860 ± 0.159	0.827 ± 0.170	0.804 ± 0.171	0.786 ± 0.172	0.7481 ± 0.187
	100%	97.20%	93.30%	90.60%	88.90%	87.80%
ROI 2	1.673 ± 0.278	1.639 ± 0.262	1.602 ± 0.273	1.610 ± 0.283	1.604 ± 0.281	1.608 ± 0.267
	100%	98.20%	95.90%	96.30%	96.00%	96.30%
ROI 3	1.697 ± 0.180	1.663 ± 0.218	1.622 ± 0.215	1.646 ± 0.191	1.677 ± 0.187	1.693 ± 0.205
	100%	97.90%	95.50%	97.00%	98.90%	99.70%
ROI 4	1.779 ± 0.218	1.775 ± 0.210	1.754 ± 0.224	1.742 ± 0.215	1.777 ± 0.250	1.780 ± 0.237
	100%	99.90%	98.60%	98.00%	99.80%	100%
ROI 5	1.718 ± 0.254	1.725 ± 0.264	1.702 ± 0.271	1.673 ± 0.394	1.767 ± 0.286	1.760 ± 0.231
	100%	100.40%	99.00%	96.50%	102.80%	102.80%
ROI 6	1.605 ± 0.267	1.599 ± 0.276	1.572 ± 0.287	1.591 ± 0.299	1.612 ± 0.311	1.637 ± 0.299
	100%	99.70%	97.80%	99.00%	100.20%	102.10%
ROI 7	1.165 ± 0.234	1.083 ± 0.204	1.011 ± 0.207	0.973 ± 0.200	0.926 ± 0.197	0.929 ± 0.223
	100%	93.20%	87.00%	83.80%	79.70%	79.90%
average	1.503 ± 0.187	1.473 ± 0.193	1.442 ± 0.195	1.434 ± 0.202	1.450 ± 0.199	1.456 ± 0.192
	100%	98.00%	95.80%	95.30%	96.40%	96.80%
<b>Symax™</b>						
ROI 1	0.965 ± 0.174	0.946 ± 0.177	0.916 ± 0.187	0.895 ± 0.181	0.873 ± 0.187	0.866 ± 0.191
	100%	97.90%	94.60%	92.60%	90.20%	89.60%
ROI 2	1.742 ± 0.291	1.711 ± 0.312	1.670 ± 0.303	1.655 ± 0.290	1.675 ± 0.294	1.681 ± 0.298
	100%	98.10%	95.90%	95.20%	96.30%	96.60%
ROI 3	1.760 ± 0.207	1.702 ± 0.208	1.698 ± 0.205	1.695 ± 0.225	1.732 ± 0.196	1.734 ± 0.193
	100%	96.80%	96.60%	96.50%	98.60%	98.70%
ROI 4	1.852 ± 0.225	1.824 ± 0.213	1.818 ± 0.226	1.844 ± 0.213	1.868 ± 0.211	1.893 ± 0.212
	100%	98.50%	98.10%	99.70%	101.00%	102.40%
ROI 5	1.770 ± 0.223	1.737 ± 0.222	1.725 ± 0.226	1.759 ± 0.233	1.796 ± 0.237	1.829 ± 0.238
	100%	98.20%	97.50%	99.40%	101.50%	103.40%
ROI 6	1.659 ± 0.177	1.635 ± 0.198	1.621 ± 0.201	1.642 ± 0.200	1.672 ± 0.215	1.713 ± 0.202
	100%	98.50%	97.60%	99.00%	100.70%	103.30%
ROI 7	1.292 ± 0.200	1.224 ± 0.179	1.167 ± 0.186	1.127 ± 0.211	1.121 ± 0.218	1.112 ± 0.223
	100%	95.10%	90.50%	87.30%	86.70%	86.00%
average	1.577 ± 0.169	1.540 ± 0.171	1.516 ± 0.175	1.522 ± 0.165	1.534 ± 0.180	1.553 ± 0.170
	100%	97.60%	96.10%	96.50%	97.20%	98.50%

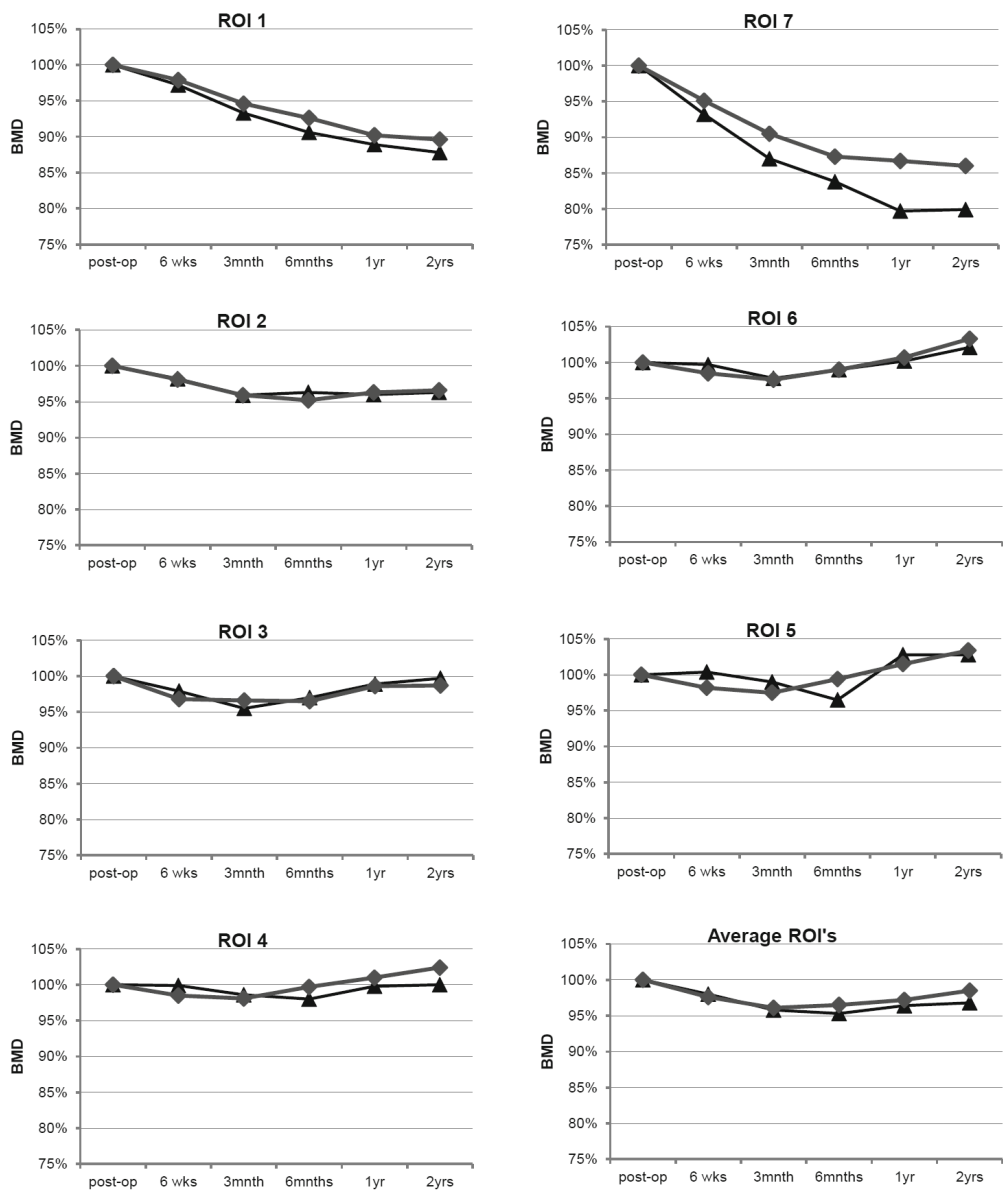


Fig. 6 Graphs showing BMD course of the ROIs 1 to 7 and net average in a longitudinal study for 2 years, comparing the Symax™ (◆) and the Omnifit® (▲) stem, with the immediate post-operative BMD set at 100 % (= baseline reference).

## Remodeling prediction versus clinical findings

There were considerable differences in predicted bone loss between the Symax™ reconstructions with and without a distal gap (Fig. 7). In the reconstruction without a distal gap bone resorption was considerably greater especially in Gruen zone 6 and 7. Bone loss at 2 years postoperatively was 35% in the Gruen zone 7 for the Symax™ reconstruction without a gap and 28% in the reconstruction with a distal gap. FE remodeling prediction for the Symax™ reconstruction with a gap was better correlated with clinical findings than the prediction for the Symax™ reconstruction without a distal gap. Thus, the Symax™ reconstruction with a distal gap was more suitable for FE remodeling prediction, especially as the clinical findings confirmed no direct contact between implant and bone distally for the Symax™ reconstructions.

There were differences in FE-predicted bone loss between the Omnifit® stem and the Symax™ stem. In Gruen zone 7 slightly greater bone loss at 2 years was predicted for the reconstruction with the Symax™ stem with a distal gap (-28% for Symax™ versus -26% for the Omnifit® stem, see Fig. 7). However, in zones 1 to 6 the Symax™ stem was expected to cause less bone resorption than the Omnifit® stem.

This FE predicted pattern of bone remodeling matched the clinical findings only partially. Although greatest bone loss for both stems was obviously correctly predicted in the proximal zones (1 and 7), the correlation between clinical data and FE predictions was rather poor for the Symax™ in zone 7, and for the Omnifit® in zone 6 (both at 2 years). In the important Gruen zone 7 DEXA-measured bone loss at 2 years was significantly smaller for the Symax™ (-14% versus -20.3% for the Omnifit®,  $p=0.01$ ), while FE simulations had predicted a slightly larger bone loss (-28 % for the Symax™ versus -26% for the Omnifit®). So the FE remodeling predictions did not concur with the clinical findings.

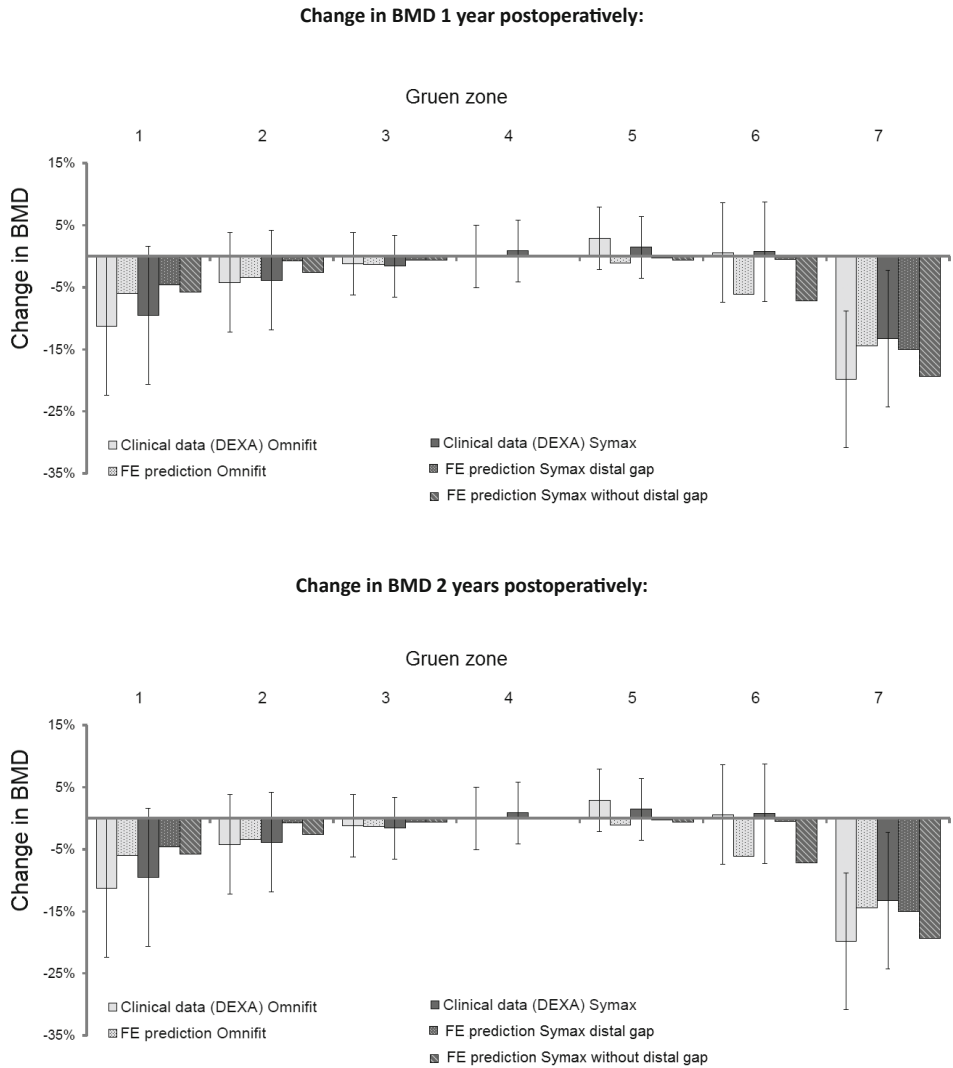


*Fig. 7 Clinical DEXA data per Gruen zone (with standard deviation) around the Omnifit® and Symax™ stem at 1 year (top) and 2 years (bottom) postoperatively, combined with the FEM predictions on remodeling. For the Symax™ predictions are given with a simulated gap around the distal stem (in other words no friction at the interface) and without a distal gap (friction at the interface).*

## Discussion

In the clinical part of this study it was tested if the design improvements implemented in the Symax™ stem will result in less bone resorption (DEXA) when compared to the Omnifit® stem. Namely, we hypothesized that the Symax™ stem will preserve bone stock better in proximal Gruen zones thanks to the design changes that optimize stresses in the periprosthetic bone and interface. Secondly, we investigated if a FE remodeling prediction will yield similar results as seen clinically for both stems.

Considering the DEXA-findings of successive generations of uncemented stems with bone loss varying between 15 and 70 %, we find the results of the Symax™ stem promising, with regard to preservation of bone quantity. There is only a modest maximal bone loss (calcar area 14 %, greater trochanter 10.4 %), which is a normal representation of proximal osseointegration, but it illustrates improved metaphyseal bone loading compared to several other designs. More distally there is hardly any BMD loss at all indicating excellent preservation of bone in the regions where no osseointegration is intended. It can therefore be confirmed that the geometry of the Symax™ stem, based on the proximal „fit and fill“ principle, in combination with the proximal BONIT®-HA coating and the distal Dotize® surface treatment, are able to improve stress transfer from the implant to bone in the important zone 7. DEXA results for the Omnifit® in our clinical trial were similar with earlier assessment performed by Sluimer et al. (16% and 20% at 2 years for zone 1 and 7 respectively, versus 13% and 20% in the present study)<sup>35</sup>. This confirms reliability and validity of our clinical DEXA data.

Taking into account the excellent long term clinical results and survival scores of the Omnifit®<sup>24,36</sup>, our study suggests that the Symax™ will perform well at mid- and longer term, with improved preservation of periprosthetic bone. This seems to be supported in a consecutive cohort of the first 1000 Symax™ stems implanted in 3 hospitals in the Netherlands, and an international multicentre trial, both showing no aseptic loosening after 5 years follow-up (personal communication).

In contrast to the clinical findings, the FE simulation predicted greater bone loss in Gruen zone 7 for the Symax™ stem. Furthermore, in the other Gruen zones FE simulation predicted greater bone loss for the Omnifit® stem when compared to the Symax™ stem (reconstruction with a distal gap), while clinically no considerable differences were found. Even though the FE remodeling prediction did not yield the same results in individual Gruen zones as the clinical DEXA study, the effect of design improvement in the Symax™ stem can be seen in the reduction of bone loss around this stem in the reconstruction with a distal gap.

In the present study we showed that the FE remodeling simulation is within certain limits capable of capturing the differences in bone remodeling between two THA reconstructions with different stems. There are a few factors that exclude the possibility of an exact match between the clinical finding and our FE predictions. Firstly, there are differ-

ences in bone quality and loading condition between the group of patients and the model. Secondly, we simulated remodeling around only one bone model (of a 81 year-old male) implanted with one implant size, while the clinical results were averaged over data of 25 patients (all younger) with variable bone quality and implant size. Thirdly, the loading condition in our simulation was not changed between the pre and postoperative situation. In reality after the post-surgery rehabilitation period patients become more active, which may reduce the resorption rates around both stems. Furthermore, there are more variables that influence DEXA changes than exclusively those incorporated in the strain adaptive bone remodeling concept. The surgical trauma of the reaming and implantation causes a catabolic reaction as a result of the inflammatory changes and degradation of bone<sup>37,38</sup>. This has to be repaired and neutralized before the (bio)mechanically induced bone apposition and resorption can exclusively be held responsible for further DEXA changes. Furthermore the recovery of the bone from pain-induced disuse atrophy will take time. The use of the 'cane for comfort' will not really influence functional scores, but does cause relative unloading of the bone<sup>39</sup>, while it is not taken into account in the FE- model. Therefore during the first three to six months there are more disturbing factors than exclusively biomechanical ones, that determine DEXA results. This may explain why the match between FE predictions and DEXA results is not high during the first postoperative year. However, at two years the remodeling balance between apposition and resorption is restored and considered to be mainly mechanically determined. At that moment correlation between predicted and real bone density should be higher.

Another limitation of the FE remodeling simulation is the fact that it neglects the dynamic process of osseointegration. Huiskes recognized that the degree of stress shielding is indeed affected by the bonding conditions of the implant-bone interface<sup>40</sup>. Therefore knowledge about the pattern and extent of osseointegration of a new uncemented implant, from retrieval analysis and histomorphometry, is paramount for generating realistic FE-remodeling predictions. As bone remodeling is a longer-term process (in the order of a few years), it is common in FE bone remodeling simulations to assume that coated areas can be considered as bonded<sup>14,41,42</sup>. Hence, in this study we also assumed that the surface area with the proximal coating was fully bonded in both stem cases. However, from retrieval studies this ideal situation has been shown not to be realistic. Porous coated prostheses usually show a bone-implant contact (BIC) of less than 20%<sup>43,44</sup>. BIC of HA-coated stems varies between 20% and 78% depending on the design<sup>23,43-45</sup>. Furthermore osseointegration is not a static but dynamic process in time and will depend on implant geometry, stem stiffness, surface treatment, type of coating and their degradation characteristics. The retrieval study of the Symax<sup>TM</sup> hip stem illustrated a progressive direct bone-implant contact in time increasing from 26.5 % (at 3 weeks) to 83.5 % (at 13 months)<sup>17</sup>, which was different from that of the Omnifit<sup>®</sup><sup>23</sup>. This progressive bonding and osseointegration will have an effect on the amount of migration and load transfer from implant to bone, and on the resultant remodeling process, but this is typically not incorporated in finite element models. Further-



more it was found that normal contact stiffness and the friction coefficient increase several times as bone grows into the rough surface of the implant and mineralises, thus providing a changing interface with improving secondary stability <sup>46</sup>. In other words, the assumption of a bonded interface at coated areas is over-simplified and probably should incorporate a time-dependent change of stem-bone bonding <sup>47</sup>. As phenomena like degradation, Ca-ion release and subsequent bone turnover are not fully quantified, it is virtually impossible to model these aspects in a valid manner.

Compared to the Omnifit<sup>®</sup>, the Symax<sup>™</sup> is distinctly different in two ways; the geometry and the surface- and coating characteristics. Literature has shown that the effects of geometry and material changes can be simulated reliably with the FE-technique. Amongst the many features held responsible for stress shielding, the mismatch in elasticity modulus between hip stems and bone is considered most important in causing stress mediated disuse atrophy of bone. Therefore focus has been on creating more flexible stems like the Epoch<sup>®</sup> and the Alloclassic<sup>®</sup> (both Zimmer, Warsaw, Indiana, USA) <sup>48</sup>. The metaphyseal fit-and-fill design of the Symax<sup>™</sup>, showing larger cross-sectional dimensions, and therefore being stiffer, was expected to cause more stress-shielding <sup>30,49</sup>. However this stem proves to preserve periprosthetic bone at least as good as flexible stems <sup>50,51</sup>, and better than almost all proximally and entirely porous or HA coated stems <sup>2,3,35,52</sup>. This illustrates that interactions between various determinants of stress shielding and resulting bone remodeling are still not completely understood and hard to capture in an exclusively mechanical model. The same applies for the effect of the distal Dotize<sup>®</sup> treatment. The effects of new coatings on interface properties appear to be even more difficult to predict. To improve predictions, simultaneous ingrowth simulation and remodeling simulation should be performed. This would require quantification of the mechano-biological aspects of coatings after which this can be implemented in FE simulations. Subsequently, these studies need to be validated with results of retrievals and measurements of qualitative and quantitative bone changes. Various scenarios can then be simulated, and it can be tested how sensitive the FE-models are for changes in bonding conditions and for the dynamics of the osseointegration-process in time.

Several attempts have been conducted to simulate and predict adaptive periprosthetic bone remodeling in computer models that combine bone remodeling theories with finite element analysis. Validation of these FE-simulations were mostly based on animal experiments <sup>53,54</sup>, post mortem retrieval studies <sup>14</sup>, and retrospective clinical densitometry studies with DEXA <sup>16</sup> or 3D-volumetric CT-analysis <sup>55</sup>. Although correlation between predicted density changes and clinical data was mostly low, it was nevertheless concluded that bone remodeling after THA could entirely be explained by a mechanical model <sup>14,42</sup>. In another study high correlation could be explained by retrospective fitting of the model on DEXA results available from earlier studies <sup>15,16,53</sup>.

This implies that preclinical FE predictions in new designs triggering unquantified biological processes may be hazardous, because it remains difficult (as in our study) to an-

ticipate on how biological tissues (like bone) will react on, for example, new implant properties (surface treatment, coating morphology, release of Ca-ions). In a recent review it was recognized that in models incorporating biological processes, the number of model parameters that have to be identified and translated into measurable physical or physiological quantities is high. Furthermore these parameters may show considerable variation between subjects of the research population. Therefore several levels of quantification and validation are required to improve the accuracy with which the model can predict physical phenomena <sup>56</sup>.

We conclude that, based on the clinical DEXA results, the theoretical concept for improved proximal bone loading of the femur by the Symax™ stem is correct. However, likely due to only partial modeling of differences between the implant-bone interface conditions in both reconstructions, the FE model could not confirm the hypothesis and support the clinical findings. Our FE simulation showed that the effect of distal stem treatment preventing bone ingrowth appears to have a positive effect on proximal bone maintenance. Further quantitative data about biological phenomena are required to feed the FE-models in order to advance from case-specific simulations to reliable preclinical predictions of bone remodeling (or even implant survival) of new designs in averaged patient populations, particularly if multiple biological aspects are changed in a prosthetic design. Only then recommendations for multifaceted design changes of implants can be reliable.

## Acknowledgements

We would like to acknowledge Liesbeth Jutten for her contribution to the study, data management and statistical assistance, Marc van Rijsbergen for his contribution to the FE part of the study, and Roel Hendrickx for analysis of the DEXA scans.

## Reference List

- 1 **Bobyn JD, Mortimer ES, Glassman AH, Engh CA, Miller JE, Brooks CE.** Producing and avoiding stress shielding. Laboratory and clinical observations of noncemented total hip arthroplasty. *Clin Orthop Relat Res* 1992;(274):79-96.
- 2 **Engh CA, McGovern TF, Bobyn JD, Harris WH.** A quantitative evaluation of periprosthetic bone-remodeling after cementless total hip arthroplasty. *J Bone Joint Surg Am* 1992;74(7):1009-20.
- 3 **Kilgus DJ, Shimaoka EE, Tipton JS, Eberle RW.** Dual-energy X-ray absorptiometry measurement of bone mineral density around porous-coated cementless femoral implants. Methods and preliminary results. *J Bone Joint Surg Br* 1993;75(2):279-87.
- 4 **Huiskes R, Chao EY.** A survey of finite element analysis in orthopedic biomechanics: the first decade. *J Biomech* 1983;16(6):385-409.
- 5 **Harrigan TP, Harris WH.** A three-dimensional non-linear finite element study of the effect of cement-prosthesis debonding in cemented femoral total hip components. *J Biomech* 1991;24(11):1047-58.
- 6 **Verdonschot N, Huiskes R.** Mechanical effects of stem cement interface characteristics in total hip replacement. *Clin Orthop Relat Res* 1996;(329):326-36.
- 7 **Huiskes R, Boeklagen R.** Mathematical shape optimization of hip prosthesis design. *J Biomech* 1989;22(8-9):793-804.
- 8 **Verdonschot N, Huiskes R.** The effects of cement-stem debonding in THA on the long-term failure probability of cement. *J Biomech* 1997;30(8):795-802.
- 9 **Stolk J, Verdonschot N, Cristofolini L, Toni A, Huiskes R.** Finite element and experimental models of cemented hip joint reconstructions can produce similar bone and cement strains in pre-clinical tests. *J Biomech* 2002;35(4):499-510.
- 10 **Janssen D, Aquarius R, Stolk J, Verdonschot N.** Finite-element analysis of failure of the Capital Hip designs. *J Bone Joint Surg Br* 2005;87(11):1561-7.
- 11 **Morlock M, Schneider E, Bluhm A, Vollmer M, Bergmann G, Muller V, Honl M.** Duration and frequency of every day activities in total hip patients. *J Biomech* 2001;34(7):873-81.
- 12 **Heller MO, Bergmann G, Deuretzbacher G, Durselen L, Pohl M, Claes L, Haas NP, Duda GN.** Musculo-skeletal loading conditions at the hip during walking and stair climbing. *J Biomech* 2001;34(7):883-93.
- 13 **Carter DR, Orr TE, Fyhrie DP.** Relationships between loading history and femoral cancellous bone architecture. *J Biomech* 1989;22(3):231-44.
- 14 **Kerner J, Huiskes R, van Lenthe GH, Weinans H, van RB, Engh CA, Amis AA.** Correlation between pre-operative periprosthetic bone density and post-operative bone loss in THA can be explained by strain-adaptive remodeling. *J Biomech* 1999;32(7):695-703.
- 15 **Panisello JJ, Canales V, Herrero L, Herrera A, Mateo J, Caballero MJ.** Changes in periprosthetic bone remodeling after redesigning an anatomic cementless stem. *Int Orthop* 2009;33(2):373-9.
- 16 **Herrera A, Panisello JJ, Ibarz E, Cegonino J, Puertolas JA, Gracia L.** Long-term study of bone remodeling after femoral stem: a comparison between dxa and finite element simulation. *J Biomech* 2007;40(16):3615-25.
- 17 **ten Broeke RH, Alves A, Baumann A, Arts JJ, Geesink RG.** Bone reaction to a biomimetic third-generation hydroxyapatite coating and new surface treatment for the Symax hip stem. *J Bone Joint Surg Br* 2011;93(6):760-8.
- 18 **Szmukler-Moncler S, Ahossi V, Pointaire P.** Evaluation of BONIT®, a fully resorbable CaP coating obtained by electrochemical deposition, after 6 weeks of healing: a pilot study in the pig maxilla. *Bioceramics* 2001;13:395-8.
- 19 **Becker P, Neumann HG, Nebe B, Luthen F, Rychly J.** Cellular investigations on electrochemically deposited calcium phosphate composites. *J Mater Sci Mater Med* 2004;15(4):437-40.
- 20 **Dalton JE, Cook SD, Thomas KA, Kay JF.** The effect of operative fit and hydroxyapatite coating on the mechanical and biological response to porous implants. *J Bone Joint Surg Am* 1995;77(1):97-110.

- 21 **Søballe K, Hansen ES, Brockstedt-Rasmussen H, Bünger C.** Hydroxyapatite coating converts fibrous tissue to bone around loaded implants. *J Bone Joint Surg Br* 1993;75(2):270-8.
- 22 **Geesink RG.** Hydroxylapatite-coated total hip replacement five year clinical and radiological results.1993;171-208.
- 23 **Bauer TW, Geesink RC, Zimmerman R, McMahon JT.** Hydroxyapatite-coated femoral stems. Histological analysis of components retrieved at autopsy. *J Bone Joint Surg Am* 1991;73(10):1439-52.
- 24 **Capello WN, D'Antonio JA, Jaffe WL, Geesink RG, Manley MT, Feinberg JR.** Hydroxyapatite-coated femoral components: 15-year minimum followup. *Clin Orthop Relat Res* 2006;453:75-80.
- 25 **Becker P, Baumann A, Lüthen F, Rychly J, Kirbs A, Beck U, Neumann HG.** Spark anodization on titanium and titanium alloys. *Proceedings of the 10th World Conference on Titanium* 2003;Vol. V:3339-44.
- 26 **Aldinger PR, Sabo D, Pritsch M, Thomsen M, Mau H, Ewerbeck V, Breusch SJ.** Pattern of periprosthetic bone remodeling around stable uncemented tapered hip stems: a prospective 84-month follow-up study and a median 156-month cross-sectional study with DXA. *Calcif Tissue Int* 2003;73(2):115-21.
- 27 **Tarala M, Janssen D, Verdonchot N.** Balancing incompatible endoprosthetic design goals: a combined ingrowth and bone remodeling simulation. *Med Eng Phys* 2011;33(3):374-80.
- 28 **Keyak JH, Falkinstein Y.** Comparison of in situ and in vitro CT scan-based finite element model predictions of proximal femoral fracture load. *Med Eng Phys* 2003;25(9):781-7.
- 29 **Heller MO, Bergmann G, Kassl JP, Claes L, Haas NP, Duda GN.** Determination of muscle loading at the hip joint for use in pre-clinical testing. *J Biomech* 2005;38(5):1155-63.
- 30 **Huiskes R, Weinans H, van RB.** The relationship between stress shielding and bone resorption around total hip stems and the effects of flexible materials. *Clin Orthop Relat Res* 1992;(274):124-34.
- 31 **Akhavan S, Matthiesen MM, Schulte L, Penoyar T, Kraay MJ, Rinnac CM, Goldberg VM.** Clinical and histologic results related to a low-modulus composite total hip replacement stem. *J Bone Joint Surg Am* 2006;88(6):1308-14.
- 32 **Gruen TA, McNeice GM, Amstutz HC.** "Modes of failure" of cemented stem-type femoral components: a radiographic analysis of loosening. *Clin Orthop Relat Res* 1979;(141):17-27.
- 33 **Rancourt D, Shirazi-Adl A, Drouin G, Paiement G.** Friction properties of the interface between porous-surfaced metals and tibial cancellous bone. *J Biomed Mater Res* 1990;24(11):1503-19.
- 34 **Engh CA, Massin P, Suthers KE.** Roentgenographic assessment of the biologic fixation of porous-surfaced femoral components. *Clin Orthop Relat Res* 1990;(257):107-28.
- 35 **Sluimer JC, Hoefnagels NH, Emans PJ, Kuijjer R, Geesink RG.** Comparison of two hydroxyapatite-coated femoral stems: clinical, functional, and bone densitometry evaluation of patients randomized to a regular or modified hydroxyapatite-coated stem aimed at proximal fixation. *J Arthroplasty* 2006;21(3):344-52.
- 36 **Havelin LI, Engesaeter LB, Espehaug B, Furnes O, Lie SA, Vollset SE.** The Norwegian Arthroplasty Register: 11 years and 73,000 arthroplasties. *Acta Orthop Scand* 2000;71(4):337-53.
- 37 **Kröger H, Miettinen H, Arnala I, Koski E, Rushton N, Suomalainen O.** Evaluation of periprosthetic bone using dual-energy x-ray absorptiometry: precision of the method and effect of operation on bone mineral density. *J Bone Miner Res* 1996;11(10):1526-30.
- 38 **Karachalios T, Tsatsaronis C, Efraimis G, Papadelis P, Lyritis G, Diakoumopoulos G.** The long-term clinical relevance of calcar atrophy caused by stress shielding in total hip arthroplasty: a 10-year, prospective, randomized study. *J Arthroplasty* 2004;19(4):469-75.
- 39 **Bryan JM, Sumner DR, Hurwitz DE, Tompkins GS, Andriacchi TP, Galante JO.** Altered load history affects periprosthetic bone loss following cementless total hip arthroplasty. *J Orthop Res* 1996;14(5):762-8.
- 40 **Huiskes R.** The various stress patterns of press-fit, ingrown, and cemented femoral stems. *Clin Orthop Relat Res* 1990;(261):27-38.
- 41 **Weinans H, Huiskes R, Grootenboer HJ.** Effects of fit and bonding characteristics of femoral stems on adaptive bone remodeling. *J Biomech Eng* 1994;116(4):393-400.
- 42 **Turner AW, Gillies RM, Sekel R, Morris P, Bruce W, Walsh WR.** Computational bone remodeling simulations and comparisons with DEXA results. *J Orthop Res* 2005;23(4):705-12.

- 43 **Porter AE, Taak P, Hobbs LW, Coathup MJ, Blunn GW, Spector M.** Bone bonding to hydroxyapatite and titanium surfaces on femoral stems retrieved from human subjects at autopsy. *Biomaterials* 2004;25(21): 5199-208.
- 44 **Coathup MJ, Blunn GW, Flynn N, Williams C, Thomas NP.** A comparison of bone remodeling around hydroxyapatite-coated, porous-coated and grit-blasted hip replacements retrieved at post-mortem. *J Bone Joint Surg Br* 2001;83(1):118-23.
- 45 **Tonino AJ, Therin M, Doyle C.** Hydroxyapatite-coated femoral stems. Histology and histomorphometry around five components retrieved at post mortem. *J Bone Joint Surg Br* 1999;81(1):148-54.
- 46 **Orlik J, Zhurov A, Middleton J.** On the secondary stability of coated cementless hip replacement: parameters that affected interface strength. *Med Eng Phys* 2003;25(10):825-31.
- 47 **Folgado J, Fernandes PR, Jacobs CR, Pellegrini VD, Jr.** Influence of femoral stem geometry, material and extent of porous coating on bone ingrowth and atrophy in cementless total hip arthroplasty: an iterative finite element model. *Comput Methods Biomech Biomed Engin* 2009;12(2):135-45.
- 48 **Glassman AH, Bobyn JD, Tanzer M.** New femoral designs: do they influence stress shielding? *Clin Orthop Relat Res* 2006;453:64-74.
- 49 **Bobyn JD, Glassman AH, Goto H, Krygier JJ, Miller JE, Brooks CE.** The effect of stem stiffness on femoral bone resorption after canine porous-coated total hip arthroplasty. *Clin Orthop Relat Res* 1990;(261):196-213.
- 50 **Glassman AH, Crowninshield RD, Schenck R, Herberts P.** A low stiffness composite biologically fixed prosthesis. *Clin Orthop Relat Res* 2001;(393):128-36.
- 51 **Kärrholm J, Anderberg C, Snorrason F, Thanner J, Langeland N, Malchau H, Herberts P.** Evaluation of a femoral stem with reduced stiffness. A randomized study with use of radiostereometry and bone densitometry. *J Bone Joint Surg Am* 2002;84-A(9):1651-8.
- 52 **van Rietbergen B, Huiskes R.** Load transfer and stress shielding of the hydroxyapatite-ABG hip: a study of stem length and proximal fixation. *J Arthroplasty* 2001;16(8 Suppl 1):55-63.
- 53 **van Rietbergen B, Huiskes R, Weinans H, Sumner DR, Turner TM, Galante JO.** ESB Research Award 1992. The mechanism of bone remodeling and resorption around press-fitted THA stems. *J Biomech* 1993;26(4-5): 369-82.
- 54 **Weinans H, Huiskes R, van RB, Sumner DR, Turner TM, Galante JO.** Adaptive bone remodeling around bonded noncemented total hip arthroplasty: a comparison between animal experiments and computer simulation. *J Orthop Res* 1993;11(4):500-13.
- 55 **Lengsfeld M, Gunther D, Pressel T, Leppek R, Schmitt J, Griss P.** Validation data for periprosthetic bone remodeling theories. *J Biomech* 2002;35(12):1553-64.
- 56 **Viceconti M, Olsen S, Nolte LP, Burton K.** Extracting clinically relevant data from finite element simulations. *Clin Biomech (Bristol, Avon)* 2005;20(5):451-4.





# Chapter

---

# 4

***Balancing incompatible  
endoprosthetic design goals.  
A combined ingrowth and  
bone remodeling simulation***



## Abstract

*In order to design a good cementless femoral implant many requirements need to be fulfilled. For instance, the range of micromotions at the bone-implant interface should not exceed a certain threshold and a good ratio between implant-bone stiffness that does not cause bone resorption, needs to be ensured. Stiff implants are known to evoke lower interface micromotions but at the same time they may cause extensive resorption of the surrounding bone. Composite stems with reduced stiffness give good remodeling results but implant flexibility is likely to evoke high micromotions proximally. Finding a good balance between these incompatible design goals is very challenging.*

*The current study proposes a finite element methodology that employs subsequent ingrowth and remodeling simulations and can be of assistance when designing new implants. The results of our simulations for the Epoch stem were in a good agreement with the clinical data. The proposed implant design made of porous tantalum with an inner CoCrMo core performed slightly better with respect to the Epoch stem and considerably better with respect to a Ti alloy stem. Our combined ingrowth and remodeling simulation can be a useful tool when designing a new implant that well balances mentioned incompatible design goals.*

## Introduction

Survival of cementless implants depends on growth of bone into and onto the implant surface. To facilitate bone ingrowth, micromotions at the implant-bone interface should be minimized as these may lead to implant loosening<sup>1</sup>. Therefore, in order to ensure an acceptable range of implant-bone motion, high-stiffness materials are used for prosthetic components. However, these components can drastically change the bone stress distribution with respect to the preoperative situation. After total hip arthroplasty (THA), loads that were originally transferred through bone are carried mainly by the prosthetic component, which results in stress shielding and subsequent bone remodeling around the implant. The stiffness mismatch between the bone and the femoral implant may cause bone resorption<sup>2,3</sup>, subsequently leading to weakening of the complete reconstruction. Therefore, to reduce peri-prosthetic stress shielding, implants with a generally low bending stiffness could be an option. Hence, on the one hand high-stiffness implants reduce micromotions, while on the other hand low-stiffness implants reduce peri-prosthetic bone remodeling.

In order to optimize a cementless implant, a balance has to be found between these two incompatible design goals<sup>4</sup>. To screen the potential effects of composition changes of a femoral stem on bone, finite element (FE) models can be used. One can create a case-specific validated model<sup>5,6</sup> and simulate the outcome of various physiological processes like bone osseointegration<sup>7</sup> or bone remodeling<sup>8</sup>. To find a balance between these incompatible design goals one needs to investigate micromotions at the implant-bone interface as commonly done in many FE studies<sup>9,10</sup> but also look at bone remodeling.

In the present study we propose an FE methodology that combines an ingrowth and remodeling simulation. This method can be of assistance when designing new prosthetic components. To our knowledge there are only two FE studies (from one group of authors) where such an approach has been employed<sup>7,11</sup>. In the study of Fernandes et al.<sup>11</sup> bone ingrowth was simulated when the relative displacement at the interface was less than a threshold value. In such a case the initial frictional interface was bonded. Simultaneously, peri-prosthetic bone remodeling was simulated. In the current study, we propose a different approach where we first simulate the early stage ingrowth process to establish an equilibrium interface condition. This interface condition is subsequently used in the remodeling simulation, which typically takes place the first few years after the operation.

We evaluated the use of porous tantalum to improve upon an already existing well-performing composite design using the FE method. As a well performing design we chose the VerSys Epoch FullCoat stem for its external surface characteristics and relatively low bending stiffness with respect to other designs<sup>12,13</sup>. Porous tantalum is a relatively new material and can be manufactured in a range of porosities with corresponding stiffness values. In addition, porous tantalum has a proven bone ingrowth capacity<sup>14,15</sup> thanks to its porosity and high frictional characteristics. These material properties have been

utilized for various cup components<sup>15</sup>, and there is one femoral stem design that utilizes Trabecular Metal material (Zimmer® Trabecular Metal™ Primary Hip Prosthesis).

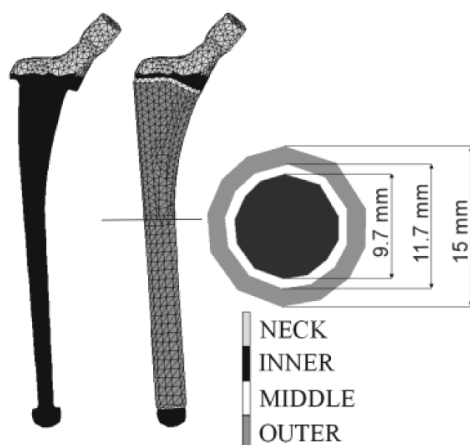
In the present study we performed analyses to investigate the effects of various constitutions of tantalum material distributions on bone ingrowth. Subsequently we selected the three best performing designs and analyzed these in a bone remodeling simulation, to examine which implant design is best capable of balancing the two incompatible design goals. We addressed the question whether our methodology of subsequent ingrowth and remodeling simulation give a good insight when designing cementless femoral implants. We therefore applied this methodology to prosthetic designs containing various configurations of tantalum material.

## Materials and Methods

Our case-specific FE model of bone was created from CT data of a human femur (81 year-old male, left femur). The bone was CT scanned along with a calibration phantom (solid, 0, 50, 100, 200 mg/ml calcium hydroxyapatite, Image Analysis, Columbia, KY, USA); subsequently the data was processed using a medical imaging software package (MIMICS 11.0). The model of the implant (VerSys Epoch FullCoat design (Zimmer, Inc., Warsaw, IN, USA)) was provided by the manufacturer and solid meshed using an FEA preprocessor (Marc 2007r1, MSC Software). All models were built from linear four-noded tetrahedral elements. The stem was positioned in the virtual bone by an experienced surgeon, using in-house software which allows the user to manipulate a solid model within the visualized CT-data (DCMTK MFC 10.8). We simulated the large amount of gaps (area of gaps of 21 %) that are usually present at the bone-implant interface<sup>16</sup> by using an in-house algorithm<sup>17</sup>. In order to create gaps at the interface an initial node-to-node surface mesh of bone and implant was created. Subsequently, the in-house algorithm was used to move the contour of intramedullary canal towards bony volume where local CT-values (Hounsfield Units, HU) were lower than a defined threshold. The isotropic properties of cortical and trabecular bone were derived from calibrated CT data. The calibration phantom was used to convert HU to calcium equivalent densities ( $\rho_{\text{CHA}}$ ). An in-house software package was used to assign a calcium equivalent density ( $\rho_{\text{CHA}}$ ) to each element, based on the average  $\rho_{\text{CHA}}$  value of all pixels in the element volume. The ash density was computed using relationships specific to the type of phantom used ( $\rho_{\text{ash}} = 0.0633 + 0.887\rho_{\text{CHA}}$ ). The elastic modulus ( $E$ , MPa) was computed for each element from ash density ( $\rho_{\text{ash}}$ ) using correlations for trabecular and cortical bone<sup>18</sup>. In the present study we used ash to apparent density ratio ( $\rho_{\text{ash}}/\rho_{\text{app}}$ ) equal to 0.6 over the whole density range<sup>19</sup>.

Table 1 Proposed stem compositions and their bending stiffness.

NAME	NECK	INNER	MIDDLE	OUTER	BENDING STIFFNESS [103 Nm <sup>2</sup> ]
EPOCH	CoCrMo	CoCrMo	PEEK	FIBER METAL	116.7
TI ALLOY	TiALV	TiALV	TiALV	TiALV	260.8
TA60	CoCrMo	60% POROSITY TA	60% POROSITY TA	60% POROSITY TA	14.4
TA80	CoCrMo	80% POROSITY TA	80% POROSITY TA	80% POROSITY TA	4.5
TA80-SOLID CORE	CoCrMo	CoCrMo	80% POROSITY TA	80% POROSITY TA	107.9



The Epoch stem is a layered composite construct consisting of a CoCrMo core, a PEEK inner layer and an outer Ti fiber metal layer. In order to analyze the various material combinations we kept the same layers but assigned them with different material properties (Table 1).

### Ingrowth Simulation

We first analyzed the effects of the varied composition on interfacial micromotions and bone ingrowth. Micromotions were defined as shear motion of implant nodes with respect to the local surface of the bone taking into account local deformation of the bone. Both the shear motion and gap opening were computed for each interface stem node. Bone osseointegration was assumed to occur when micromotions at the implant-bone interface remained below  $40 \mu\text{m}^1$  and the interfacial gap remained smaller than  $500 \mu\text{m}^{20}$  for 5 subsequent increments (Fig. 1). Though, this number does not represent real time period it gives an

indication that the local conditions allowing for ingrowth were constant under varied loading configurations (unloaded-loaded, loaded-unloaded) for a defined time. Ingrowth was simulated by means of activating springs between a stem node and its adjacent bone node. The stiffness of a spring could be changed at any time (spring activation = ingrowth). The spring constant was defined taking into account the local bone material properties. We assumed the newly created bone had mechanical properties similar to that of the surrounding bone since the ingrowth and shear strength of the interface is greater in the cortical region<sup>20,21</sup>. The spring constant was therefore defined as the summation of the adjacent bone elements' Young Modulus multiplied by 1/3 of the corresponding element face area (each face had 3 nodes connected to it), divided by the original spring length (equal to the gap between implant and bone node). In some cases, activating a spring locally caused excessive stresses at the implant-bone interface. If the local bone stresses exceeded 25 MPa, the springs were deactivated again, assuming failure of the bond. Reconstructions were subjected to normal walking loading conditions<sup>22</sup>.

As potential implant compositions, we chose porous tantalum (Ta) in three constitutions: Ta60, Ta80 and Ta80-solid core (Table 1). The Ta60 and Ta80 compositions were built of porous tantalum with corresponding porosities (60 and 80 %), while the implant neck was made of Co-CrMo alloy. The Ta80-solid core composition consisted of a CoCrMo alloy core surrounded by a layer of porous tantalum (80 % porosity). In addition, as reference stems we used the Epoch stem (existing design) and a solid Ti alloy stem with the grid blasted surface finish (hypothetical design, used to allow comparison to a commonly utilized construct). For each material corresponding material properties and frictional characteristics were applied (Table 2).

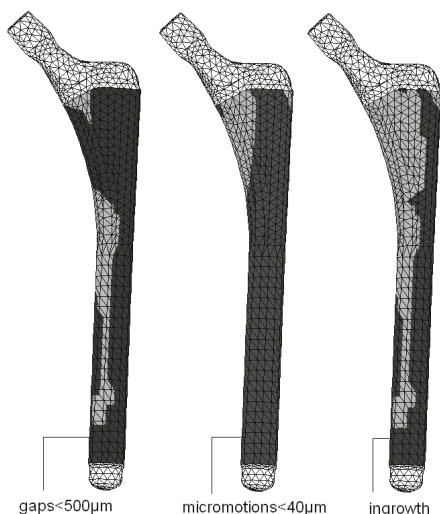


*Fig. 1 Distribution of factors (gaps and micromotions) that govern the ingrowth process (Ta80). Note that ingrowth can be also jeopardize by high local bone stresses (proximally for the current figure).*

Table 2 Material properties used in FE models.

MATERIAL	YOUNG MODULUS [GPa]	POISSON'S RATIO	IMPLANT-BONE FRICTION COEFFICIENT
CoCrMo	240	0.3	n/a
PEEK	3.4	0.3	n/a
FIBER MESH	6.9	0.3	0.5 <sup>23</sup>
TiALV	105	0.3	0.5 <sup>24</sup>
60 % POROSITY TA	5.8	0.34	0.88 <sup>25</sup>
80 % POROSITY TA	1.8	0.37	0.88 <sup>25</sup>

### Bone Remodeling Simulation

Secondly, the three best-performing reconstructions (area of bone ingrowth) as predicted by the bone ingrowth simulations were analyzed in a bone remodeling simulation. We used strain adaptive remodeling theory to simulate changes in bone mineral density in time ( $dp/dt$ )<sup>26</sup>. The difference in local strain energy density per unit of bone mass between the preoperative ( $R_{ref}$ ) and postoperative situation was taken as a stimulus ( $S$ ) for bone remodeling when outside a dead zone ( $((1-D)*R_{ref}) \div ((1+D)*R_{ref})$ ),  $D$ -dead zone value). When  $S$  falls within the dead zone, no remodeling is assumed to occur ( $dp/dt=0$ ). When  $S$  is smaller or greater than the dead zone, bone resorption or apposition will take place, respectively. In the current model the remodeling signal was averaged over the three following loading conditions ( $S=(S_1+S_2+S_3)/3$ ). The reconstructions were subjected to an alternating loading history of normal walking and stair climbing. The normal walking consisted of two peak hip joint forces occurring during the walking cycle (the beginning and end of single support phase). The stair climbing load consisted of the peak force occurring during a stair climbing cycle. The local rate of mass change was also dependent on the density, based on the assumption that the remodeling rate depends on the size of the available free bone surface. Typically, the free surface is low in case of low bone density and in case of very high density<sup>27</sup>. Time in the remodeling simulation (computer time unit, ctu) depends on the maximum stimulus per iteration, the greater the stimulus the smaller the time iteration. Our FE remodeling prediction was fitted to clinical data<sup>28</sup> on the Epoch design to define the adequate 'dead zone' value and to allow for scaling of the time unit in the bone remodeling simulation. The clinical data used for the correlation existed of a 2 year clinical follow-up study by Akhavan et al. of the Epoch stem, in which the bone mineral density was monitored<sup>28</sup> (Fig. 2).

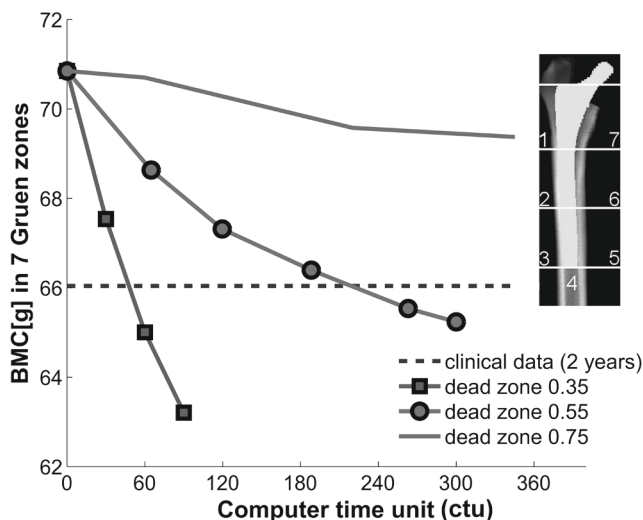


Fig. 2 Tuning of remodeling simulation with choice of three dead zones. Dead zones 0.35 and 0.55 gave good prediction for the bone mineral content (BMC) within resonable time unit (ctu).

The best fit was obtained for dead zone value 0.35 and time unit 60 (meaning that 60 ctu correspond to 2 year clinical reality) (Fig. 3). The implant-bone interface was assumed to be bonded only at locations where ingrowth was predicted in the previous simulations, with frictional contact in the remaining area. To allow for clinically relevant interpretation of the remodeling results, we used an in-house software package (DCMTK MFC 10.8) to project the results of the remodeling simulation onto 2D DEXA images. First, a 3D (X,Y,Z) voxel mesh is mapped onto the FE reconstruction (Fig.4). Subsequently, for each bone tetrahedral element its intersection volume with each voxels is calculated. The intersection volume is then multiplied by calcium equivalent of the element and added to the calcium equivalent of the corresponding voxels. Subsequently, a 2D pixel mesh with known calcium equivalent is created according to the chosen DEXA plane (e.g. (X,Y)). Each pixel has a calcium equivalent value corresponding to the summation of the values of 3D voxels ( $X_1, Y_1, Z_{1:n}$ ) along the same ( $X_1, Y_1$ ) coordinates. Non-bone elements do not contribute to the amount of calcium. In fact, if they were present along the ( $X_1, Y_1$ ) coordinate when converting to the 2D pixel mesh, the pixel will be visualized as a stem pixel on the DEXA. We defined the seven Gruen zones<sup>29</sup> and computed bone density ( $\text{g}/\text{cm}^2$ ) and local bone mineral content (BMC) (g) at different time points. We calculated bone density at each Gruen zone after one, two, three, four, five and ten years postoperatively for each implant composition. The bone loss predicted by our simulations was defined as a percentage of the pre-operative bone mass.

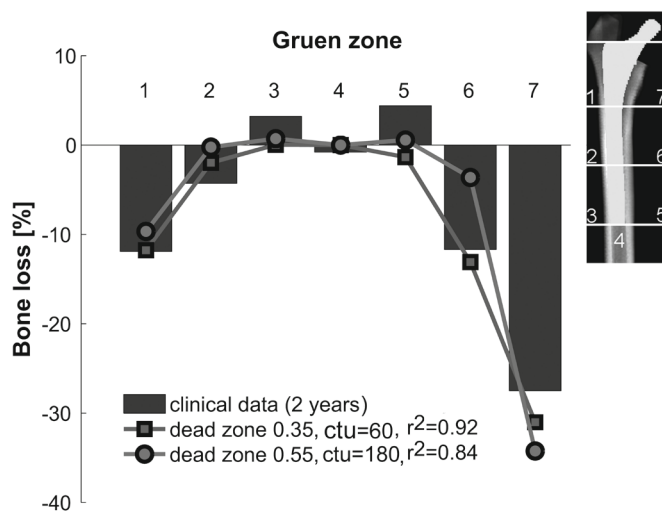


Fig. 3 Correlation results between the clinical (2 years in situ) data and data obtained from the remodeling simulations allowed us to define the best dead zone and real time.

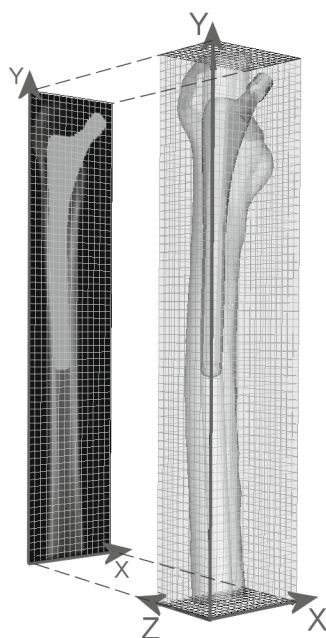


Fig. 4 An in-house software for converting numerical data.



Results

Of the proposed stem compositions three performed equally well in terms of predicted ingrowth. The Ti-alloy reached the ingrowth level of 80 % the fastest, followed by the Ta80-solid core (which showed the highest ingrowth area of all after 4 cycles) and the Epoch ( Fig. 5). The two stems composed only of porous tantalum (Ta60 and Ta80) achieved a similar ingrowth level (60 % of the implant surface). Hence, the stems composed only of porous tantalum were too flexible, causing micromotions above 40  $\mu\text{m}$  which occurred primarily at the proximal level.

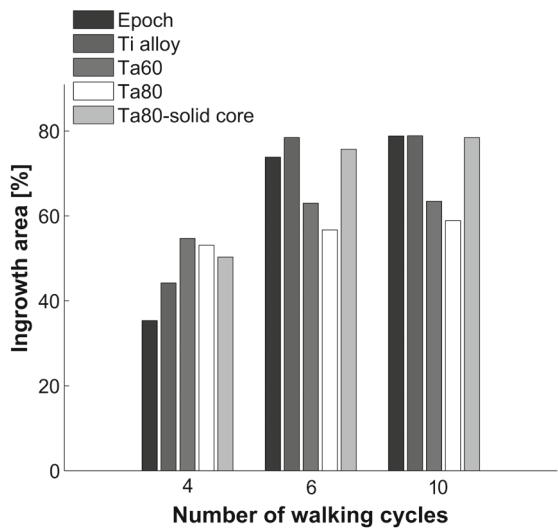


Fig. 5 Ingrowth area (%) for two standard designs (Epoch, Ti alloy) and three potential porous tantalum designs (Ta60, Ta80, Ta80-solid core).



Fig. 6 Change in bone mineral content (BMC) predicted at 5 years by the FE remodeling simulation

Bone remodeling simulations were subsequently performed with the other 3 stem types (Epoch, Ti alloy and Ta80-solid core). The stem made of Ti alloy caused the greatest bone resorption in almost all Gruen zones. For all three designs the bone loss mainly occurred in the proximal part of the femur, with the greatest bone resorption in Gruen zone 7 (up to 75 % after 10 year for Ti alloy stem). There was only a small difference between the remodeling of the Epoch and Ta80-solid core reconstructions (Fig. 6). These implants caused minimal bone loss in the distal region and the greatest in Gruen zone 7. These findings are consistent with the clinical measurements reported by Akhavan et al.<sup>28</sup>. The Ta80-solid core reconstruction had the least bone loss, although the difference with the Epoch was marginal.

Quantitatively, the bone loss in the reconstruction with the Ti alloy stem was 23 g after 10 years. After 10 years the Ta80-solid core stem and the Epoch stem displayed a bone loss of 11 g and 12 g, respectively. The change in BMC stabilized in time, the greatest changes were predicted to occur during the first 5 years, for all the models ( Fig. 7).

Besides the DEXA prediction of bone loss, we calculated the total BMC of the complete bone in time, including the regions obscured by the implant in the DEXA measurements. The overall change in BMC corresponded with the changes seen in the 7 Gruen zones. After 10 years, the total bone loss was equal to 36 g, 19 g and 16 g for the Ti alloy, Epoch and Ta80-solid core stems, respectively. Considering the differences in bone loss measured with the DEXA and computed for the complete bone, one can note that considerable change also occurred in the bone obscured by the stem on the DEXA scans.

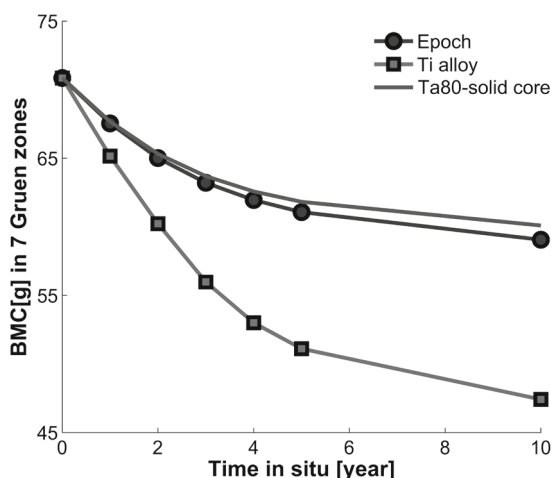


Fig. 7 Bone loss predicted by FE simulation at seven Gruen zones (1-7).

## Discussion

In the present study by means of a combined design philosophy we attempted to improve upon the VerSys Epoch FullCoat stem using porous tantalum material. A common approach is to change implant composition and design so that micromotions and interface stresses are reduced and will allow bone ingrowth. Our in-house ingrowth simulation allowed us to follow the ingrowth process of different implant compositions. The osseointegration simulation showed its sensitivity to the different reconstructions. Initially there were considerable differences in the ingrowth process between designs. Tantalum design with a solid core performed the best initially, achieving maximum ingrowth as the Epoch and Ti-alloy design when the process stabilized. Tantalum designs without a solid metal core showed to be too flexible for successful fixation. This finding was consistent with the results already presented in literature<sup>30</sup> where high interface stresses occurred proximally for an iso-elastic stem. The Ta60 and Ta80 stems represented iso-elastic femoral implants since their material properties (1.8 GPa and 5.8 GPa) were in the lower range of bone stiffness.

This study adopts a combined FE approach to improve prosthetic design. We defined an ingrowth process based on acceptable ranges of micromotions and gaps for osseointegration. Our choice was supported by the outcome of clinical studies where thresholds for shear motion and gaps were defined for optimal bone ingrowth<sup>1,20</sup>. We recreated the actual interface gaps that represent the irregularity of the implant-bone interface making the ingrowth prediction more realistic. Furthermore, our remodeling simulation was successfully validated against clinical data which allowed us to select an optimal dead zone and subsequently correlate computer time units with real time. The changes in bone density predicted by our bone remodeling theory were quantitatively similar to the clinical data with respect to the region of occurrence. In many previous studies, a converged state was taken as a final remodeling result<sup>11</sup> while another study shows that this state tends to overestimate bone remodeling of bone<sup>31</sup>.

The remodeling simulations showed that the composite stems performed better than the stem made of solid Ti alloy. This finding was consistent with the results of Turner et al.<sup>32</sup>, where a decrease of bone mineral density around the Epoch stem was half of that surrounding the titanium alloy stem in Gruen zone 7. Our combined FE approach indicates that, from a theoretical point of view, the Epoch design and Ta80-solid core stem are best suitable to balance the incompatible design goals for cementless femoral implants.

A limitation to our study was that the ingrowth and remodeling analyses were separated in the current study, while *in vivo* there may actually be an overlap of the two processes. We based our assumption on previous studies on bone ingrowth and remodeling. Ingrowth occurs directly after implantation if the local conditions allow it (acceptable range of micromotions<sup>1,33</sup>, no infection<sup>34</sup>). For instance, porous tantalum achieves an almost complete incorporation within 16 weeks, with little change after 1 year<sup>14</sup>. Bone

remodeling, however, is a more long term process, although density changes already take place during the first few months after operation. Bodén et al.<sup>35</sup> reported that the decrease in bone mineral density (BMD) continued after 2 years and in Gruen zone 7 it was faster than the rate of bone loss on the control side. Also Mueller et al.<sup>36</sup> reported decrease in trabecular and cortical bone density especially in the calcar region between the 1 and 6 year examinations. Although these studies indicate there are differences between the stages during which ingrowth and remodeling takes place, currently there is no data available that would allow for a reliable determination of the relative timeframes.

Limitations of this study are also related to the bone remodeling theory and FE modeling. The remodeling rule is limited to the internal remodeling and no correction for geometrical changes was made. Additionally, our study was limited to only one implant shape, while other prosthetic designs may display greater sensitivity to the optimization process with porous tantalum material. The outcome of our study was also bone-quality dependent. An inverse relationship has earlier been reported between decrease of bone mineral content of an implanted femur with the bone mineral content of the contralateral control femora<sup>37</sup>. The results could be different when e.g. an osteoporotic bone or a prosthesis with a different fit (proximal vs. distal) were chosen.

The main limitation of our osseointegration simulation were the assumptions made for the ingrowth process. Ingrowth factors were identical for all stem compositions, whereas these may be more favorable for porous tantalum relative to the fiber mesh of the Epoch stem or grit-blasted Ti alloy stem. For instance, the differences in porosity of various coatings result in weaker or stronger bone apposition and interface shear strength<sup>38,39</sup> but this factor was not implemented in our simulation. On the other hand, our assumption might be considered necessary in order to be able to compare and choose the best performing design. In spite of the assumptions made, the ingrowth area predicted for the Epoch reconstruction was corresponding with the clinical data<sup>28</sup> where 73.57 % ( $\pm 8.48$ ) along the entire length of the stem showed bone ingrowth after 48 months in situ. One can speculate that tantalum implants may have a higher ingrowth potential than predicted by our simulations<sup>14,15</sup>.

Furthermore, it needs to be mentioned that we analyzed only one case-specific model, based on a single CT-scan and on one implant design. Although the selected femur was considered to be average in terms of shape, size and bone mineral density, the current results are influenced by the bone quality and implant position in the intramedullary canal.

In addition, we chose a specific stem design for our analyses. Evidently, the type of stem analyzed in this study is different from regular stem designs that are being used more frequently. Due to the low structural stiffness, one would expect to find micromotions higher than those found in regular stems. However, as the study of Kärrholm et al. (2002)<sup>40</sup> suggests, the subsidence of the Epoch stem is similar to that of a stiffer implant, which would disqualify the theoretical risk of increased interfacial micromotions. In the

current study, we also included a stiff titanium alloy design, based on the Epoch shape. Our results indicate that the micromotions of the 'stiff' Epoch and the original isoelastic Epoch stem are very similar. Additionally, also in the study of Kärholm et al. a stiffer design was associated with more proximal bone loss than the Epoch stem. Although this does not provide a direct proof, it gives an indication of the validity of our results and their applicability to other straight stem designs.

We performed subsequent ingrowth and remodeling simulations which could be argued a simplification of reality since the processes occur simultaneously. However, the relative relationship between the processes is not known sufficiently to allow reliable predictions by FE models. Since we separated the two processes and the interface conditions of the ingrowth simulation are implemented as an input of the remodeling process, the implant-bone interface will remain constant in the second simulation. Even high stresses occurred at the interface, the behavior between bone and implant will not be changed from bonded to frictional.

In conclusion, based on the results of this study we believe that a micromotion analysis in itself may not be sufficient to predict implant primary stability as commonly done in *in vitro*<sup>41-43</sup> and FE studies<sup>10,44</sup>. As shown in previous studies<sup>45,46</sup> and confirmed in the current, stiffer implants (e.g. Ti alloy stem) increase the interface stability and therefore give good results in ingrowth simulations. However, due to a discrepancy in bone and implant stiffness, our results indicate such implants have the potential to increase bone resorption compared to more flexible composite stems. We showed that to be able to judge implant stability one should perform an interfacial micromotions prediction study followed by a remodeling simulation. The methodology proposed in the present study can be a useful tool when designing a new implant or improving upon existing designs.

## Acknowledgements

This study was funded in part by Zimmer, Inc., Warsaw, IN, USA.

## Reference List

- 1 **Jasty M, Bragdon C, Burke D, O'Connor D, Lowenstein J, Harris WH.** In vivo skeletal responses to porous-surfaced implants subjected to small induced motions. *J Bone Joint Surg Am* 1997;79(5):707-14.
- 2 **Huiskes R, Weinans H, Van RB.** The relationship between stress shielding and bone resorption around total hip stems and the effects of flexible materials. *Clin Orthop Relat Res* 1992;(274):124-34.
- 3 **Head WC, Bauk DJ, Emerson RH, Jr.** Titanium as the material of choice for cementless femoral components in total hip arthroplasty. *Clin Orthop Relat Res* 1995;(311):85-90.
- 4 **Huiskes R.** Failed innovation in total hip replacement. Diagnosis and proposals for a cure. *Acta Orthop Scand* 1993;64(6):699-716.
- 5 **Taddei F, Pancanti A, Viceconti M.** An improved method for the automatic mapping of computed tomography numbers onto finite element models. *Med Eng Phys* 2004;26(1):61-9.
- 6 **Trabelsi N, Yosibash Z, Milgrom C.** Validation of subject-specific automated p-FE analysis of the proximal femur. *J Biomech* 9-2-2009;42(3):234-41.
- 7 **Folgado J, Fernandes PR, Jacobs CR, Pellegrini VD, Jr.** Influence of femoral stem geometry, material and extent of porous coating on bone ingrowth and atrophy in cementless total hip arthroplasty: an iterative finite element model. *Comput Methods Biomech Biomed Engin* 2009;12(2):135-45.
- 8 **Van Rietbergen B, Huiskes R, Weinans H, Sumner DR, Turner TM, Galante JO.** ESB Research Award 1992. The mechanism of bone remodeling and resorption around press-fitted THA stems. *J Biomech* 1993;26(4-5):369-82.
- 9 **Reggiani B, Cristofolini L, Varini E, Viceconti M.** Predicting the subject-specific primary stability of cementless implants during pre-operative planning: preliminary validation of subject-specific finite-element models. *J Biomech* 2007;40(11):2552-8.
- 10 **Viceconti M, Brusi G, Pancanti A, Cristofolini L.** Primary stability of an anatomical cementless hip stem: a statistical analysis. *J Biomech* 2006;39(7):1169-79.
- 11 **Fernandes PR, Folgado J, Jacobs C, Pellegrini V.** A contact model with ingrowth control for bone remodelling around cementless stems. *J Biomech* 2002;35(2):167-76.
- 12 **Glassman AH, Crowninshield RD, Schenck R, Herberts P.** A low stiffness composite biologically fixed prosthesis. *Clin Orthop Relat Res* 2001;(393):128-36.
- 13 **Hartzbard MA, Glassman AH, Goldberg VM, Jordan LR, Crowninshield RD, Fricka KB, Jordan LC.** Survivorship of a low-stiffness extensively porous-coated femoral stem at 10 years. *Clin Orthop Relat Res* 2010;468(2):433-40.
- 14 **Bobyn JD, Stackpool GJ, Hacking SA, Tanzer M, Krygier JJ.** Characteristics of bone ingrowth and interface mechanics of a new porous tantalum biomaterial. *J Bone Joint Surg Br* 1999;81(5):907-14.
- 15 **Levine BR, Sporer S, Poggie RA, la Valle CJ, Jacobs JJ.** Experimental and clinical performance of porous tantalum in orthopedic surgery. *Biomaterials* 2006;27(27):4671-81.
- 16 **Prymka M, Wu L, Hahne HJ, Koebke J, Hassenpflug J.** The dimensional accuracy for preparation of the femoral cavity in HIP arthroplasty. A comparison between manual- and robot-assisted implantation of hip endoprosthesis stems in cadaver femurs. *Arch Orthop Trauma Surg* 2006;126(1):36-44.
- 17 **Waanders D, Janssen D, Miller MA, Mann KA, Verdonchot N.** Fatigue creep damage at the cement-bone interface: an experimental and a micro-mechanical finite element study. *J Biomech* 13-11-2009;42(15):2513-9.
- 18 **Keyak JH, Falkinstein Y.** Comparison of in situ and in vitro CT scan-based finite element model predictions of proximal femoral fracture load. *Med Eng Phys* 2003;25(9):781-7.
- 19 **Schileo E, Dall'ara E, Taddei F, Malandrino A, Schotkamp T, Baleani M, Viceconti M.** An accurate estimation of bone density improves the accuracy of subject-specific finite element models. *J Biomech* 7-8-2008;41(11):2483-91.
- 20 **Sandborn PM, Cook SD, Spires WP, Kester MA.** Tissue response to porous-coated implants lacking initial bone apposition. *J Arthroplasty* 1988;3(4):337-46.

- 21 **Clemow AJ, Weinstein AM, Klawitter JJ, Koeneman J, Anderson J.** Interface mechanics of porous titanium implants. *J Biomed Mater Res* 1981;15(1):73-82.
- 22 **Heller MO, Bergmann G, Deuretzbacher G, Dürselen L, Pohl M, Claes L, Haas NP, Duda GN.** Musculo-skeletal loading conditions at the hip during walking and stair climbing. *J Biomech* 2001;34(7):883-93.
- 23 **Rancourt D, Shirazi-Adl A, Drouin G, Paiement G.** Friction properties of the interface between porous-surfaced metals and tibial cancellous bone. *J Biomed Mater Res* 1990;24(11):1503-19.
- 24 **Shirazi-Adl A, Dammak M, Paiement G.** Experimental determination of friction characteristics at the trabecular bone/porous-coated metal interface in cementless implants. *J Biomed Mater Res* 1993;27(2):167-75.
- 25 **Zhang Y, Ahn PB, Fitzpatrick DC, Heiner AD, Poggie RA, Brown TD.** Interfacial frictional behavior: cancellous bone, cortical bone, and a novel porous tantalum biomaterial. *Journal of Musculoskeletal Research* 1999;3(4):245-51.
- 26 **Huiskes R, Weinans H, Grootenboer HJ, Dalstra M, Fudala B, Slooff TJ.** Adaptive bone-remodeling theory applied to prosthetic-design analysis. *J Biomech* 1987;20(11-12):1135-50.
- 27 **Martin RB.** Porosity and specific surface of bone. *Crit Rev Biomed Eng* 1984;10(3):179-222.
- 28 **Akhavan S, Matthiesen MM, Schulte L, Penoyar T, Kraay MJ, Rinnac CM, Goldberg VM.** Clinical and histologic results related to a low-modulus composite total hip replacement stem. *J Bone Joint Surg Am* 2006;88(6):1308-14.
- 29 **Gruen TA, McNeice GM, Amstutz HC.** "Modes of failure" of cemented stem-type femoral components: a radiographic analysis of loosening. *Clin Orthop Relat Res* 1979;(141):17-27.
- 30 **Weinans H, Huiskes R, Grootenboer HJ.** Effects of material properties of femoral hip components on bone remodeling. *J Orthop Res* 1992;10(6):845-53.
- 31 **Kerner J, Huiskes R, van Lenthe GH, Weinans H, Van RB, Engh CA, Amis AA.** Correlation between pre-operative periprosthetic bone density and post-operative bone loss in THA can be explained by strain-adaptive remodelling. *J Biomech* 1999;32(7):695-703.
- 32 **Turner AW, Gillies RM, Sekel R, Morris P, Bruce W, Walsh WR.** Computational bone remodelling simulations and comparisons with DEXA results. *J Orthop Res* 2005;23(4):705-12.
- 33 **Pilliar RM, Lee JM, Maniopoulos C.** Observations on the effect of movement on bone ingrowth into porous-surfaced implants. *Clin Orthop Relat Res* 1986;(208):108-13.
- 34 **Cameron HU, Yoneda BT, Pilliar RM, Macnab I.** The effect of early infection on bone ingrowth into porous metal implants. *Acta Orthop Belg* 1977;43(1):71-4.
- 35 **Bodén HS, Sköldenberg OG, Salemyr MO, Lundberg HJ, Adolphson PY.** Continuous bone loss around a tapered uncemented femoral stem: a long-term evaluation with DEXA. *Acta Orthop* 2006;77(6):877-85.
- 36 **Mueller LA, Nowak TE, Haeberle L, Mueller LP, Kress A, Voelk M, Pfander D, Forst R, Schmidt R.** Progressive femoral cortical and cancellous bone density loss after uncemented tapered-design stem fixation. *Acta Orthop* 2010;81(2):171-7.
- 37 **Engh CA, McGovern TF, Bobyn JD, Harris WH.** A quantitative evaluation of periprosthetic bone-remodeling after cementless total hip arthroplasty. *J Bone Joint Surg Am* 1992;74(7):1009-20.
- 38 **Friedman RJ, An YH, Ming J, Draughn RA, Bauer TW.** Influence of biomaterial surface texture on bone ingrowth in the rabbit femur. *J Orthop Res* 1996;14(3):455-64.
- 39 **Kienapfel H, Sprey C, Wilke A, Griss P.** Implant fixation by bone ingrowth. *J Arthroplasty* 1999;14(3):355-68.
- 40 **Kärrholm J, Anderberg C, Snorrason F, Thanner J, Langeland N, Malchau H, Herberts P.** Evaluation of a femoral stem with reduced stiffness. A randomized study with use of radiostereometry and bone densitometry. *J Bone Joint Surg Am* 2002;84-A(9):1651-8.
- 41 **Schneider E, Kinast C, Eulenberger J, Wyder D, Eskilsson G, Perren SM.** A comparative study of the initial stability of cementless hip prostheses. *Clin Orthop Relat Res* 1989;(248):200-9.
- 42 **Götze C, Steens W, Vieth V, Poremba C, Claes L, Steinbeck J.** Primary stability in cementless femoral stems: custom-made versus conventional femoral prosthesis. *Clin Biomech (Bristol, Avon)* 2002;17(4):267-73.
- 43 **Bühler DW, Berlemann U, Lippuner K, Jaeger P, Nolte LP.** Three-dimensional primary stability of cementless femoral stems. *Clin Biomech (Bristol, Avon)* 1997;12(2):75-86.

- 
- 44 **Pancanti A, Bernakiewicz M, Viceconti M.** The primary stability of a cementless stem varies between subjects as much as between activities. *J Biomech* 2003;36(6):777-85.
- 45 **Kuiper JH, Huiskes R.** Friction and stem stiffness affect dynamic interface motion in total hip replacement. *J Orthop Res* 1996;14(1):36-43.
- 46 **Harvey EJ, Bobyn JD, Tanzer M, Stackpool GJ, Krygier JJ, Hacking SA.** Effect of flexibility of the femoral stem on bone-remodeling and fixation of the stem in a canine total hip arthroplasty model without cement. *J Bone Joint Surg Am* 1999;81(1):93-107.





***Effect of intra-operative  
impaction force on the primary  
stability and probability  
of bone damage in  
cementless reconstructions  
of varied bone quality***

## Abstract

*Good primary stability of cementless implants is achieved when implant-bone micromotions are below a threshold which assures bone ingrowth. Surgeons are advised to impact the prosthesis in order to obtain an adequate implant-bone contact. However, an excessive impaction force can cause intra-operative damage to the bone, which can subsequently lead to implant-bone interface failure. The goal of the present study was to find a balance between the stabilizing effect of the intra-operative impaction force and the risk of bone damage caused by this force.*

*We created finite element models of composite isoelastic and solid Ti-alloy stems implanted in bones of varied quality in order to analyze the effect of different magnitudes of impaction force on implant primary stability and chance of bone damage.*

*An impaction force of 1kN caused no or negligible damage to the bone, but did not provide a good initial implant stability. However, the stability improved for the reconstructions with good and medium bone quality when implant seating was achieved. An impaction force beyond 2kN assured a very good stability, but caused extensive bone damage, especially in poor quality bones.*

*A balance between a good initial implant stability and a low risk of intra-operative bone damage is to apply an impaction force of 2kN in bones of good and medium quality. An impaction force of 1kN and a longer low load bearing period is advised in bones of poor quality, in order to prevent intra-operative bone damage and allow for secondary fixation by bone ingrowth.*

## Introduction

The survival of cementless hip prostheses highly depends on their primary and secondary stability. Primary stability is achieved during the surgery and depends on factors such as bone quality and bone-implant contact area <sup>1</sup>. Secondary stability is achieved through osseointegration of the implant. An inadequate fit may jeopardize bone ingrowth and may result in aseptic loosening of the implant, which is reported to be the main cause for revision <sup>2</sup>.

In order to obtain a good postoperative stability surgeons are advised to stabilize the prosthesis by impaction, causing the implant to be clamped within the femoral canal. However, excessive impaction can lead to bone fissures <sup>3</sup> during rasping or insertion of the stem. The probability of cracks is related to bone quality, where osteoporotic bones are at greater risk <sup>4</sup>. Hence, a balance should be found between achieving an adequate stability by stem impaction and preventing bone damage.

The primary stability influences the secondary stability, as bone ingrowth or ongrowth depends on the micromotions at the implant-bone interface. In an *in-vivo* study on dogs <sup>5</sup>, relative motions between implant and bone smaller than 28µm allowed bone to grow into the pores of a coated implant, while micromotions beyond 150µm were found to prevent bone formation. In another canine study, micromotions below 20µm have been reported to assure stable bone ingrowth into porous-coated implants <sup>6</sup>. Similarly to these studies, a retrieval study of porous-coated implants showed failed ingrowth in areas with micromotions of 150µm, while cortex-implant motions up to 40µm were found in the areas showing signs of ingrowth <sup>7</sup>. Based on the results of these studies 20µm seems an acceptable threshold value for micromotions below which stable bone ingrowth will certainly occur.

The Finite Element Method (FEM) is suitable for computing implant-bone micromotions to quantify implant stability. Several FEM studies tested the effects of surgical factors on implant stability, looking at the effect of implant size, malalignment <sup>8</sup>, implant-bone interface gaps, bone properties <sup>1,9</sup>, interference fit <sup>10</sup> and loading conditions <sup>11</sup>. Implant stability can be defined by the magnitude of interface micromotions as often done in FEM <sup>11,12</sup> and in-vitro studies <sup>13</sup>. FEM studies showed that stair climbing loads generate higher peak micromotions than other physiological loads<sup>11</sup>. However, the effect of intra-operative impaction on implant stability and the accompanying risk of bone damage has not yet been studied. FEM can be used here to assess the conflict issues related to an adequate implant stability and acceptable risk of bone damage. Bone damage can be predicted using either a stress- or a strain-based criterion <sup>14</sup>. But as showed in that study, the prediction of the level of failure risk and the location of fracture onset can differ between these criterions.

In the present study, in an FEM model of a THA reconstruction with a low stiffness composite and a Ti-alloy stem, we analyzed the effect of intra-operative impaction force on the primary stability, at various levels of bone quality. In addition, we evaluated the effect of impaction on bone at risk of damage. We used two damage criterions, the stress criterion (Von Mises stress) and strain criterion (maximum principal strain).

In order to investigate the conflict between implant stability and bone damage prevention we addressed the following research questions:

- 1 How is implant stability affected by the level of impaction force, bone quality and implant stiffness?
- 2 In what situation (bone quality, impaction force) is bone at risk for damage and does it change upon *in vivo* loading?
- 3 Does FE damage prediction depend on whether stress or strain-based damage criteria are used?

## Materials and Methods

An FEM model of a human femoral bone (81 year-old male, left femur) was created from CT data. The bone was scanned along with a phantom constructed of different hydroxyapatite samples (0, 50, 100, 200mg/cm<sup>3</sup>; Image Analysis, Columbia, KY, USA). A geometrical model of the implant (VerSys Epoch FullCoat) was provided by the manufacturer (Zimmer, Inc., Warsaw, IN, USA). An experienced surgeon positioned the stem in a virtual model of the bone using in-house software (DCMTK MFC 10.8). Gaps at the implant-bone interface were simulated using an in-house algorithm<sup>15</sup>. A brief explanation of this algorithm is given here. To create an FEM model with a realistic gap distribution, first a model with an ideal contact was built. Subsequently, the intramedullary surface of bone was moved towards the bone volume based on the CT information (Hounsfield Units, HU). If locally the HU value was below the threshold for bone tissue, the surface area was moved to account for the gap between implant and bone. The resulting gap area was equal to 49%; 51% of the implant ingrowth surface was initially in direct contact with the bone, which is typically seen in manually reamed cavities<sup>16</sup>. The gap width ranged between 0 and 1mm. Both the bone and stem model were solid meshed using an FEM preprocessor (Marc 2007r1, MSC Software). The bone and implant models consisted of ~65,000 and ~14,000 four-noded tetrahedral elements, respectively.

The calibrated CT scan allowed for mapping of the isotropic bone properties onto the model<sup>17</sup>. Two implant types were simulated based on the Epoch geometry: the original isoelastic implant and a solid Ti-alloy version. The implant material properties were provided by the manufacturer for the EPOCH design (240GPa for the CoCrMo core, 3.4GPa for the polyether ether ketone (PEEK) and 6.9GPa for the outer fiber mesh). The elastic modulus of the Ti-alloy stem was set to 105GPa. A Poisson's ratio of 0.3 was assumed for all materials. As bone ingrowth was not simulated physically, we modeled double-sided contact at the implant-bone interface with a friction coefficient of 0.5<sup>18</sup>.

To assess the effect of bone quality on the implant stability and bone risk of damage, three bone qualities were simulated. The 'neutral' bone stiffness ranged from 196MPa to 13.7GPa (BQmid). Two additional bone quality configurations were simulated by changing

the original calcium equivalent by plus and minus 30%, resulting in an elastic modulus ranging from 153MPa to 7GPa and from 244MPa to 22.6GPa, for the lower (BQmin) and higher bone quality (BQmax), respectively.

In order to evaluate the effect of intra-operative impaction three impaction forces were simulated. Based on the findings reported by Bishop et al.<sup>19</sup> a firm hammer blow with which a surgeon implants the prosthesis is equal to 5kN. We simulated the following impaction forces: 1kN, 2kN and 5kN, which we considered gentle, normal and firm, respectively (Fig. 1). An operative impaction force was simulated by applying a quasi-static force in the direction along the shaft. Directly after application of the impaction force, the sequential loading cycles of normal walking and stair climbing loads were alternately applied. A cycle consisted of a loaded increment, during which the corresponding peak force was applied, and an unloaded increment, during which a residual force of 50N was applied. Hence, each total cycle consisted of four increments: walking-loaded, walking-unloaded, stair climbing-loaded, stair climbing-unloaded. The loading pattern was repeated until a converged subsidence state was obtained (Fig. 1).

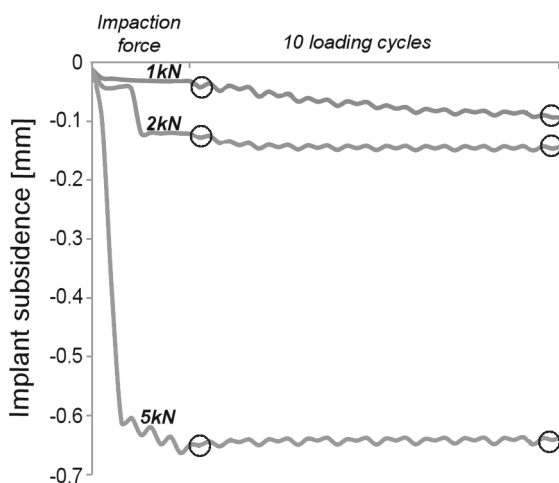


*Fig. 1 Implant stability and bone volume at risk of damage were defined after impaction and after approximately 10 loading cycles (in circles).*

In total, eighteen simulations were performed in which the impaction force and bone quality were varied to evaluate their effect on implant stability and bone volume at risk of damage (2 implant types, 3 impaction magnitudes, 3 bone qualities).

Implant stability was assessed by analyzing the implant-bone micromotions. The applied loading pattern allowed to define micromotions under walking and stair climbing in a single simulation. A threshold of 20 $\mu$ m was selected as the implant-bone motion which allows for stable bone ingrowth<sup>6</sup>. Micromotion was defined as the shear motion of implant

nodes with respect to the local bone surface, taking into account local deformation of the bone. During each loading cycle (walking or stair climbing), the area with micromotions beyond 20 $\mu$ m threshold was calculated. This area, taken as a percentage of the total ingrowth area (8,445 mm<sup>2</sup>), was used to represent the overall implant stability.

The bone volume at risk of intra-operative damage (directly after impaction) and post-operative damage (after cyclic loading) was defined by two failure criterions. We chose a stress-based criterion<sup>20</sup> and a strain-based criterion<sup>21</sup>. In the stress-based criterion the volume of bone at risk of damage was calculated by quantifying the volume of elements for which the von Mises stress exceeded the Yield Strength, which was defined based on the local bone density<sup>20</sup>. In the strain-based criterion the volume of bone at risk of damage was calculated by quantifying the volume of elements for which principal strain in tension or compression exceeded the yield properties for trabecular bone. The yield strain in tension and compression were set to 0.62% and 1.04%<sup>21</sup>, respectively. Elements adjacent to muscle attachment points were excluded, as these were subjected to stress and strain artifacts.

## Results

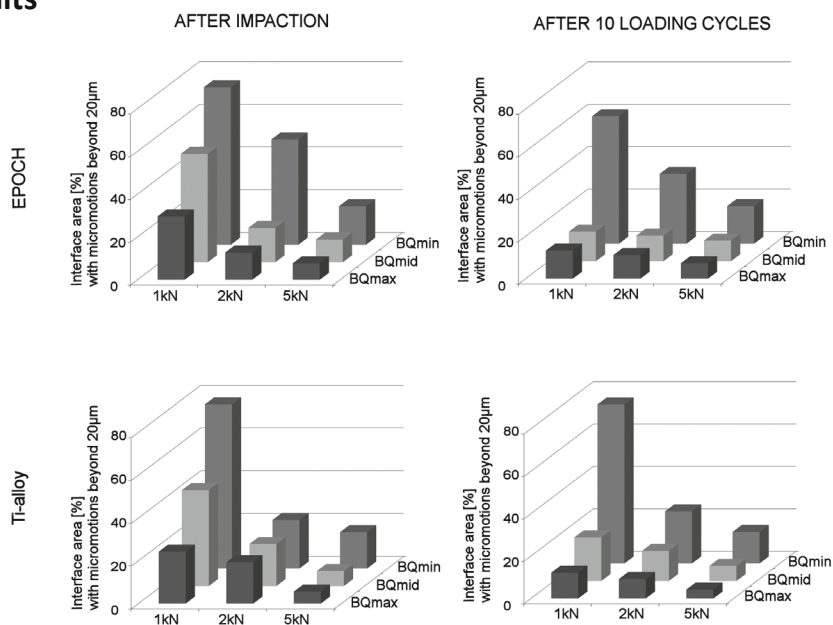


Fig. 2 Implant stability during walking defined by the area with micromotions beyond 20 $\mu$ m.

Implant stability increased with increasing magnitude of impaction force and bone quality (Fig. 2). After impaction with a 1kN force the initial implant stability was considerably smaller compared with cases impacted with greater forces. The stability improved after approximately 10 loading cycles, but only in the reconstructions with BQmax and BQmid

(Fig. 2-3). In poor quality bones (BQmin), neither the intraoperative gentle impaction nor the in-vivo loading assured implant stability. Good initial stability of implants was obtained when an impaction force beyond 1kN was applied (Fig. 2), especially in reconstructions with the Ti-alloy stem. In the reconstruction with the Epoch stem impacted with a 2kN impaction force in bone of poor quality, the stability was not as good as in the corresponding case with the Ti-alloy stem. The Ti-alloy stem was found to be slightly more stable than the composite stem. The most stable interface condition was achieved when the Ti-alloy stem was implanted using a 5kN impaction force in BQmax and BQmid (Fig. 2).

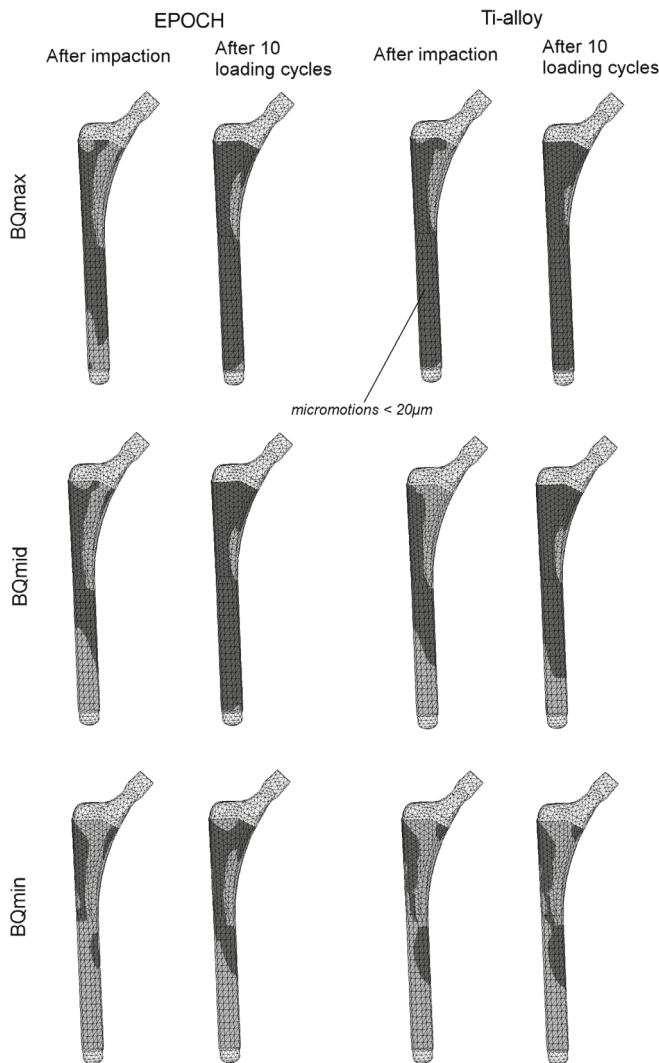


Fig. 3 Interface micromotions after using an impaction force of 1kN.



Bone volume at risk of damage increased with decreasing bone quality (Table 1, Fig. 4). The greatest damage to the bone was predicted when an impact force of 5kN was applied to a reconstruction with BQmin. Bone damage was small or even negligible when an impact of 1kN was applied in bones of all qualities, and when an impact force of 2kN was used in bones of good and medium quality (Fig. 4). If any damage due to impact occurred in these cases, it was localized mainly at the interface area with trabecular bone. In the reconstructions with 2kN (poor bone quality) and 5kN impact force (all bone qualities), the majority of the damage was caused intra-operatively, but some damage was also caused by the walking and stair climbing loads. There were negligible differences in intra-operative damage prediction between reconstructions with the Epoch and Ti-alloy stem (Fig. 4). The total predicted bone damage was somewhat greater for the reconstructions with the Epoch stem.

*Table 1 Prediction of bone damage caused by the intra-operative impact force and the applied loading condition. Two damage criteria were used: a stress-based and strain-based criterion.*

		BONE VOLUME AT RISK OF DAMAGE [MM3] (OF WHICH DAMAGE [%] CAUSED BY IMPACTION)		
	IMPACTION FORCE	BONE QUALITY	STRESS-BASED CRITERION	STRAIN-BASED CRITERION
EPOCH	1KN	BQMAX	10 (0%)	10 (0%)
		BQMID	17 (0%)	10 (0%)
		BQMIN	239 (9%)	68 (46%)
	2KN	BQMAX	49 (30%)	10 (0%)
		BQMID	737 (40%)	172 (54%)
		BQMIN	1045 (60%)	369 (72%)
	5KN	BQMAX	3123 (79%)	1543 (81%)
		BQMID	2406 (76%)	1901 (77%)
		BQMIN	9971 (86%)	6816 (89%)
TI-ALLOY	1KN	BQMAX	10 (0%)	10 (0%)
		BQMID	19 (0%)	10 (0%)
		BQMIN	260 (7%)	56 (23%)
	2KN	BQMAX	17 (0%)	10 (0%)
		BQMID	348 (78%)	190 (99%)
		BQMIN	1046 (62%)	423 (77%)
	5KN	BQMAX	700 (74%)	256 (88%)
		BQMID	3239 (81%)	1886 (82%)
		BQMIN	8192 (88%)	5524 (89%)

There were quantitative differences in damage predictions between the two failure criteria (Table 1). Bone damage predicted by the stress-based damage criterion was greater than the damage predicted by the strain-based criterion (Fig. 5). The localizations of damaged bone were similar between the two criteria.

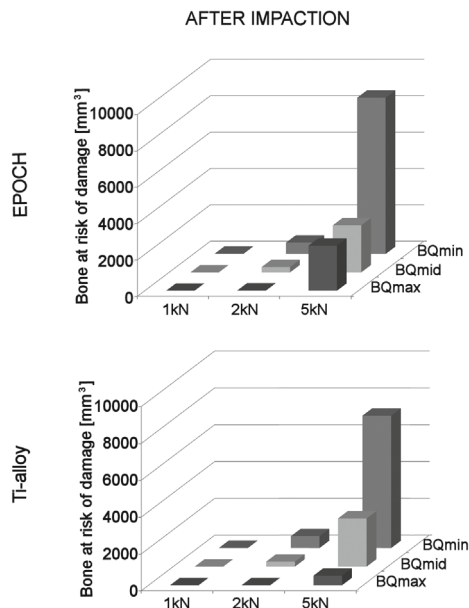


Fig. 4 Bone volume at risk of damage after impactation based on the stress-based criterion.

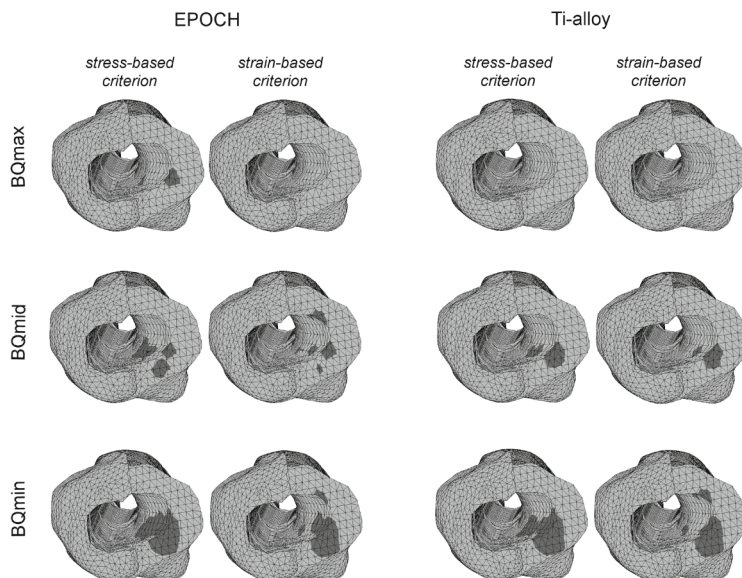


Fig. 5 Prediction of bone damage caused by an impaction force of 2kN using the stress- and strain-based criterions.

## Discussion

In the present study the effect of intra-operative impaction on the stability of composite and Ti-alloy implants and risk of intra-operative damage to bone was studied, at various levels of bone quality and using two damage criterions.

The first question we wanted to answer concerned the magnitude of the impaction force required to obtain a good implant stability under conditions of varied bone quality and implant stiffness (as assumed in the current study). As expected, implant stability increased with increasing magnitude of impaction force and bone quality. An impaction beyond 1kN was found to assure good implant stability in bones of all qualities. Interestingly, even though an impaction force of 1kN was not sufficient initially, the stability was achieved already after a few *in-vivo* loading cycles, but only in bones of good and medium quality. Stiffer stem showed greater stability than the composite implant when impacted at the same level.

Our second question concerned the magnitude of the impaction force that would cause bone damage. The results showed that an impaction force of 1kN for all bone qualities and an impaction force of 2kN in good and medium bone quality was causing no or negligible damage to the bone tissue. An impaction force of 2kN in bones of poor quality and 5kN in all bone qualities were shown to cause damage to bone.

Finally, our study compared bone damage predictions when the stress-based and strain-based criterions were implemented. We found that the Von Mises stress criterion gave a greater damage prediction than the maximum principle strain criterion. In both predictions the damage locations were similar.

Several secondary findings of the present study were consistent with data reported in the literature. Firstly, the difference in magnitude of micromotions when different loading conditions were applied to the reconstructions have been reported <sup>11</sup>. Similarly to these findings, our study showed that stair climbing causes higher peak micromotions than walking. Secondly, the increase of micromotions with reduced bone quality has been shown in other FEM studies <sup>9,22</sup>. Abdul-Kadir and Kamsah (2009) also showed a distal localization of peak micromotions in implantations in bone of poor quality.

The chosen magnitude of the intra-operative impaction load was similar to those used in *in-vitro* studies <sup>12,19</sup>. Additionally, the magnitudes of the functional loads (walking/stair climbing) were in the range of joint loads during every day activities, which has been reported sufficient to obtain good primary stability in press-fit uncemented femoral resurfacing implants <sup>23</sup>. Additionally, the models had an actual mapping of the gaps present at the bone-implant interface and therefore represent a realistic case. Commonly, the interface gaps are not simulated in the FEM models, although they do have an influence on the initial stability of the cementless implants as indicated by Viceconti et al. <sup>1</sup>. Furthermore, we implemented two failure criterions to fairly judge bone damage in our FEM models. Even though Von Mises stress criterion is commonly used in predicting failure <sup>24</sup>, we decided to

include a strain-based failure criterion as well. Furthermore, the maximum principal strain criterion has been reported to correctly identify the level of failure risk and the location of fracture onset in a subject-specific FEM models, while Von Mises or principal stress criterions were less accurate <sup>14</sup>.

The present study has also several limitations. Firstly, we did not account for the formation of bone damage mechanically, as no plasticity of bone loaded beyond the yield strength was implemented physically. Due to this simplification, our simulations may have underestimated the volume at risk of damage. Secondly, the range of Young's Moduli for the bone with the poorest quality was relatively low with respect to values reported for osteoporotic femoral bone ( $9.66 \pm 0.78 \text{ GPa}$  <sup>25</sup>). However, osteoporosis does not only affect calcium values, but also the thickness of the cortical bone <sup>26</sup>, and the size and shape of the intramedullary canal. In the present study the shape and size were kept constant. Therefore, the effect of the relatively low Young's Modulus values was compensated for in our models by the size and shape of the original bone. The pre-stresses caused by implant hammering were applied by the impaction force. Lastly, our choice of  $20 \mu\text{m}$  for bone ingrowth threshold needs to be justified. One could argue that  $40$  or  $150 \mu\text{m}$  (also mentioned in animal studies (Pilliar et al., 1986; Engh et al., 1992; Jasty et al., 1997)) could be chosen instead. When the  $40 \mu\text{m}$  bone ingrowth threshold was chosen, equivalent conclusions on implant stability could be drawn, although evidently the values defining the stability were smaller. As in our simulations the micromotions remained smaller than  $150 \mu\text{m}$ , a maximum stability would have been predicted when adopting that specific threshold.

In conclusion, our study showed that implant stability and bone at risk of damage depend mainly on bone quality and magnitude of impaction force. Initial implant stability increased with increasing impaction force and bone quality. Bone at risk of damage depended on the chosen damage criterion and increased with decreasing bone quality and increasing impaction force. A gentle impaction force appeared not to seat the implant completely, although good implant stability was later achieved in bones of good and medium quality during functional loading. An impaction force beyond  $2 \text{ kN}$  provided an excellent stability, but also increased the risk of bone damage. It seems difficult to obtain an adequate stability intra-operatively in low quality bones. However, the stability can improve thanks to the in-vivo loading. If these patients are treated with cementless implants, it may be advisable to prolong a period of partial weightbearing in order to allow for bone ingrowth and secondary stability.

## Acknowledgements

We would like to thank Zimmer, Inc., Warsaw, IN, USA for the models of the Epoch Ver-Sys FullCoat stem.

## Reference List

- 1 **Viceconti M, Brusi G, Pancanti A, Cristofolini L.** Primary stability of an anatomical cementless hip stem: a statistical analysis. *J Biomech* 2006;39(7):1169-79.
- 2 **Ulrich SD, Seyler TM, Bennett D, Delanois RE, Saleh KJ, Thongtrangan I, Kuskowski M, Cheng EY, Sharkey PF, Parvizi J, Stiehl JB, Mont MA.** Total hip arthroplasties: what are the reasons for revision? *Int Orthop* 2008;32(5):597-604.
- 3 **Lindahl H.** Epidemiology of periprosthetic femur fracture around a total hip arthroplasty. *Injury* 2007;38(6):651-4.
- 4 **Toni A, Ciaroni D, Sudanese A, Femino F, Marraro MD, Bueno Lozano AL, Giunti A.** Incidence of intraoperative femoral fracture. Straight-stemmed versus anatomic cementless total hip arthroplasty. *Acta Orthop Belg* 1994;60(1):43-54.
- 5 **Pilliar RM, Lee JM, Maniopoulos C.** Observations on the effect of movement on bone ingrowth into porous-surfaced implants. *Clin Orthop Relat Res* 1986;(208):108-13.
- 6 **Jasty M, Bragdon C, Burke D, O'Connor D, Lowenstein J, Harris WH.** In vivo skeletal responses to porous-surfaced implants subjected to small induced motions. *J Bone Joint Surg Am* 1997;79(5):707-14.
- 7 **Engh CA, O'Connor D, Jasty M, McGovern TF, Bobyn JD, Harris WH.** Quantification of implant micromotion, strain shielding, and bone resorption with porous-coated anatomic medullary locking femoral prostheses. *Clin Orthop Relat Res* 1992;(285):13-29.
- 8 **Abdul-Kadir M, Hansen U, Klabunde R, Amis A.** The effect of malalignment and undersizing on primary stability of cementless stems. *J Biomech* 2006;39(Supplement 1):S514.
- 9 **Abdul-Kadir M, Kamsah N.** The effect of bone properties due to skeletal diseases on stability of cementless hip stems. *American Journal of Applied Sciences* 2009;6(12):1988-94.
- 10 **Abdul-Kadir MR, Hansen U, Klabunde R, Lucas D, Amis A.** Finite element modelling of primary hip stem stability: the effect of interference fit. *J Biomech* 2008;41(3):587-94.
- 11 **Pancanti A, Bernakiewicz M, Viceconti M.** The primary stability of a cementless stem varies between subjects as much as between activities. *J Biomech* 2003;36(6):777-85.
- 12 **Viceconti M, Muccini R, Bernakiewicz M, Baleani M, Cristofolini L.** Large-sliding contact elements accurately predict levels of bone-implant micromotion relevant to osseointegration. *J Biomech* 2000;33(12):1611-8.
- 13 **Pettersen SH, Wik TS, Skallerud B.** Subject specific finite element analysis of implant stability for a cementless femoral stem. *Clin Biomech (Bristol, Avon)* 2009;24(6):480-7.
- 14 **Schileo E, Taddei F, Cristofolini L, Viceconti M.** Subject-specific finite element models implementing a maximum principal strain criterion are able to estimate failure risk and fracture location on human femurs tested in vitro. *J Biomech* 2008;41(2):356-67.
- 15 **Waanders D, Janssen D, Miller MA, Mann KA, Verdonchot N.** Fatigue creep damage at the cement-bone interface: An experimental and a micro-mechanical finite element study. *J Biomech* 12-8-2009;
- 16 **Prymka M, Wu L, Hahne HJ, Koebke J, Hassenpflug J.** The dimensional accuracy for preparation of the femoral cavity in HIP arthroplasty. A comparison between manual- and robot-assisted implantation of hip endoprosthesis stems in cadaver femurs. *Arch Orthop Trauma Surg* 2006;126(1):36-44.
- 17 **Keyak JH, Falkinstein Y.** Comparison of in situ and in vitro CT scan-based finite element model predictions of proximal femoral fracture load. *Med Eng Phys* 2003;25(9):781-7.
- 18 **Rancourt D, Shirazi-Adl A, Drouin G, Paiement G.** Friction properties of the interface between porous-surfaced metals and tibial cancellous bone. *J Biomed Mater Res* 1990;24(11):1503-19.
- 19 **Bishop NE, Burton A, Maheson M, Morlock MM.** Biomechanics of short hip endoprosthesis--the risk of bone failure increases with decreasing implant size. *Clin Biomech (Bristol, Avon)* 2010;25(7):666-74.
- 20 **Keyak JH, Kaneko TS, Tehranzadeh J, Skinner HB.** Predicting proximal femoral strength using structural engineering models. *Clin Orthop Relat Res* 2005;(437):219-28.

- 
- 21 **Bayraktar HH, Morgan EF, Niebur GL, Morris GE, Wong EK, Keaveny TM.** Comparison of the elastic and yield properties of human femoral trabecular and cortical bone tissue. *J Biomech* 2004;37(1):27-35.
  - 22 **Wong AS, New AM, Isaacs G, Taylor M.** Effect of bone material properties on the initial stability of a cementless hip stem: a finite element study. *Proc Inst Mech Eng H* 2005;219(4):265-75.
  - 23 **Gebert A, Peters J, Bishop NE, Westphal F, Morlock MM.** Influence of press-fit parameters on the primary stability of uncemented femoral resurfacing implants. *Med Eng Phys* 2009;31(1):160-4.
  - 24 **Derikx.** Implementation of asymmetric yielding in case-specific finite element models improves the prediction of femoral fractures. *Computer Methods in Biomechanics and Biomedical Engineering* 2010;
  - 25 **Coats AM, Zioupos P, Aspden RM.** Material properties of subchondral bone from patients with osteoporosis or osteoarthritis by microindentation testing and electron probe microanalysis. *Calcif Tissue Int* 2003;73(1):66-71.
  - 26 **Thiele OC, Eckhardt C, Linke B, Schneider E, Lill CA.** Factors affecting the stability of screws in human cortical osteoporotic bone: a cadaver study. *J Bone Joint Surg Br* 2007;89(5):701-5.



***Towards a method to simulate  
the process of bone ingrowth  
in cementless THA using finite  
element method***



## Abstract

*In cementless total hip arthroplasty, long-term implant stability is achieved by bone ingrowth. The strength of the new bond gradually increases in time, due to bone maturation and progression of ingrowth. This process is, affected by micromotions and gaps at the interface.*

*Ingrowth can be simulated using the finite element method, by monitoring peri-prosthetic micromotions. However, the bone maturation process and its effect on implant stabilization are omitted in current simulations. The aim of the present study was to simulate maturation of the bond between implant and bone and to test its effect on reconstructions of variable bone quality and interface conditions.*

*The predicted bone ingrowth depended on bone quality and implant-bone contact area. In the ideal situation, 91% of ingrowth could be achieved, while in the worst case only 17% was reached. Initial contact area had a significant effect on the outcome, overruling the effect of variations in bone quality. The progression of ingrowth had a stabilizing effect on adjacent regions, especially in high contact area cases. Further development and validation of the presented algorithm requires more information on the nature of the relation between the ingrowth rate, and the magnitude of micromotions and the gap size.*

## Introduction

Bone ingrowth in cementless total hip arthroplasty (THA) provides secondary fixation after the initial press-fit fixation that is achieved during surgery. This secondary fixation depends on the post-operative conditions, and on implant characteristics <sup>1</sup>.

From a biomechanical perspective, the most important parameters involved in osseointegration of cementless implants are micromotions <sup>2,3</sup> and gaps <sup>4,5</sup> at the implant-bone interface. Peri-prosthetic micromotions below 40µm have been reported to result in bone formation and osseointegration, while motions exceeding 150µm will cause the formation of fibrous tissue around the implant <sup>3</sup>. Moreover, animal experiments have shown that bone is able to bridge interface gaps as large as 2 mm.

However, it appears there are considerable differences in the strength of the bone-implant bond <sup>5</sup>. The strength of the new interface increases with bone ingrowth depth, time after implantation, and with decreasing initial gap size. Other studies <sup>6,7</sup> also reported that the time after implantation is a factor in bone osseointegration. Hofmann et al. showed significant progression of bone ingrowth of human trabecular bone into load-bearing porous-coated titanium implants up to 9 months postoperatively, after which bone ingrowth did not proceed further. This plateau has also been demonstrated in animal experiments, showing almost complete incorporation of tantalum specimens by 16 weeks, with little change at 52 weeks.

The type of bone and the bone density also play a role in bone ingrowth <sup>8,9</sup>. Shih et al. reported that type of bone contacting the implant is the key factor affecting the amount and pattern of bone ingrowth into the porous implant. Significantly more bone ingrowth can be achieved in areas with cortical bone contact, than in areas with trabecular bone contact.

Based on the aforementioned studies one can conclude that bone ingrowth is a multifactorial and complex process. Simulation of this process can only be performed by making certain assumptions and simplifications. Previously, the process of osseointegration has been simulated using the finite element method (FEM) <sup>10-13</sup>. Commonly, bone ingrowth is modeled as an instantaneous event, affected by the magnitude of interface micromotions, and the size of the interface gap. Spears et al. simulated bone ingrowth in a press-fit acetabular cup, in which ingrowth was assumed to occur when during six simulated activities the local micromotion remained below 40µm, the local gap was ever less than 100µm and always below 500µm. A similar approach was implemented by Andreykiv et al. where the ingrowth was assumed to occur when micromotions did not exceed 20µm throughout one loading period.

A drawback of current FEM simulations is that bone ingrowth usually is simulated as an instant change in the mechanical behavior of the implant-bone interface: sliding contact is instantly changed into a rigid bond, rather than that a gradual process is simulated. Moreover, the effect of bone quality and the size of the gap at the interface on ingrowth and the ingrowth rate usually are neglected.

The aim of the present study was to build on previous FEM bone ingrowth simulations and propose a new methodology to simulate bone ingrowth as a time dependent process,

and to investigate its effect on implant stability. For this purpose, the gradual process of bone maturation and osseointegration was incorporated in an FEM-based algorithm. In our approach the biological process of bone bond maturation was simulated as a gradual increase of the local stiffness of the bond. To account for the effect of bone quality on bone ingrowth, we based the value of the local implant-bone interface stiffness on the local bone quality. Furthermore, we included the effect of the magnitude of micromotions and the size of the gaps on the bone ingrowth progression: the rate of ingrowth was increased in areas with lower micromotions and smaller gaps. In order to test our new osseointegration simulation, we created multiple FEM models of femoral reconstructions with variations in bone quality and initial contact area, and investigated the sensitivity to these parameters.

## Materials and Methods

### Ingrowth process simulation

In our FEM osseointegration algorithm we simulate bone ingrowth as a gradual process by accounting for bone maturation in time. This gradual process was simulated by implementing a gradual increase in the local stiffness of the implant-bone bond. This gradual increase depended on the local magnitude of the interface micromotions and the local gap size. Hence, the smaller the micromotions and the smaller the gap, the faster bone ingrowth was assumed to occur, resulting in a faster increase of the stiffness of the bond. Since bone ingrowth is known to depend on the quality of host bone <sup>8,9</sup>, we based the ultimate stiffness of the bond on the local bone quality.

Ingrowth could only occur in areas where the magnitudes of micromotions ( $M$ ) and gaps ( $G$ ) did not exceed certain thresholds. Micromotions were defined in our FEM study by looking at the relative motion between the stem nodes and bone faces of the FEM mesh. The relative motion was computed as the difference between the loaded and unloaded state, expressed as the perpendicular projections of a stem node onto the plane of an adjacent bone face. The local gap was defined as the shortest distance between a stem node and an adjacent bone face. The micromotion threshold below which bone ingrowth could occur was  $40\mu\text{m}$ , based on a study by Jasty et al. <sup>3</sup>. The maximum gap, below which ingrowth could occur was set to 1mm, given that bone was shown to be able to bridge up to 2mm gap <sup>5</sup> and that interface gaps of the manually implanted prostheses have an average height of 0.8mm <sup>14</sup>. Furthermore, we assumed that a gap of 0.5mm could be bridged faster than the gap beyond this threshold, and that the rate of ingrowth in gaps between 0.5 and 1mm was constant.

Based on a study by Bobyn et al. <sup>6</sup>, we assumed complete ingrowth to occur within 16 weeks, under ideal circumstances. In our simulation we defined a time unit as one loading period (consisting of 4 subsequent increments: peak walking load-unloaded, peak stair climbing load-unloaded). Hence, one loading period corresponded to 4 weeks *in situ* in our

simulation. Under the ideal conditions (micromotions (M) and gaps (G) equal to zero) bone ingrowth would occur after 16 weeks (4 loading periods). If the conditions were not ideal, the ingrowth process would take longer. At the end of each loading period, the incremental ingrowth potential  $P_i$  was computed for each stem node at the interface, based on the magnitude of local micromotions and gaps occurring during the past that loading period (Fig. 1).

The computation was made using the following equation (Eq. 1):

$$P_i = \frac{1}{4} \left( 1 - \frac{M_{max}}{40\mu m} \right) (1 - G_{max}) \quad G_{max} \leq 0.5 \text{ mm} \quad (1)$$

$$P_i = \frac{1}{4} \left( 1 - \frac{M_{max}}{40\mu m} \right) 0.5 \quad G_{max} > 0.5 \text{ mm}$$

$M_{max}$  - maximum micromotions in the loading period (range 0÷40 $\mu$ m)

$G_{max}$  - maximum gap in the loading period

The incremental ingrowth potential  $P_i$  was added to the total ingrowth potential  $P$  ( $P = \sum P_i$ ), for each node couple at the interface. Ultimate ingrowth was achieved when  $P \geq 1.0$ . The maximum incremental ingrowth potential ( $P_i$ ) was equal to  $\frac{1}{4}$ , so under ideal conditions in  $P$  would be equal to 1.0 within 4 loading periods. An incremental ingrowth potential was equal to zero ( $P_i = 0$ ) if either the local micromotions were greater than 40 $\mu$ m or the gap was greater than 1mm.

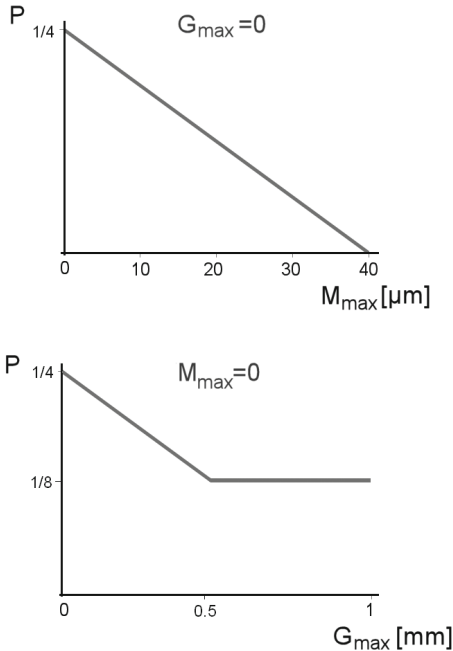


Fig. 1 (top) Relation between ingrowth potential  $P$  and magnitude of micromotions  $M_{max}$  assuming interface gaps equal to 0. (bottom) Relationship between ingrowth potential  $P$  and magnitude of interface gaps  $G_{max}$  assuming interface micromotions equal to 0. (See Eq. 1)

The mechanical effect of ingrowth was implemented through a true direction spring (Marc 2007r1, MSC Software) that was added at the interface. The stiffness of the bond (spring stiffness) was adjusted depending on the calculated ingrowth potential, and on the local bone quality. Hence, the newly created bond would obtain the stiffness of the adjacent bone. Each stem node would therefore be linked to three bone nodes; the three bone nodes forming the element face of the bone with respect to which micromotions and gaps were calculated. The maximum stiffness of each spring ( $S_{max}$ ), was computed as follows. Each surface node of the bone is connected to  $n$  elements with various material properties, dependent on the local bone density. Hence, the weighed Young's modulus ( $E$ ) of each node was determined. Given that each bone face with a certain area ( $A$ ) is connected to three bone surface nodes, each node portions  $1/3$  of that interface face area. To produce a spring stiffness, the weighed stiffness was then multiplied by the bone surface face area ( $A$ ), and subsequently divided by the original spring length  $l_0$  (equal to the gap between implant and bone at the time of spring activation) (Fig. 2, Eq. 2).

$$S_{max}(\rho) = \frac{\sum_{i=1}^n \frac{1}{3} E_i A_i}{l_0} \quad (2)$$

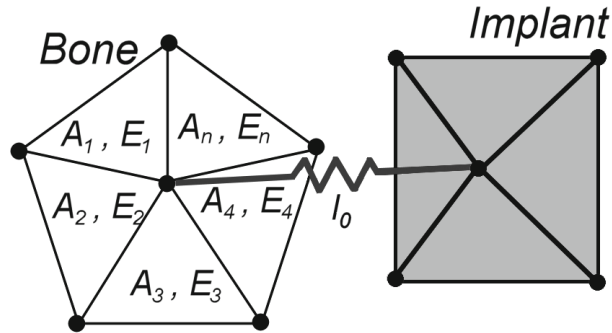


Fig. 2 Maximal stiffness of a spring  $S_{max}$  connecting adjacent bone and stem node, was based on the local stiffness of the bone elements  $E_{(1 \pm n)}$ ,  $1/3$  of each bone contact area  $A_{(1 \pm n)}$  and spring length during spring's activation  $l_0$ . We considered  $1/3$  of each bone contact area adjacent to a node given that each element face consists of 3 nodal points and the contribution to a nodal area is equal to  $1/3$  of each adjacent face area.

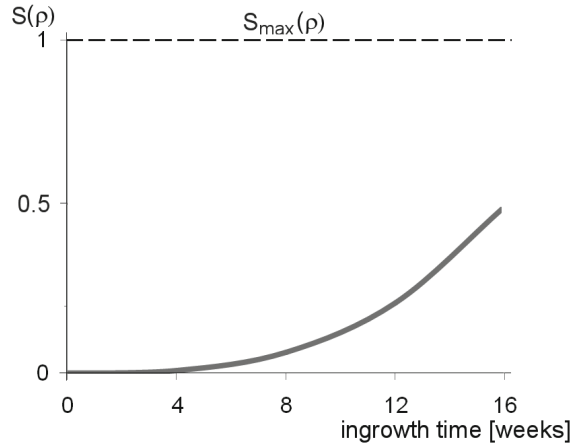


Fig. 3 Magnitude of spring stiffness  $S(\rho)$  depended on time. We assumed that within 16 weeks complete maturation of bone will not take place, but reach 50%. (See Eq. 3)

For each bone interface node with an ingrowth potential ( $P$ ) greater than 0, a spring was activated and assigned with a stiffness value  $S$  (Fig. 3). A non linear maturation of bone was assumed, resulting in a non-linear progression of the spring stiffness with ingrowth potential (Eq. 3). Furthermore, the ultimate mineralization of the new bond could not occur within 16 weeks;  $S$  could therefore reach only 50% of the maximum spring stiffness ( $S_{\max}$ ) (Eq. 3).

$$S(\rho) = \frac{1}{2} S_{\max}(\rho) P^2 \quad (3)$$

## FEM models

The ingrowth algorithm was applied to FEM models in order to test its feasibility. At first, we created a default model: a model of a cementless THA reconstruction based on a CT scan of a human femur (81 yrs, male) implanted with the VerSys Epoch FullCoat stem (Zimmer, Inc., Warsaw, IN, USA). The elastic modulus of the bone was computed from the local ash density<sup>15</sup>, which was measured using a calibration phantom (0, 50, 100, 200mg/cm<sup>3</sup>; Image Analysis, Columbia, KY, USA). In this model, full (100%) contact between the implant and the bone was simulated.

The default bone model was subjected to a number of variations in initial contact area, resulting in four additional models: initial contact areas (CA) equal to 100, 68, 51 and 35 per cent (CA100, CA68, CA51, CA35). Partial contact was created within the models by creating gaps at the implant-bone interface. The interface gaps were created using an in-house erosion algorithm<sup>16</sup>, which displaces bone interface nodes by

a defined value, based on the local CT grey scale values. The magnitude of interfacial gaps ranged between 0 and 1mm (at locations with extremely low grey scale values). Both the bone and stem models were solid meshed using an FEM preprocessor (Marc 2007r1, MSC Software). The bone consisted on average of ~66,000 elements, while the implant consisted of ~14,000 4-noded tetrahedral elements. Linear elements as these function better in conjunction with the node-to-surface contact algorithm adopted here for modeling frictional contact (Marc 2007r1, MSC Software). Material properties of the implant were provided by the manufacturer (Table 1). We modeled three different bone qualities based on the original calcium equivalent distribution. The values of the Young's Modulus of bones ranged up to 7GPa, 13.7GPa and 22.6GPa, from the poorest to the best bone quality (BQ) (BQmin - BQmid - BQmax), respectively. A Poisson's ratio of 0.3 was assumed for both bone and implant. The friction coefficient between the stem and bone was set to 0.5<sup>17</sup>.

The reconstructions were subjected to the loading condition of normal walking and stair climbing<sup>18</sup> assuming a body weight of 80kg. As mentioned earlier, one loading period consisted of 4 increments, composed of: peak normal walking force, unloading, peak stair climbing force and again unloading (Table 2). During the unloaded phase a compressive force of 50N was applied for stability purposes.

*Table 1 Material properties used in FE models.*

MATERIAL	YOUNG MODULUS [GPA]	POISSON'S RATIO
CoCrMo	240	0.3
PEEK	3.4	0.3
FIBER MESH	6.9	0.3

*Table 2 The magnitude and directions of joint force and muscle forces applied to the FEM model to simulate the peak loading during walking and stair climbing (data from Heller et al.<sup>18</sup>) assuming body weight of 80kg. To simulate the in-vivo loading conditions four sequential loading increments were applied in the following manner: peak normal walking force - unloading (hip contact force of -50N in Z direction) - peak stair climbing force- unloading (hip contact force of -50N in Z direction).*

		FORCE [N]		
		X	Y	Z
WALKING	BW=800N			
	HIP CONTACT	-432	-263	-1833
	ABDUCTOR AND TENSOR FASCIA LATAE	518	122	646
	VASTUS LATERALIS	-7	148	-743
STAIR CLIMBING	HIP CONTACT	-475	-485	-1890
	ABDUCTOR, ILIO-TIBIAL TRACT AND TENSOR FASCIA LATAE	664	237	618
	VASTUS LATERALIS	-18	179	-1081
	VASTUS MEDIALIS	-70	317	-2137

## Settling of the prosthesis into the bone

In the clinical situation the ingrowth process is not likely to start before the implant has migrated into a settled position. Hence, before the ingrowth simulation was activated, the settling process of the stem was simulated. This was done by applying the loading conditions while following the stem subsidence. Implant subsidence was defined as the relative motion between the averaged position of the surface nodes around the stem tip and averaged position of bone surface nodes inside the intramedullary canal at the same level. The stem was assumed to have settled when a converged subsidence was achieved. The criterion was fulfilled when the difference between the incremental subsidence values in subsequent loading periods (between the unloaded increment after the stair climbing load) was smaller than 1% of the total subsidence.

## Testing of the ingrowth process simulation

In total we performed 12 simulations where our new ingrowth simulation was tested for its sensitivity to variations in implant-bone contact area (CA100, CA68, CA51, CA35) and bone quality (BQmin - BQmid - BQmax). We calculated the total area of bone ingrowth by multiplying the area of each stem node and its ingrowth potential and summing it over the complete available ingrowth area. The actual ingrowth area was computed at 4, 8, 12 and 16 weeks of simulated ingrowth time.



## Results

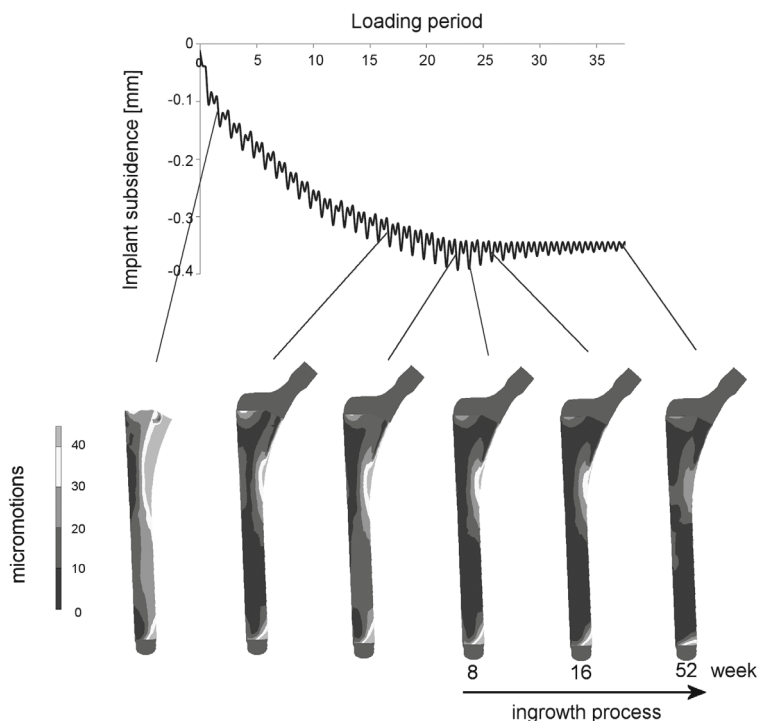


*Fig. 4 Stabilizing effect of bone ingrowth process on implant subsidence and magnitude of local micromotions (CA51 BQmin).*

All simulations displayed a distinct settling period, during which the subsidence rate and the micromotions gradually decreased (Fig. 4). In general, implant subsidence was inversely correlated with bone quality. In the case with the poorest bone quality and initial contact area of 51% (CA51; BQmin) the Subsidence was the greatest (0.4 mm) in the case with the poorest bone quality and an initial contact area of 51% (CA51; BQmin). After the settling period the ingrowth algorithm was started, which further reduced the micromotions at the interface and stopped implant subsidence (Fig. 4).

Increasing the contact area between implant and bone caused an acceleration of the ingrowth process (Fig. 5). In models with a low contact area, the progression of ingrowth with time was linear, while this relation became increasingly non-linear with increased contact area, illustrating the stabilizing effect of ingrowth on adjacent areas in cases with a better bone quality.

Contact area had a similar influence on the effect of bone quality. Models with a low contact area were insensitive to variations in peri-prosthetic bone quality, while a better bone quality improved the ingrowth process and implant fixation in the models with a higher contact fraction (Table 3). In the ideal situation (complete initial bone-stem contact, best bone

quality), the ultimate ingrowth area was 91% after 16 weeks, while this was considerably smaller (17%) in the worst case (initial contact area 35%, poorest bone quality) (Table 3).

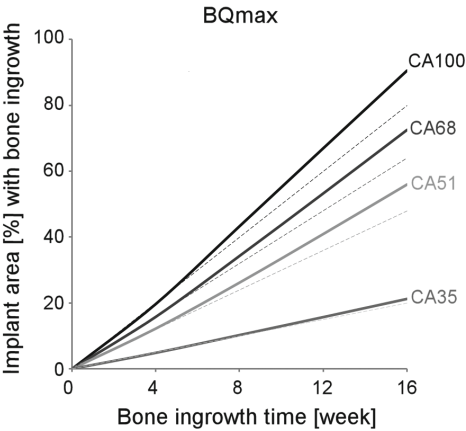


Fig. 5 Relationship between bone ingrowth area and time. Dashed lines indicate a linear relationship (based on the result at 4 weeks). For the CA100, CA68 and CA51 reconstructions there is a nonlinear increase of implant area with bone ingrowth in time indicating stabilizing effect of the acticated springs.

Table 3 Ingrowth area as a percentage of the total interface area.

INITIAL CONTACT AREA[%]	BONE QUALITY	INGROWTH AREA [%]			
		4 WEEKS	8 WEEKS	12 WEEKS	16 WEEKS
CA100	BQMAX	20	43	67	91
	BQMID	15	37	60	84
	BQMIN	18	38	58	79
CA68	BQMAX	16	34	53	73
	BQMID	12	29	47	65
	BQMIN	12	27	44	60
CA51	BQMAX	12	26	41	56
	BQMID	9	20	32	44
	BQMIN	7	16	26	38
CA35	BQMAX	5	10	16	21
	BQMID	5	10	16	22
	BQMIN	4	8	12	17

## Discussion

The aim of the present study was to build on previous FEM bone ingrowth simulations and propose a methodology to simulate bone ingrowth as a time dependent process. By changing the mechanical response of springs at the implant-bone interface mimicking the new bond, we were able to simulate gradual changes as seen during bone ingrowth and bone maturation.

We tested the sensitivity this new approach to variations of implant-bone contact area and peri-prosthetic bone quality. The bone ingrowth algorithm yielded results that depended on bone quality and implant-bone contact area. In the ideal situation, a maximum of 91% of ingrowth could be achieved, indicating that in a small portion of the implant-bone interface the micromotions due to external loads remained too high to allow full ingrowth. However, in the worst case (lowest contact area, poor bone quality) only 17% of ingrowth was reached, stressing the effect of initial contact area and bone quality. The progression of ingrowth had a stabilizing effect on adjacent regions, especially in high contact area cases.

Initial contact area had a significant effect on the outcome of the current simulations, and even overruled the effect of variations in bone quality. This stresses the importance of including realistic implant-bone contact, as it has been shown that a manually reamed cavity yields approximately 60% of contact between the bone and implant <sup>14</sup>. Most FEM studies, however, assume an idealized (full) contact at the implant-bone interface, which may lead to a substantial over prediction of implant stability and subsequent ingrowth.

Evidently, micromotions are reduced when the implant is surrounded by bone of good quality. Hence, the current models predicted a higher ingrowth rate and a larger ultimate area of bone ingrowth in models with superior bone quality. This is supported by migration data measurements that have linked early migration to failure <sup>19,20</sup>.

Typically, FEM simulations analyzing implant stability of cementless femoral implants do not allow for initial settling of the implant. In the current simulations, each run started with a settling period, during which rather large micromotions and implant subsidence were found. After a series of loading blocks the micromotions decreased, and the implant reached a steady position. This behavior was seen in every simulation, and stresses the importance of allowing for implant settling. This was also reported by Pettersen et al. <sup>21</sup>, who showed that the interface motions were considerably greater in the first couple of load increments.

Our study obviously has a number of limitations concerning the FEM models and ingrowth process simulation itself. First of all, the implants were implanted without pre-stresses occurring during press-fit insertion. These pre-stresses were accounted for by allowing the implant to settle and seek its ultimate position. Secondly, only a specific set of loads was selected to represent patient activity (walking and stair climbing). Although these activities are the most common activities, a wider variation of activities may affect the ingrowth process. Furthermore, our ingrowth algorithm only simulated mechanical fac-

---

tors involved in implant osseointegration, while biological effects such as vascularization<sup>22</sup> had to be omitted. Although we did not perform a convergence study to assess mesh dependencies for this particular reconstruction, we have adopted the same approach to build the models as we did in a previous study, in which FEM models were validated against experimental deflection measurements of cementless THA reconstructions<sup>23</sup>.

The aim of the present study was to improve on current FEM approaches to model implant osseointegration. The parameters influencing the process (micromotion magnitude, gap size) are related to clinical and experimental findings, but evidently, assumptions have been made to relate their effect to the rate of ingrowth (linear/non-linear, speed). It is extremely difficult to validate these parameters against clinical data, as it is currently not possible to assess the *in situ* bone ingrowth situation in a post-operative situation. Nevertheless, although the assumptions made in the current algorithm lack a fundamental basis, one should bear in mind that this is also the case for the approach that is generally used to model ingrowth. That approach assumes ingrowth is an instantaneous event provided that micromotions stay below a certain threshold and the gaps are small enough, while it is known from experimental and clinical data that the bond between bone and implant matures in time. Possibly, additional data may be retrieved from animal experiments, providing more information on the nature of the relation between the ingrowth rate, and the magnitude of micromotions and the gap size.

## Reference List

- 1 **Kienapfel H, Sprey C, Wilke A, Griss P.** Implant fixation by bone ingrowth. *J Arthroplasty* 1999;14(3):355-68.
- 2 **Engl CA, O'Connor D, Jasty M, McGovern TF, Bobyn JD, Harris WH.** Quantification of implant micromotion, strain shielding, and bone resorption with porous-coated anatomic medullary locking femoral prostheses. *Clin Orthop Relat Res* 1992;(285):13-29.
- 3 **Jasty M, Bragdon C, Burke D, O'Connor D, Lowenstein J, Harris WH.** In vivo skeletal responses to porous-surfaced implants subjected to small induced motions. *J Bone Joint Surg Am* 1997;79(5):707-14.
- 4 **Sandborn PM, Cook SD, Spires WP, Kester MA.** Tissue response to porous-coated implants lacking initial bone apposition. *J Arthroplasty* 1988;3(4):337-46.
- 5 **Dalton JE, Cook SD, Thomas KA, Kay JF.** The effect of operative fit and hydroxyapatite coating on the mechanical and biological response to porous implants. *J Bone Joint Surg Am* 1995;77(1):97-110.
- 6 **Bobyn JD, Stackpool GJ, Hacking SA, Tanzer M, Krygier JJ.** Characteristics of bone ingrowth and interface mechanics of a new porous tantalum biomaterial. *J Bone Joint Surg Br* 1999;81(5):907-14.
- 7 **Hofmann AA, Bloebaum RD, Bachus KN.** Progression of human bone ingrowth into porous-coated implants. Rate of bone ingrowth in humans. *Acta Orthop Scand* 1997;68(2):161-6.
- 8 **Shih LY, Shih HN, Chen TH.** The effects of sex and estrogen therapy on bone ingrowth into porous coated implant. *Journal of Orthopaedic Research* 2003;21(6):1033-40.
- 9 **Fini M, Giavaresi G, Rimondini L, Giardino R.** Titanium alloy osseointegration in cancellous and cortical bone of ovariectomized animals: histomorphometric and bone hardness measurements. *Int J Oral Maxillofac Implants* 2002;17(1):28-37.
- 10 **Fernandes PR, Folgado J, Jacobs C, Pellegrini V.** A contact model with ingrowth control for bone remodelling around cementless stems. *J Biomech* 2002;35(2):167-76.
- 11 **Folgado J, Fernandes PR, Jacobs CR, Pellegrini VD, Jr.** Influence of femoral stem geometry, material and extent of porous coating on bone ingrowth and atrophy in cementless total hip arthroplasty: an iterative finite element model. *Comput Methods Biomech Biomed Engin* 2009;12(2):135-45.
- 12 **Spears IR, Pfeleiderer M, Schneider E, Hille E, Bergmann G, Morlock MM.** Interfacial conditions between a press-fit acetabular cup and bone during daily activities: implications for achieving bone in-growth. *J Biomech* 2000;33(11):1471-7.
- 13 **Andreykiv A, Prendergast PJ, van KF, Swieszkowski W, Rozing PM.** Bone ingrowth simulation for a concept glenoid component design. *J Biomech* 2005;38(5):1023-33.
- 14 **Prymka M, Wu L, Hahne HJ, Koebke J, Hassenpflug J.** The dimensional accuracy for preparation of the femoral cavity in HIP arthroplasty. A comparison between manual- and robot-assisted implantation of hip endoprosthesis stems in cadaver femurs. *Arch Orthop Trauma Surg* 2006;126(1):36-44.
- 15 **Keyak JH, Falkinstein Y.** Comparison of in situ and in vitro CT scan-based finite element model predictions of proximal femoral fracture load. *Med Eng Phys* 2003;25(9):781-7.
- 16 **Waanders D, Janssen D, Miller MA, Mann KA, Verdonschot N.** Fatigue creep damage at the cement-bone interface: An experimental and a micro-mechanical finite element study. *J Biomech* 12-8-2009;
- 17 **Rancourt D, Shirazi-Adl A, Drouin G, Paiement G.** Friction properties of the interface between porous-surfaced metals and tibial cancellous bone. *J Biomed Mater Res* 1990;24(11):1503-19.
- 18 **Heller MO, Bergmann G, Kassi JP, Claes L, Haas NP, Duda GN.** Determination of muscle loading at the hip joint for use in pre-clinical testing. *J Biomech* 2005;38(5):1155-63.
- 19 **Kärrholm J, Borssén B, Löwenhielm G, Snorrason F.** Does early micromotion of femoral stem prostheses matter? 4-7-year stereoradiographic follow-up of 84 cemented prostheses. *J Bone Joint Surg Br* 1994;76(6):912-7.
- 20 **Freeman MA, Plante-Bordeneuve P.** Early migration and late aseptic failure of proximal femoral prostheses. *J Bone Joint Surg Br* 1994;76(3):432-8.
- 21 **Pettersen SH, Wik TS, Skallerud B.** Subject specific finite element analysis of implant stability for a cementless femoral stem. *Clin Biomech (Bristol, Avon)* 2009;24(6):480-7.

- 
- 22 **Murphy WL, Simmons CA, Kaigler D, Mooney DJ.** Bone regeneration via a mineral substrate and induced angiogenesis. *J Dent Res* 2004;83(3):204-10.
- 23 **Tarala M, Janssen D, Telka A, Waanders D, Verdonshot N.** Experimental versus computational analysis of micromotions at the implant-bone interface. *Proc Inst Mech Eng H* 2011;225(1):8-15.



# Chapter

---

# 7

## *Towards a more realistic prediction of peri-prosthetic micromotions*



## Abstract

*The finite element (FE) method has become a common tool to evaluate peri-prosthetic micromotions in cementless total hip arthroplasty. Often, only the peak joint load and a selected number of muscle loads are applied to determine micromotions. Furthermore, the applied external constraints are simplified (diaphyseal fixation), resulting in a non-physiological situation.*

*In this study, a scaled musculoskeletal model was used to extract a full set of muscle and hip joint loads occurring during a walking cycle. These loads were applied incrementally to an FE model to analyze micromotions. The relation between micromotions and external loads was investigated, and how micromotions during a full loading cycle compared to those calculated when applying a peak load only. Finally, the effect of external constraints was analyzed (full model vs. diaphyseal fixation and reduced number of muscle loads).*

*Relatively large micromotions were found during the swing phase when the hip joint forces were relatively low. Maximal micromotions, however, did concur with the peak hip joint force. Applying only a peak joint force resulted in peak micromotions similar to those found when full walking cycle loads were applied. The magnitude and direction of the micromotions depended on the applied muscle loads, but not on external constraints.*

## Introduction

The long term stability of a cementless hip implant depends on the growth of bone into and onto the prosthetic surface<sup>1</sup>. Bone ingrowth depends on peri-prosthetic micromotions at the bone-implant interface and several studies have shown that bone can only attach to the implant when these micromotions remain below approximately 40µm<sup>2-4</sup>. Larger micromotions can lead to the formation of fibrous tissue and subsequent loosening of the prosthesis<sup>5</sup>. Thus, the magnitude of interface micromotions can be used as an indicator of implant stability and ingrowth potential.

Finite element (FE) analysis is a valuable tool to evaluate interface mechanics in total hip arthroplasty (THA). FE analysis allows for the computation of micromotions around the complete bone-implant interface under a wide range of loading conditions and patient specific configurations. The magnitude and direction of micromotions can be determined by calculating the relative displacement between bone and implant upon dynamic loading. In most FE studies investigating peri-prosthetic micromotions, the loads that occur during activities of daily living (e.g. walking or stair climbing) are represented by applying joint and muscle loads at a single time point during the activity<sup>6,7</sup>. The most commonly applied loading configuration for any activity is the instant when the maximum joint reaction forces of a movement cycle occur (peak joint load). Although this seems to be an obvious choice, it is unknown how the magnitude and the direction of micromotions develop during the complete activity and whether maximal micromotions do actually occur at the instant of maximal joint reaction force. Furthermore, loading conditions are often simplified in FE simulations by including only a selection of muscles that attach to the femur<sup>6,8,9</sup>. It has been shown that by applying joint reaction forces only, is likely to overestimate femoral stresses by 150% compared to a physiological situation<sup>10</sup>. Duda et al. therefore recommend the use of a full muscle model in FE calculations to obtain a more realistic loading pattern<sup>10</sup>.

Muscle loads can be derived from musculoskeletal models, in which certain assumptions are made regarding the bone geometry. Usually, such a standard set of muscle loads is applied to FE models, regardless whether or not the bone geometry matches that of the musculoskeletal model. However, a recent study by Jonkers et al.<sup>11</sup> has shown that the inclusion of subject-specific muscle and hip joint contact forces drastically influences the stress distribution in the proximal femur. This highlights the importance of using a set of muscle loads that is consistent with the bone geometry used in the FE study.

During a movement cycle, a physiological femur is not in static equilibrium but undergoes continuously changing accelerations. However, during an FE analysis, the model should be free of rigid body motions, which is achieved by applying constraints. The manner in which these constraints are applied varies between studies. Boundary conditions that constrain the femur in the diaphysis are commonly applied<sup>6,7</sup>, but do not represent a physiological situation. Other FE studies aim to obtain a more realistic constraints by using a complete bone and applying fixations at the epicondyles<sup>10,12</sup> and the hip joint<sup>13</sup>, or

use a weak spring suspension <sup>14</sup>. Given the large number of configurations, there is little consensus which method provides the most realistic representation <sup>13</sup>, especially under the variable loading configurations that occur activities of daily living.

In the present study, an FE model of a complete cementless THA reconstruction including a set of muscle forces that was consistent with the bone geometry was used to answer the following research questions:

- 1 How do the magnitude and direction of interface micromotions develop during a gait cycle and how are these distributed over the stem surface?
- 2 Is there a relationship between the magnitude of the hip joint reaction force during the gait cycle and the concurrent micromotions at the implant-bone interface and does maximal micromotion occur when the maximal hip joint reaction force occur?
- 3 Is the magnitude of maximum micromotion different when a loading cycle is applied to the FE model compared to single time point loading?
- 4 How does the magnitude and the direction of micromotions depend on the used set of boundary conditions?

## Materials and Methods

A combination of data acquisition and modeling techniques were used to obtain results (Fig. 1). An FE model of a human femur was created based on cadaver CT scan data (81 year old male, right femur) using medical imaging software Mimics 11.0 (Materialise, Belgium) and the FE preprocessor Marc Mentat 2007r1 (MSC Software Corporation, USA). A solid model of an implant was provided by the manufacturer (CLS Spotorno stem, Zimmer Inc., USA). The implant was positioned in the bone model using an in-house software package (DCMTK MFC 10.8) under supervision of an experienced surgeon. Proximally, a node-to-node fit between the implant and the bone was modeled (no interface gaps), whereas distally an interface gap of 100 $\mu$ m was created to simulate a more realistic interface condition obtained during surgery. The mesh in the present study is based on mechanical convergence studies of a previous FE study investigating THA reconstructions whereby the deflection of physiological femurs was compared to the deflection of numerical models <sup>7</sup>. The same element type was in this study (linear four node tetrahedrons), resulting in a total number of ~27000 and ~129000 elements for the implant and the bone model, respectively.

The implant, made of TiAlV alloy, was assigned a Young's modulus of 105 GPa. As the bone was scanned along with a calibration phantom (solid, 0, 50, 100, 200 mg/ml calcium hydroxyapatite, Image Analysis, USA) the Young's modulus of the cortical and trabecular bone could be related to their density <sup>15</sup>. Frictional contact ( $\mu=0.3$ ) was simulated at the bone-implant interface using a node-to-surface algorithm (MSC.MARC 2007r1, MSC Software Corporation, Santa Ana, CA) <sup>16</sup>.

- Import geometry of femur FE model in Anybody	- Run kinematic analysis	- Apply muscle and joint reaction forces to FE model	- Calculate micromotions
- Import motion and ground reaction force data in Anybody	- Optimize human model	- Apply boundary conditions	
	- Calculate muscle and joint reaction forces	- FE analysis	

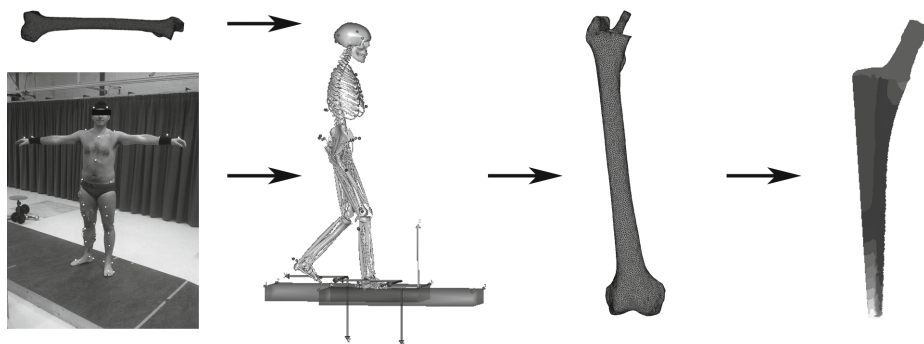


*Fig. 1 Schematic view of study procedure. The Anybody™ model was built after the geometry of a femur model was imported, resulting in a geometrically consistent set of muscles. Motion data was used to obtain muscle forces during a gait cycle. The micromotions were calculated using Marc Mentat 2007r1.*

To study the magnitude and direction development of micromotions during the gait cycle, the FE model was subjected to forces occurring during a walking cycle. The cycle was divided into 37 steps, starting with the last part of a stance phase, followed by the swing phase and stance phase of the right leg. The muscle forces were calculated using the musculoskeletal modeling system Anybody™ v5 (Anybody Technology A/S, Denmark)<sup>17</sup>. The femur geometry of the FE model was imported into the musculoskeletal modeling system, after which the anatomical data set was adapted. The muscle attachment and via points were displaced such that they matched the FE model (i.e. the muscle attachment points were located at the femur surface), in order to obtain a set of muscle loads that was geometrically consistent with the femur geometry. Besides time dependent loads from the musculoskeletal model, the effect of single time point loading on micromotions was studied as well, by applying muscle and hip joint reaction forces of the increment when the greatest hip joint reaction forces occurred during the gait cycle.

Peri-prosthetic micromotion was defined as the relative displacement of the implant stem with respect to the adjacent inner surface of the bone. An in-house algorithm<sup>18</sup> was used to track the micromotion development over time. For every time increment, the position of the stem node was projected on the corresponding contact face, which allowed quantification of the magnitude and direction of micromotions. Incremental micromotions were defined as the distances between subsequent nodal projections onto the bony sur-

face, whereas maximal micromotion was defined as the greatest distance between these projections (Fig. 2). Six nodes were selected (two proximally, two mid stem and two distally) on the surface of the implant for analysis to quantify micromotions at these locations.

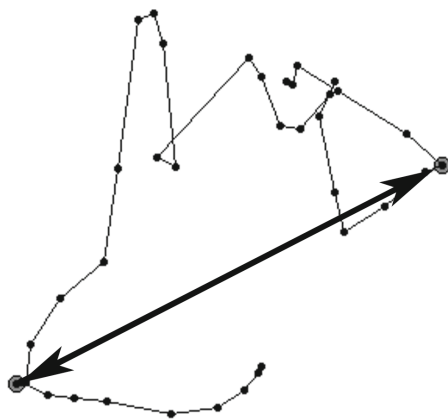


*Fig. 2 Example of incremental nodal projections and maximal micromotion definition (large arrow).*

In order to study the dependency of various constraint configurations on interface micromotions, one default and three additional constraint sets were applied to the FE model (Fig. 3): (1) Default constraints: 3 translational d.o.f. constrained at hip joint centre (implant) and 3 rotational d.o.f. constrained at the knee joint. (2) Simplified constraints: All d.o.f. constrained at the diaphysis ~60mm below implant tip. (3) Spring constraints: FE model suspended using weak springs as suggested by Wagner et al.<sup>14</sup> (4) Linear constraints: the hip joint was free to move in the direction of the axis pointing from the hip joint towards the knee joint, but was constrained in all other translational d.o.f. as suggested by Speirs et al.<sup>13</sup>. In total, seven individual cases were analyzed which are listed in Table 1.

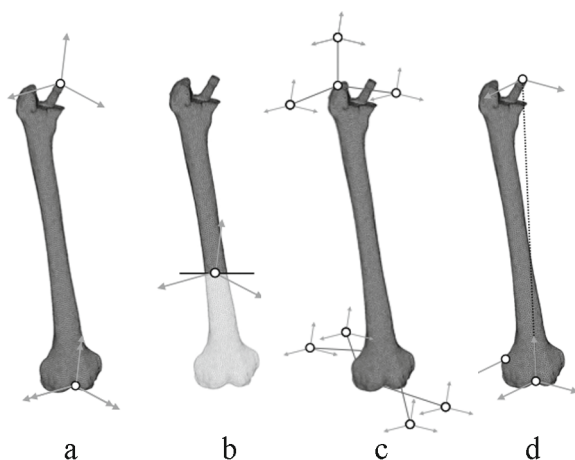


*Fig. 3 Constraint configurations. Single arrows represent translational d.o.f., whereas double arrows represent rotational degrees of freedom. a) default constraints, b) simplified constraints, c) spring constraints and d) linear constraints.*

Table 1 Overview of the cases (A-G) analyzed in this study and their configurations, the interfacial micromotions in the six points analyzed (a-f), the maximal micromotion occurring during the simulation, and the area subjected to selected ranges of micromotions.

CASE	CONSTRAINTS	MUSCLE MODEL	LOADING CONFIGURATION
A	Default	Full muscle set	Full cycle
B	Diaphysis	Hip joint force, abductors, Vastus Lateralis	Full cycle
C	Diaphysis	All muscles above fixation	Full cycle
D	Springs	Full muscle set	Full cycle
E	Linear	Full muscle set	Full cycle
F	Default	Full muscle set	Single point
G	Linear	Full muscle set	Single point

CASE	INTERFACIAL MICROMOTIONS [μm]						MICROMOTION-AREA DISTRIBUTION [%]			
	a	b	c	d	e	f	Max	0-40μm	41-80μm	81-120μm
A	32	39	4	3	96	39	101	91	7	2
B	31	35	6	11	111	50	126	90	7	3
C	31	40	3	4	92	38	98	91	8	1
D	30	38	2	4	90	50	100	90	8	2
E	31	39	3	5	92	39	97	91	7	2
F	28	37	2	2	78	15	86	94	6	0
G	28	36	1	3	78	15	84	94	6	0

Results

The magnitude and path of interface micromotions was dependent on the measurement location on the implant (Fig. 4). In the proximal region, a unidirectional pattern is visible in proximal-distal direction. Mid stem micromotions occur in a combined proximal-distal and anterior-posterior (lateral side of the implant) and medial-lateral (anterior side of the implant) direction. In the distal region, micromotions had a tendency to develop

in anterior-posterior and medial-lateral direction. The maximal micromotions under the default boundary conditions during the gait cycle were  $39\mu\text{m}$ ,  $4\mu\text{m}$  and  $96\mu\text{m}$  for the proximal, middle and distal part of the implant, respectively (Table 1, case A). The absolute maximal micromotions were found at the distal tip of the prosthesis and were marginally larger compared to the anterior-distal node e.

At any point on the implant, the greatest incremental micromotion appeared to be generated near the time increment when the greatest hip joint reaction forces occurred (immediately after swing phase). However, large incremental micromotions were also found during the swing phase when the hip joint reaction forces were relatively low (e.g. node f, Fig. 4).

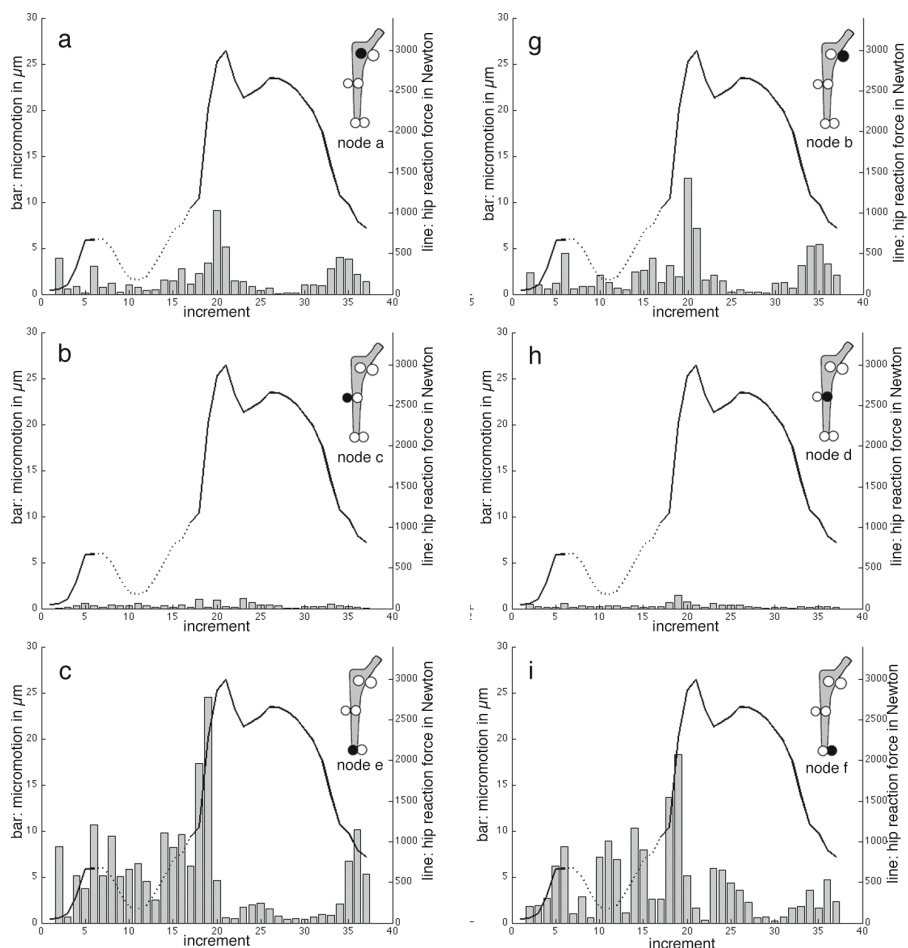


*Fig. 4 A bar diagram shows for each of six selected nodes the magnitude of the incremental micromotion per time increment (a-f). In the same subfigure, a line graph represents the hip joint reaction force. A pictogram shows to which node the graph belongs. In all subfigures, dotted lines represent the swing phase of the leg, whereas a continuous line represents the stance phase.*

Models loaded at a single time point (cases F and G) resulted in maximal micromotions very similar to those found in time dependent loaded cases, although micromotions at the distal area seemed to be smaller (Table 1). The percentage of micromotions on the stem below 40 $\mu\text{m}$  was similar for all cases (Fig. 5).

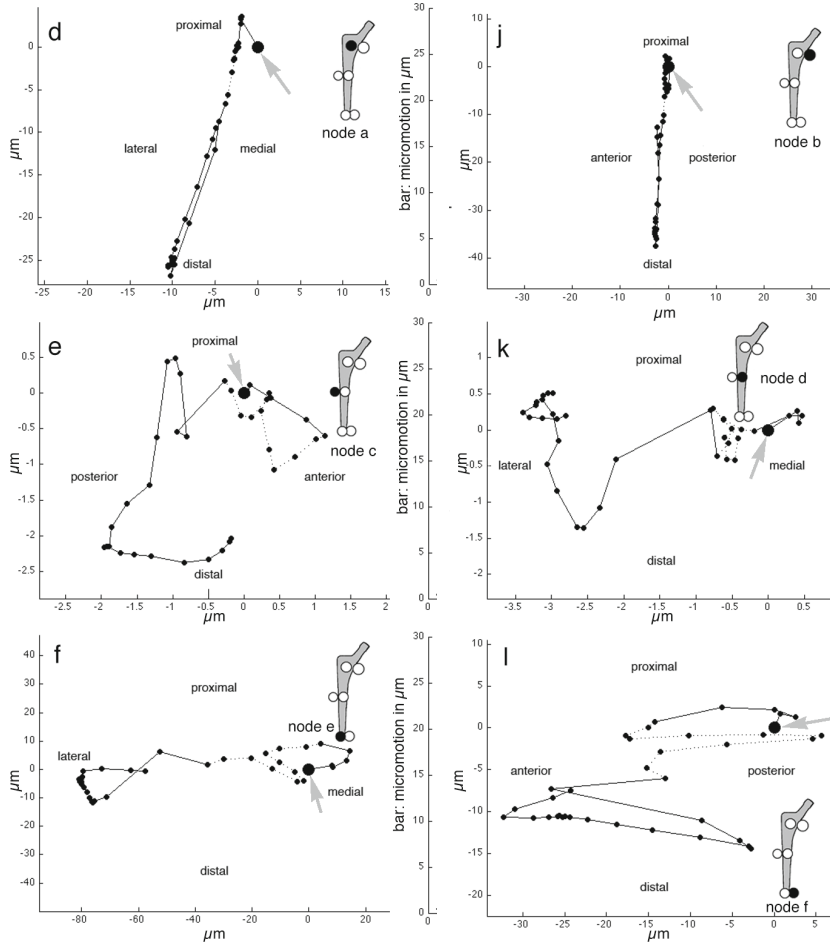


Fig. 5. For each of the six selected nodes (a-f), the path of interfacial micromotions is shown during the walking cycle. The initial position (large dot) is indicated by an arrow. In all subfigures, dotted lines represent the swing phase of the leg, whereas a continuous line represents the stance phase.



Consistent magnitude and path development of interface micromotions was calculated for all time dependent cases including a complete set of muscles (cases A, C, D and E, Fig. 6). Simplified constraints of the FE model in combination with a simplified muscle set (case B) did reveal different micromotion magnitudes and direction development paths with respect to the other time dependent loaded cases. Obviously, the single time point loaded cases (cases F and G) produced straight micromotion paths (Fig. 6), which clearly deviated from those obtained with the time dependent loaded cases.

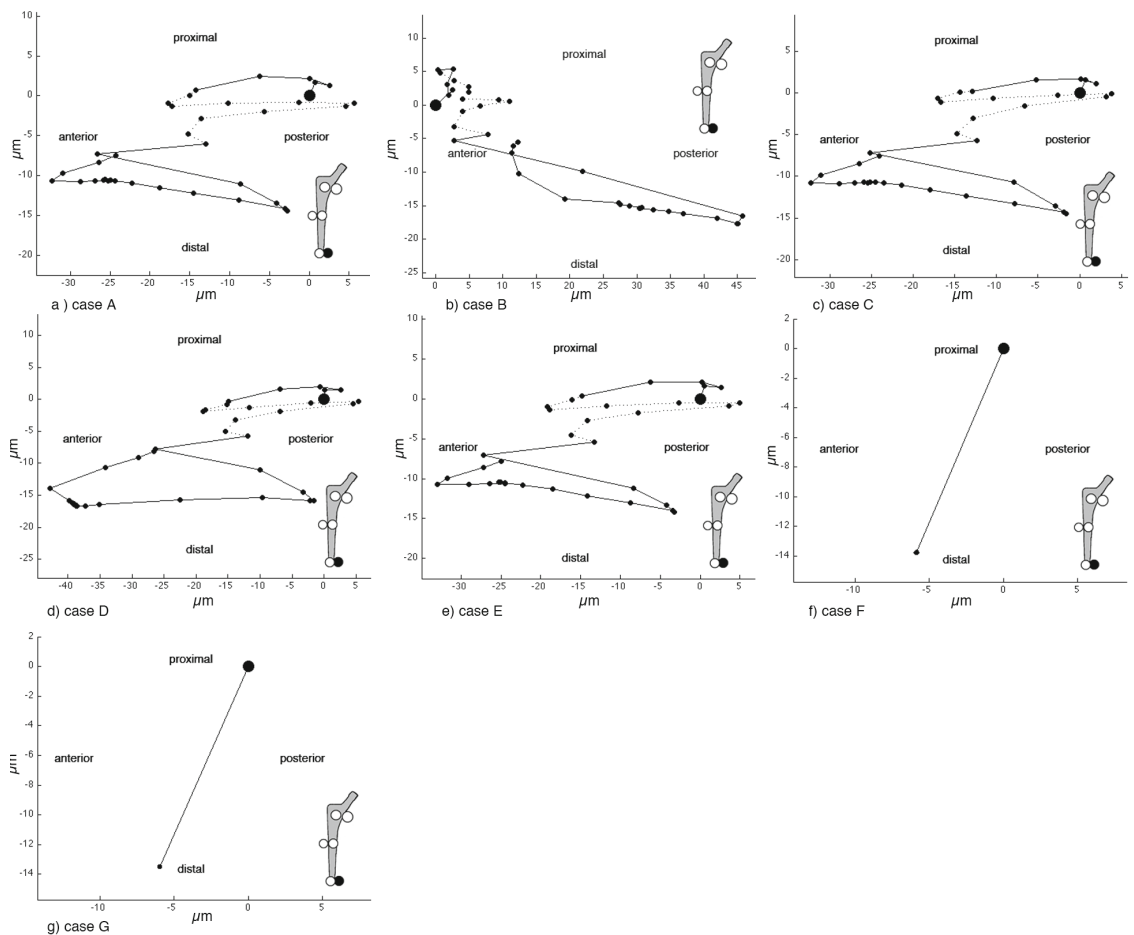


Fig. 6 A single node (node f) was selected to show the effect of different boundary conditions on the micromotion development. Little differences were found, with exception of the simplified loading and constraint configuration (case B).

---

## Discussion

In the present study, an FE model with geometry consistent muscle forces was used to study the effect of time dependent loading and constraining effects on the magnitude and direction development of interface micromotions at various locations of a cementless THA implant throughout a gait cycle. In answer to the research questions, when simulating full cycle loads, we found a) distinct differences in the direction and magnitude of the micromotions occurring between the different regions of the implant-bone interface. Moreover, b) large incremental micromotions were found during the swing phase when the hip joint reaction forces were relatively low, although c) the maximum micromotions did concur with the peak hip joint force. Finally, d) the magnitude and direction of the maximum micromotions did not depend on the boundary conditions, although they did depend on the applied muscle loads.

Obviously, there are a number of limitations which should be noted before interpreting the results. Firstly, a single THA reconstruction was used during this study, meaning that only a single bone, implant and interface configuration was analyzed. The interface characteristics depend on many factors, such as stem shape, surface roughness, reaming procedure and bone quality. During the implantation procedure of a wedge shaped stem as used in the present study, it is often difficult to obtain a good distal fit of the prosthesis<sup>19</sup>. Therefore, a distal gap was modeled to obtain a more realistic situation. The results of applying variable interface conditions was not accounted for, since this study focused on the effects of dynamic loading and boundary conditions. In fact, this study shows the feasibility of the combination of musculoskeletal and FE models and the potential effect of the parameters as assessed in this study. Future studies can now be performed to assess the effects of the most sensitive factors that influence peri-prosthetic micromotions, e.g. applying more realistic gap distribution models<sup>7</sup>, or by using a probabilistic approach<sup>20</sup>.

Secondly, this study applies a loading configuration obtained from a single gait trail without consideration of the variability of kinetics and kinematics occurring during gait. Also, a single activity was analyzed (walking), whereas more demanding activities such as stair climbing, squatting or rising from a chair will provide different muscle loads. Subject and activity specific muscle and joint reaction forces have a large influence on femoral stress and strain distribution<sup>11</sup> and are recommended for inclusion in future studies to investigate if these forces drastically influence individual micromotion predictions as well.

Thirdly, multiple loading cycles were not included in the present study. Due to friction at the interface one might expect a settling pattern to be visible after a number of cycles, such as found by Pettersen et al.<sup>21</sup> To assess this phenomenon, pilot studies were performed to analyze if multiple loading cycles would affect micromotion predictions. These studies revealed that this effect was negligible. It should be mentioned that the micromotions found in this study may be largely influenced by the limitations as described above. The results should therefore be interpreted with the aims as posed in the introductions (i.e. the quali-

tative effects of full loading conditions, variability of constraints, calculation of micromotions during a full gait cycle or just during the maximal hip reaction force).

Previous FE studies on peri-prosthetic micromotions report maximal micromotions in the same order of magnitude as in the present study <sup>7,21,22</sup>. Comparison against in vitro tests is, however, more complex due to measurement errors and restrictions of the loads that can be applied in an experimental set-up. Such in vitro measurements of micromotions are typically performed using either linear variable differential transducers (LVDTs) <sup>23,24</sup> or optoelectronic tracking devices <sup>25</sup>, which in some cases are attached at a distance from the actual interface. More sophisticated methods have been developed to facilitate measurements closer to the interface <sup>26</sup>, which have shown to minimize errors due to elastic deformations of the bone, implant and the interface. A remaining limitation to experimental techniques, however, is the fact that only a limited number of muscle forces can be applied. Moreover, using current experimental techniques it is not possible to simulate a full walking cycle, which makes it impossible to verify the micromotion patterns predicted by FE simulations. The mechanical validation of the current FE model therefore consists of a comparison against experimental deflexion measurements that were performed with a femoral hip reconstruction in the bone that was used to create the models.

Due to optimal contact conditions and the wedged shape at the proximal area of the implant, the movement path in that area was primarily directed along the longitudinal axis of the implant, and showed a unidirectional micromotion pattern. Mid-stem and distal gaps around the implant allowed the stem to move in multiple directions, resulting in a more cross-sheared micromotion path. Distal motions were primarily in anterior-posterior and medial-lateral directions, while little axial movement was found, showing a windshield wiper effect. Low mid-stem micromotions suggest that this area acts as a pivot point of the prosthesis.

Given the threshold of 40µm for structural bone ingrowth, this study indicates that walking should not jeopardize proximal bone ingrowth as the majority of the surface had micromotion values below this threshold, which concurs with general clinical observations. Furthermore, with the progression of bone ingrowth, micromotions will become smaller in time, ensuring secondary stability of the stem.

At all positions on the implant, the greatest incremental micromotions occurred when the highest hip joint reaction forces occurred. However, due to the elastic stress release of a reconstruction when unloaded, relatively high incremental micromotions were also found during the swing phase of the leg. Hence, incremental micromotions appear to be related to both the hip joint reaction forces and the incremental deflection of the bone.

Due to time dependent loading, incremental micromotions add up during a movement cycle. Subsequently, the maximum resulting micromotions were expected to be much higher than single time point loaded cases. However, the magnitudes of maximal micromotions were actually quite close for these cases, indicating that using only a single loading moment when maximal hip joint reaction forces occur could provide a good estimate of the distribu-

tion of micromotions occurring during walking. The greatest differences were found near the distal part of the implant, where due to the presence of a gap, the stem was more free to move compared to the proximal part.

In the current study all full bone models showed surprisingly small differences in magnitude and direction of interface micromotion development. Even the FE model with diaphyseal constraints with all remaining muscles above the fixation point provided similar results. This result demonstrates the Saint Venant principle, which dictates that constraint effects have no influence on the results of the simulation if the region of interest is far away from the constrained area. Diaphyseal constraints combined with a simplified muscle set did produce different micromotion magnitudes and development patterns compared to all other cases. The proximal maximal micromotions were smaller, while distal maximal micromotions were larger compared to the default configuration. Since consistent results were obtained for all constraint sets and differences were only found for a different loading configuration, these results indicate that within the limitations of this study, the inclusion of a full consistent set of muscle forces is of greater influence on the development of interface micromotions than the application of different femur constraints.

We would like to emphasize that a wide choice of variables can potentially influence micromotion predictions, e.g. other activities such as stair climbing, different implant types and other bone-implant interface conditions. We therefore recommend further research to assess the robustness of our findings and to further assess whether different boundary conditions (in combination with single time point loads) yield similar results under these variable conditions.

In conclusion, in our current model, conventional FE model constraints for THA reconstructions (diaphyseal constraints) and single time point loading (when maximal hip reaction forces occur) provided similar results in terms of magnitude and distribution of micromotions, when compared to a simulation of a full walking cycle. Applying different constraints did not result in different micromotions, whereas a reduction of the number of included muscles did have an effect on micromotions. The application of time-dependent loading revealed that quite large micromotions occur, also when the hip joint force is relatively low (e.g. during the swing phase), which was quite surprising considering the general assumption that high micromotions occur under high external loads. The next step to further develop simulations of interfacial micromotions, is to analyze the effect of parameters such as interface gaps, peri-prosthetic bone quality, implant type and loading configurations.

## Acknowledgements

We thank Zimmer Inc. (Warsaw, Indiana, USA) for providing us with the solid model of the implant. Gait data was provided by the TLEMSafe project ([www.tlemsafe.eu](http://www.tlemsafe.eu)) which is funded by the European Commission FP7 Programme.

## Reference List

- 1 **Tarala M, Janssen D, Verdonschot N.** Balancing incompatible endoprosthetic design goals: a combined in-growth and bone remodeling simulation. *Med Eng Phys* 2011;33(3):374-80.
- 2 **Kienapfel H, Sprey C, Wilke A, Griss P.** Implant fixation by bone ingrowth. *J Arthroplasty* 1999;14(3):355-68.
- 3 **Bragdon CR, Burke D, Lowenstein JD, O'Connor DO, Ramamurti B, Jasty M, Harris WH.** Differences in stiffness of the interface between a cementless porous implant and cancellous bone in vivo in dogs due to varying amounts of implant motion. *J Arthroplasty* 1996;11(8):945-51.
- 4 **Jasty M, Bragdon C, Burke D, O'Connor D, Lowenstein J, Harris WH.** In vivo skeletal responses to porous-surfaced implants subjected to small induced motions. *J Bone Joint Surg Am* 1997;79(5):707-14.
- 5 **Burke DW, Bragdon CR, O'Connor DO, Jasty M, Haire T, Harris WH.** Dynamic measurement of interface mechanics in vivo and the effect of micromotion on bone ingrowth into a porous surface device under controlled loads in vivo. *Transcripts of the 37th Annual Meeting of the Orthopaedic Research Society* 1991;16:103.
- 6 **Viceconti M, Muccini R, Bernakiewicz M, Baleani M, Cristofolini L.** Large-sliding contact elements accurately predict levels of bone-implant micromotion relevant to osseointegration. *J Biomech* 2000;33(12):1611-8.
- 7 **Tarala M, Janssen D, Telka A, Waanders D, Verdonschot N.** Experimental versus computational analysis of micromotions at the implant-bone interface. *Proc Inst Mech Eng H* 2011;225(1):8-15.
- 8 **Bitsakos C, Kerner J, Fisher I, Amis AA.** The effect of muscle loading on the simulation of bone remodelling in the proximal femur. *J Biomech* 2005;38(1):133-9.
- 9 **Heller MO, Bergmann G, Kassi JP, Claes L, Haas NP, Duda GN.** Determination of muscle loading at the hip joint for use in pre-clinical testing. *J Biomech* 2005;38(5):1155-63.
- 10 **Duda GN, Heller M, Albinger J, Schulz O, Schneider E, Claes L.** Influence of muscle forces on femoral strain distribution. *J Biomech* 1998;31(9):841-6.
- 11 **Jonkers I, Sauwen N, Lenaerts G, Mulier M, Van der Perre G, Jaecques S.** Relation between subject-specific hip joint loading, stress distribution in the proximal femur and bone mineral density changes after total hip replacement. *J Biomech* 5-12-2008;41(16):3405-13.
- 12 **Kleemann RU, Heller MO, Stoeckle U, Taylor WR, Duda GN.** THA loading arising from increased femoral anteversion and offset may lead to critical cement stresses. *J Orthop Res* 2003;21(5):767-74.
- 13 **Speirs AD, Heller MO, Duda GN, Taylor WR.** Physiologically based boundary conditions in finite element modelling. *J Biomech* 2007;40(10):2318-23.
- 14 **Wagner DW, Divringi K, Ozcan C, Grujicic M, Pandurangan B, Grujicic A.** Combined musculoskeletal dynamics/structural finite element analysis of femur physiological loads during walking. *Multidiscipline Modeling in Materials and Structures* 2010;6(4):417-37.
- 15 **Keyak JH, Falkinstein Y.** Comparison of in situ and in vitro CT scan-based finite element model predictions of proximal femoral fracture load. *Med Eng Phys* 2003;25(9):781-7.
- 16 **Pancanti A, Bernakiewicz M, Viceconti M.** The primary stability of a cementless stem varies between subjects as much as between activities. *J Biomech* 2003;36(6):777-85.
- 17 **Rasmussen J, Damsgaard M, Voigt M.** Muscle recruitment by the min/max criterion -- a comparative numerical study. *J Biomech* 2001;34(3):409-15.
- 18 **Waanders D, Janssen D, Miller MA, Mann KA, Verdonschot N.** Fatigue creep damage at the cement-bone interface: an experimental and a micro-mechanical finite element study. *J Biomech* 13-11-2009;42(15):2513-9.
- 19 **Taylor M, Abel EW.** Finite element analysis of poor distal contact of the femoral component of a cementless hip endoprosthesis. *Proc Inst Mech Eng H* 1993;207(4):255-61.
- 20 **Viceconti M, Brusi G, Pancanti A, Cristofolini L.** Primary stability of an anatomical cementless hip stem: a statistical analysis. *J Biomech* 2006;39(7):1169-79.
- 21 **Pettersen SH, Wik TS, Skallerud B.** Subject specific finite element analysis of implant stability for a cementless femoral stem. *Clin Biomech (Bristol, Avon)* 2009;24(6):480-7.

- 
- 22 **Abdul-Kadir MR, Hansen U, Klabunde R, Lucas D, Amis A.** Finite element modelling of primary hip stem stability: the effect of interference fit. *J Biomech* 2008;41(3):587-94.
  - 23 **Engh CA, O'Connor D, Jasty M, McGovern TF, Bobyn JD, Harris WH.** Quantification of implant micromotion, strain shielding, and bone resorption with porous-coated anatomic medullary locking femoral prostheses. *Clin Orthop Relat Res* 1992;(285):13-29.
  - 24 **Baleani M, Cristofolini L, Toni A.** Initial stability of a new hybrid fixation hip stem: experimental measurement of implant-bone micromotion under torsional load in comparison with cemented and cementless stems. *J Biomed Mater Res* 15-6-2000;50(4):605-15.
  - 25 **Bühler DW, Berlemann U, Lippuner K, Jaeger P, Nolte LP.** Three-dimensional primary stability of cementless femoral stems. *Clin Biomech (Bristol, Avon)* 1997;12(2):75-86.
  - 26 **Monti L, Cristofolini L, Viceconti M.** Methods for quantitative analysis of the primary stability in uncemented hip prostheses. *Artif Organs* 1999;23(9):851-9.



*The effect of bone ingrowth  
depth on the tensile and shear  
strength of the implant-bone  
E-beam produced interface*



## Abstract

*New technologies, such as selective electron beam melting, allow to create complex interface structures to enhance bone ingrowth in cementless implants. The efficacy of such structures can be tested in animal experiments. Although animal studies provide insight into the biological response of new structures, it remains unclear how ingrowth depth is related to interface strength. Theoretically, there could be a threshold of ingrowth, above which the interface strength does not further increase.*

*To test the relationship between depth and strength we performed a finite element study on micro models with simulated uncoated and hydroxyapatite (HA) coated surfaces. We examined whether complete ingrowth is necessary to obtain a maximal interface strength.*

*An increase in bone ingrowth depth did not always enhance the bone-implant interface strength. For the uncoated specimens a plateau was reached at 1500µm of ingrowth depth. For the specimens with a simulated HA coating, a bone ingrowth depth of 500µm already yielded a substantial interface strength, and deeper ingrowth did not enhance the interface strength considerably. These findings may assist in optimizing interface morphology (its depth) and in judging the effect of bone ingrowth depth on interface strength.*

## Introduction

The success of cementless total hip arthroplasty (THA) relies on bone ingrowth into the metal structure. A good interface strength between metal and bone promotes long term stability of the implant. Surface characteristics of the metal structure, such as porosity, pore size and shape have a considerable effect on cell migration, adhesion and bone formation <sup>1-3</sup>.

High implant porosity provides more space for bone ingrowth and bone interlocking, which improves the strength of the implant-bone bond. Shear strength and the percentage of implant-bone contact of porous implants compared to rough ones was reported to be significantly increased <sup>4</sup>. Another study, which compared bone-implant contact in three different groups of nickel-titanium bone graft substitutes, reported the greatest implant-bone contact in the group with the highest porosity <sup>5</sup>.

There also appears to be an optimal pore size for bone ingrowth. An early study by Hulbert et al. <sup>6</sup> showed that pores below 100µm may prohibit mineralization of bone tissue, and pores below 75µm were reported to allow only fibrous tissue formation. In contrast, a study by Itala et al. <sup>7</sup> showed no threshold value for new bone ingrowth in pore sizes ranging from 50 to 125 µm under non-load-bearing conditions. A review study on implant fixation by bone ingrowth indicated the optimum pore size for bone ingrowth in the range of 100-400µm <sup>8</sup>. However, several studies showed that also larger pores allow ingrowth to occur <sup>2,9</sup>. One can conclude that, due to the wide variety of analyzed materials and pore shapes, the optimum range might be different for each particular structure and the site of application, requiring in-vivo testing of each combination.

Several studies have shown that bone ingrowth and its strength can be enhanced by applying an additional surface coating to improve surface bioactivity and osteoconductivity <sup>10</sup>. Coating materials such as calcium phosphate (CaP) and Hydroxyapatite (HA) can improve the area of bone ingrowth, the bone-to-implant contact fraction <sup>11,12</sup> and the implant-bone interface strength <sup>13</sup>. It has recently been shown in a rabbit study that laser-treated implants with an HA coating achieved higher removal torque values than uncoated specimens <sup>14</sup>.

Using new technologies, complex 3-dimensional shapes can be produced in which pore size and shape, and level of porosity of the interface structures can be easily varied. An example is the electron beam melting (EBM) technique. This technique allows to create structures of any desired shape, based on 3D computer-guided design <sup>15</sup>. The principle of this technology is the selective melting of powder layers by an electron beam under vacuum. The structures built with this technique are composed of Ti alloy (TiAlV).

The efficacy of new surface structures can be tested in animal experiments. In such studies, the bone ingrowth depth into the metal structure <sup>16,17</sup> or the interface shear strength at different time points is measured <sup>18,19</sup>. Typically, both histology and mechanical tests are performed in this type of research, requiring a large number of animals. However, it is not known how much ingrowth is actually needed to provide an adequate interface strength,

and how ingrowth depth and strength are related. The finite element method (FEM) is a valuable method to test such phenomena.

The present FEM study was designed to test the relationship between bone ingrowth depth and interface strength. We focused on the following research questions:

- 1 What is the relationship between interface strength and bone ingrowth depth for the uncoated and HA coated specimens?
- 2 Is a maximum ingrowth depth necessary to obtain an optimal interface strength? If not, which bone ingrowth depth can be considered sufficient?
- 3 Does interface coating enhance the interface strength?

## Materials and Methods

The FEM models were based on micro CT data of a titanium cubic enlarged structure (73% porosity and a pore size of 1.25mm) (Fig. 1), provided by the manufacturer (EURO-COATING Spa, Italy). In the previous animal experiment <sup>17</sup>, this particular structure yielded the greatest bone ingrowth depth compared to other EBM-produced structures. The size of the current FEM models (5x5x5 mm) embraced four symmetric pieces of the cubic enlarged structure. The bone structure was modeled in two ways: by solidly filling the cavities in the surface structure (simulating complete ingrowth with cortical bone), and by completely filling the cavities with a porous bone structure (Fig. 1). The porous bone structure had a face-centered cubic (fcc) arrangement of the empty pores, with a pore size of 740µm, resulting in 80% porosity of the bone structure <sup>20</sup>. The models were 3D meshed with four-noded tetrahedral elements using an FEM software package (MSC.Mentat 2007r1, MSC Software Corporation, Santa Ana, CA, USA). Mesh density (number of elements/model volume) of the metal structure was ~780/mm<sup>3</sup> and mesh density of the solid and porous bone structures ~815/mm<sup>3</sup> and ~8,750/mm<sup>3</sup>, respectively.

To assess the relationship between interface strength and bone ingrowth depth we simulated different ingrowth depths. We used the models with maximal ingrowth depth (2.3mm) to subsequently generate models with a reduced ingrowth depth. Thus, for both bone structures (solid and porous) five additional models were created (250, 500, 750, 1000, 1500µm ingrowth depth) by removing the elements below the levels of the corresponding ingrowth depths <sup>21</sup> (Fig. 1), which resulted in 12 unique FEM micro models in total. Both bone and metal were modeled isotropic, with a Young's modulus of 6.8GPa <sup>22</sup> and 105GPa (provided by the manufacturer) for the bone and the metal structure, respectively. Poisson's ratio was set to 0.3 for the metal and bone structures.

To measure interface strength under tension and shear, the models were loaded until failure. To simulate this process the bottom part of the model (metal) was fixed, while the bone was displaced with an incremental displacement in the tension or shear direction, while monitoring the reaction force of the top bone nodes (Fig. 1).

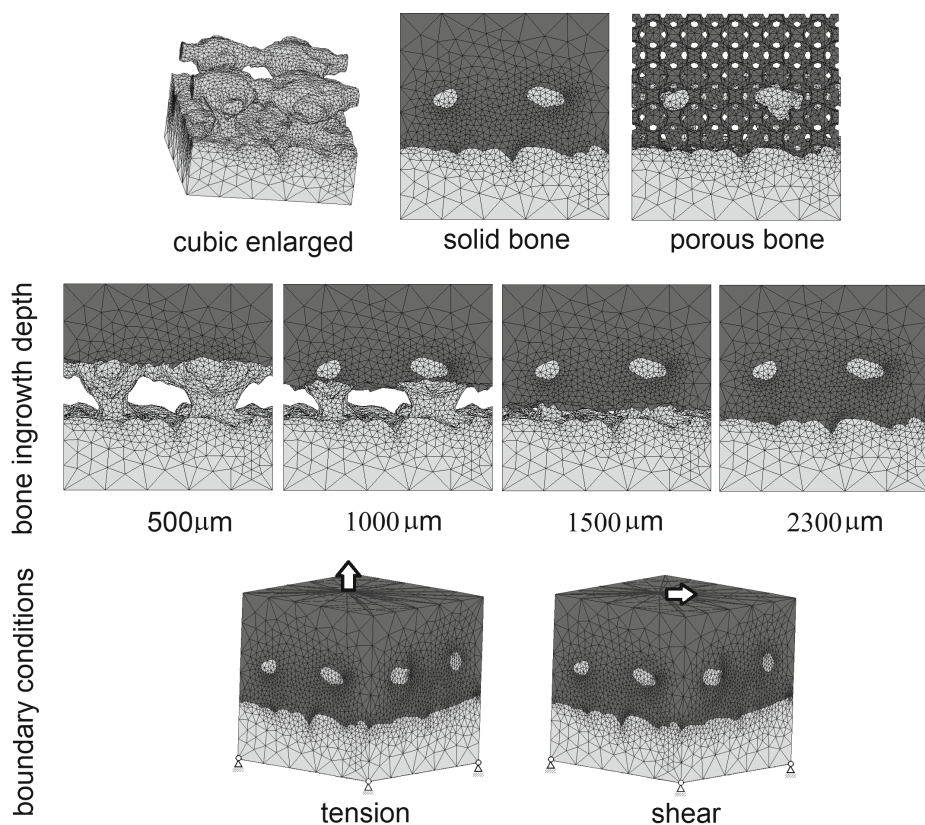


*Fig. 1 FEM micro models of the bone-implant interface with bone tissue modeled solid and porous. Various bone ingrowth depths were modeled. In order to quantify bone-implants interface strength, the metal part of the model was fixed at the bottom, while the bone was displaced with an incremental displacement in the tension or shear direction, while monitoring the reaction force of the top bone nodes.*

The apparent stress in tension or shear was computed by dividing the corresponding reaction force by the cross-sectional area of the interface (Fig. 2). The interface strength was defined as the maximum applied load divided by the cross-sectional area of the metal–bone interface. We simulated damage to the bone and metal using a modified in-house failure algorithm<sup>23</sup>. Only static failure was allowed to occur<sup>21</sup>. A crack could occur perpendicular to the principal stress direction when the stress of bone or metal exceeded their ultimate strength. The ultimate tensile bone strength was set to 47.5 MPa and was calculated from the equation proposed by Keyak et al.<sup>24</sup>. The ultimate tensile strength of the TiAlV alloy structure was set to 900MPa. Cracks could occur in any of the principal directions (three per element). A crack occurrence was simulated by setting the Young’s modulus perpendicular to the principal stress direction to 0.1MPa, while leaving the stiffness in the

other directions intact. If multiple cracks would occur, the stiffness in multiple directions would be reduced to 0.1 MPa resulting in a very compliant element.

To test the effect of an interface coating on the magnitude of interface strength we simulated two different interface conditions: (1) uncoated, simulated as a frictional interface (friction coefficient 0.3<sup>25</sup>), and (2) HA coated, modeled as a bonded interface. The bonded interface was simulated using the 'glue' option in MSC.MARC, while frictional contact between metal and bone was modeled using a double-sided node-to-surface coulomb contact algorithm<sup>26</sup>.

To assess whether implant fixation enhances with increasing bone ingrowth depth, the results for models with reduced ingrowth depths were compared with the values obtained for the model with simulated full ingrowth.

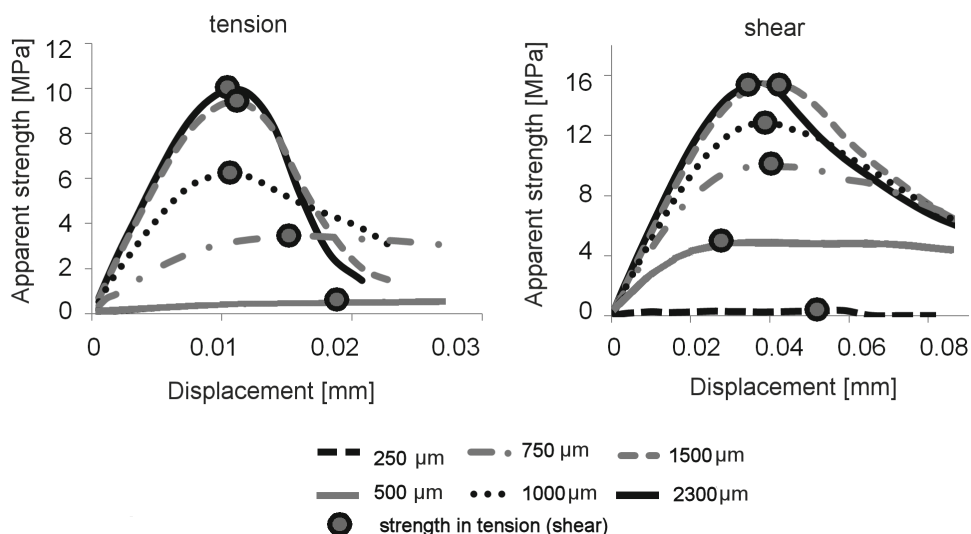


Fig. 2 An apparent strength-displacement curve was used to define the specimens' (implant plus bone) strength in tension and shear.

## Results

For the uncoated reconstructions, the interface strength increased with increasing ingrowth depth, but the relationship was not linear (Fig. 3). For these uncoated models 250 μm of ingrowth depth provided no tensile or shear strength at all, while only a slight strength occurred at 500 μm ingrowth depth. A close to maximal fixation strength for these models was obtained when the ingrowth depth reached 1500 μm (94% and 99% of max for the tensile and shear strength, respectively).

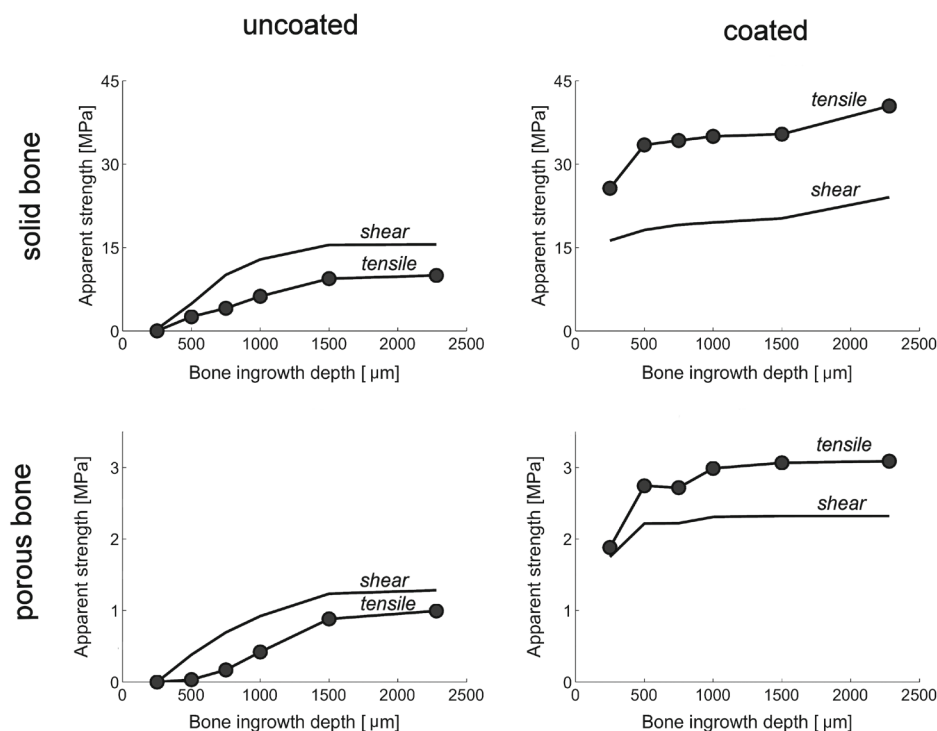


Fig. 3 For the uncoated specimens, the interface strength increased with increasing bone ingrowth depth. This relationship was considerably weaker for the HA coated specimens.

For the HA coated models the interface strength at 250μm ingrowth depth was already substantial (63% and 68% of max for the tensile and shear strength, respectively. Fig. 3). An ingrowth depth above 500μm for these models provided interface strength values in shear and tension that were comparable with those in the fully ingrown case scenario (83% and 76% of max for the tensile and shear strength, respectively). The ultimate shear strength of models with a fully ingrown interface did not differ considerably between the models with a simulated HA coating and the uncoated ones. However, the tensile strength was considerably improved for the HA coated interfaces. There was a strong relationship between the tensile and shear strength of the metal-bone interface ( $r^2 > 0.86$ , Fig. 4), which depended on the surface treatment. The strength of the metal-bone interface in shear was about 1.25 times stronger than in tension for the uncoated specimens and approximately 2 times stronger in tension than in shear for the HA coated ones. The crack pattern appeared to depend on the surface treatment. Damage under tension occurred only to the bone, while some damage also occurred to the metal under shear in the lower part of the porous cubic enlarged structure, but only for the specimens with solid bone and a simulated HA coating. The models with a simulated coating under tension produced cracks above the metal-bone

interface, while the other models produced cracks at the weakest point of the contact interface (Fig. 5). In all cases, more cracks were formed under shear than under tensile loading. For the uncoated models, the crack volume did not increase considerably with ingrowth depth when loaded in tension, while in shear this was the case. For the coated models, the crack volume increased with ingrowth depth (both in shear and tension).

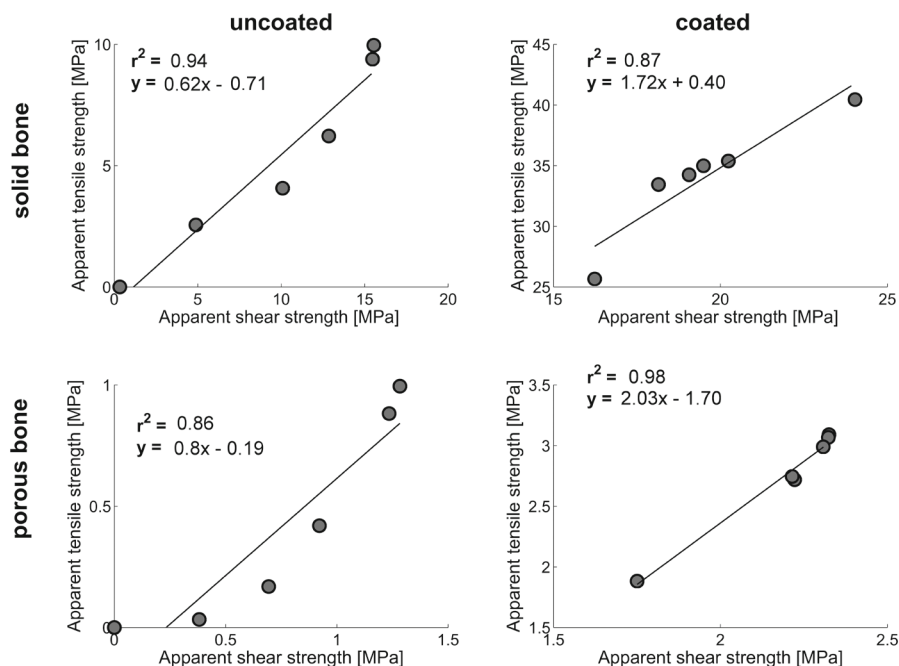
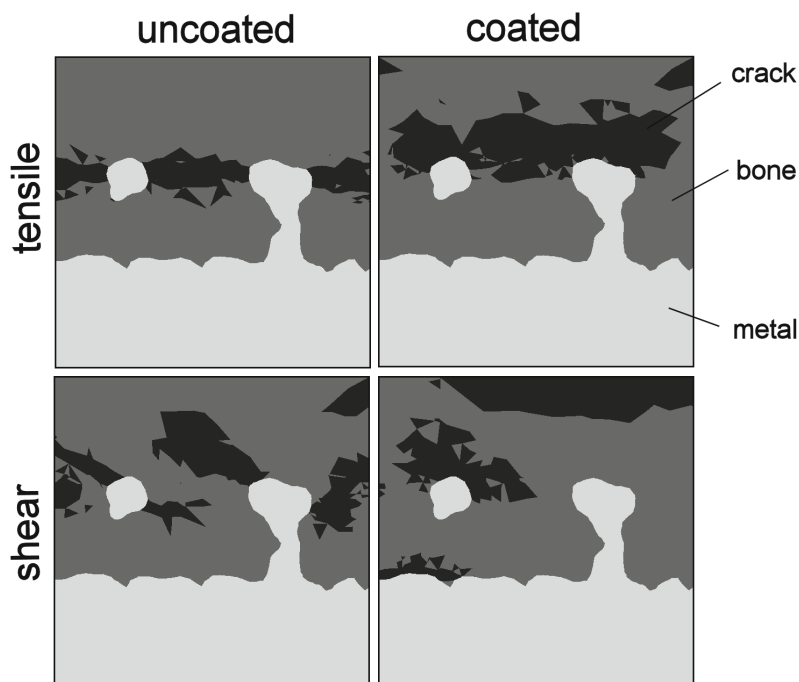


Fig. 4 The metal-bone interface was approximately 1.25 times stronger in shear than in tension for the uncoated specimens and approximately 2 times stronger in tension than in shear for the HA coated specimens.

There were quantitative but no qualitative differences between the strength of models with solid bone and porous bone (Fig. 3). Strong correlations were found between two bone representations for the uncoated models ( $r^2=0.99$ ,  $r^2=0.94$ ), and moderate ones for the models with the HA coated interfaces ( $r^2=0.87$ ,  $r^2=0.54$ ). The apparent ultimate strength in shear and tension was mainly 9 times smaller for the models with porous bone with respect to the solid bone models. A factor of 12 between the shear strengths of the solid and porous bone groups was present in the uncoated models. There were no differences in the localization of cracks between the two groups of models.



*Fig. 5 Crack formation in the metal-bone interface in tension and in shear for uncoated and HA coated specimens. The cross-sectioned view is taken through the center of the specimen.*

## Discussion

The current study presents the first FEM approach to assess the theoretical effect of bone ingrowth depth on the strength of metal-bone porous structures. The study was designed to give an insight into the clinical findings on porous interface structures. We built FEM micro models with variations in bone ingrowth depth and interface treatment (uncoated and HA coated). Subsequently, we computed the bone-metal interface strength for each model with reduced ingrowth and compared the value with maximum interface strength obtained for the complete bone ingrown case.

The first question we wanted to answer concerned the relationship between bone ingrowth depth and bone-implant interface strength. Our results suggest a strong relationship for the uncoated specimens, for which bone interface strength enhanced with increasing bone ingrowth depth. However, when a bone ingrowth of 1500 $\mu\text{m}$  was achieved the interface strengths both in shear and tension were comparable to the ones obtained in the completely ingrown case. For the HA coated specimens, increasing bone ingrowth depth did not considerably enhanced interface strength. Already at an ingrowth depth of 500 $\mu\text{m}$ , an interface strength comparable to the complete ingrown case was reached.



The aforementioned findings allowed us to answer the second question. Under the modeling conditions as simulated in this study (equal ingrown depth throughout the model without consideration of partial bonding effects), complete ingrowth does not seem to be necessary to obtain optimal interface conditions. However, the bone ingrowth depth threshold value for HA coated and uncoated specimens differed considerably. While 500 $\mu\text{m}$  of bone ingrowth depth appeared to be sufficient for the HA coated specimens, at least 1500 $\mu\text{m}$  was required for the uncoated ones.

Our third question concerned the effect of the HA coating on the interface strength in tension and shear. Furthermore, we were interested in the crack patterns that occur at the interface when uncoated and coated interfaces are modeled. Considering only mechanical effect of HA coating (and ignoring the biological potential of HA coatings), the results showed that in tension an HA coated interface is considerably stronger than the uncoated one, while the shear strength in models with complete ingrowth was not considerably improved by a coating treatment.

Although quadratic elements are better capable of capturing the bending behavior, the models in the present study were built of linear tetrahedrons. The reason for this choice is the current problem is clearly contact-driven, and linear elements are more suitable for the node-to-surface contact algorithm adopted here for modeling frictional contact (MSC. Marc). Moreover, we balanced computational expense with model accuracy.

The size of the elements in our models was chosen to well model complex morphologies of the metal structure and assure relatively low computational time. Further refinement of elements would require massive computational power. In the same lines, we only meshed a representative section to make sure we could run the models, even though the specimens which we based our models on were larger. One could argue that our failure algorithm is mesh dependent, meaning that bigger elements have to absorb more energy to fail than the small ones. However, the mesh (element size and element distribution) was the same in each model, therefore the mesh dependence effect of failure algorithm was constant. Although we did not perform a convergence study to assess mesh dependencies for this particular bone-metal interfacial behavior we have performed extensive experimental verification studies in the past with similar meshes focusing on bone-cement interface micro-mechanics<sup>21</sup> and we therefore expect that the mesh density as used in this study is adequate for our purposes.

In a parametric study, we also analyzed the effect of the friction coefficient (uncoated models) by setting friction coefficient to 0.05, 0.3 and 1 and it turned out that the friction coefficient had relatively little effect on the interfacial strength. For a model with simulated full ingrowth, the interface shear strength was equal to 14.4MPa, 16MPa and 17.2MPa for  $\mu=0.05$ ,  $\mu=0.3$  and  $\mu=1$ , respectively. The interface tensile strength was 10.2MPa, 10.2 MPa and 8.9MPa for  $\mu=0.05$ ,  $\mu=0.3$  and  $\mu=1$ , respectively. For the model with 1000 $\mu\text{m}$  bone ingrowth, the interface shear strength was 11.2MPa, 13.2MPa and 15.3MPa for  $\mu=0.05$ ,  $\mu=0.3$  and  $\mu=1$ , respectively, while the tensile strength was equal to 5.8MPa, 6.4MPa and

6.8MPa for  $\mu=0.05$ ,  $\mu=0.3$  and  $\mu=1$ , respectively. Interface strengths for models with  $\mu=1$  were much lower than models with bonded interfaces indicating that high friction cannot mechanically replace an actual bonding interfacial characteristic. In summary, the interface strength increased with friction coefficient, mainly noticeable in the shear direction. Unfortunately we do not have experimental data to validate the current choice of friction coefficient, although our results allow for a qualitative comparison of the effect of ingrowth depth on interface strength.

The models presented in the current study represent theoretical cases of ingrowth depth variations, and their possible effect on the interface strength under tensile and shear loads. The models were not based on actual ingrown surfaces retrieved from our previous animal study [17], as it was not possible to discern the interdigitated bone tissue on micro CT scans. Hence, representation of partial bonding or differentiation of bony properties were not included in the model leading to the fact that the results of this study should be considered at a qualitative basis. Unfortunately, no mechanical tests were performed in the animal study, which would have enabled us to verify the strength values predicted by our models. However, it is worth mentioning that the values of tensile strength simulated in the present study for the HA coated specimen with porous bone (1.8-2.1 MPa) were in the same range as those reported in a previous study on a plasma-sprayed HA coating–titanium implant<sup>27</sup> (0.66-1.12 MPa) given the fact that both studies differed in exact geometry, bone properties and bonding characteristics.

Additional limitations to the current FEM models further impede a direct comparison with mechanical tests performed with specimens retrieved from animal experiments. In our FEM models the degradation and delamination in time of the interface coating was not modeled physically, thus, its degradation and delamination in time could not be simulated. In addition, the effect of bone maturation on its strength in time was neglected, while a previous study<sup>27</sup> reported three different mechanisms of bone-implant interface failure, in the localization of failure (bone or coating) strongly depended on time. As neither the HA coating nor bone maturation was simulated physically, we were unable to reproduce failure patterns corresponding to that study. However, failure modes similar to the ones predicted by our FEM models have been shown in physical experiments. A previous study reported the fracture line close to the implant surface for the smooth cylinders, while at a distance of 1-2 mm from the implant surface for the implants with axial groves<sup>28</sup>. Bone was represented in our models either as a solid or a porous structure. Both representations do not capture the “true” ingrowth morphology, but interestingly, the models with solid and porous bone showed a similar relationship between bone ingrowth depth and interface strength. This may suggest that interface failure does not qualitatively depend on the method in which bone structure is simulated but that the increase in strength is more driven by the morphology of the porous structure of the metal surface. However, whether this hypothesis is true can only be assessed by studying various metal-bone interfaces in animal experiments. To avoid CT image artifacts of the metal components, high resolution

images of sequential histological sections of retrieved specimens from animal experiments are required for model creation.

Evidently, the results presented here are valid only for one particular surface structure. However, this methodology offers evaluation of the mechanical response of novel surface structures, without needing to perform a large scale animal experiment. Hence, this approach may be very suitable particularly in the design phase of new interface structures, requiring only the creation and analysis of FEM models of the particular structure.

Despite its limitations the findings of the present study can aid in judging the theoretical efficacy of bone ingrowth reported in animal studies. For instance, an in-house animal experiment with goats<sup>17</sup> reported ingrowth depth values into uncoated cubic enlarged structure of  $850\mu\text{m}\pm 223\mu\text{m}$  and  $1,258\mu\text{m}\pm 414\mu\text{m}$  at 2 and 6 weeks postoperatively, respectively. Based on the current results, the ingrowth depth at 2 weeks postoperatively may not be sufficient to guarantee a maximal interface strength for the uncoated specimens. However, for the HA coated structures it would already ensure good stability. Bone ingrowth depth reported at 6 weeks postoperatively would be already optimal for both the HA coated and uncoated cubic enlarged interface structures. However, as explained above one needs to be careful when interpreting the results obtained in the current study since it is difficult to judge which interface strength is sufficient *in vivo*. All the comparisons we make are with respect to the cases with complete bone ingrowth. It is well possible that a stable interface condition does not require maximal strength, and already a percentage of the maximum possible strength is sufficient. Alternatively, it may be possible that the maximal strength may not be sufficient to fixate an implant adequately. As a result, in the present study we are only able to state whether the values measured with the deficient ingrowth models are different or not from the case with complete ingrowth.

Our FEM study tested the theoretical relationship between bone ingrowth depth and interface strength. The results suggest that an increase in bone ingrowth depth does not always enhance bone-implant interface strength. Therefore, the maximum ingrowth depth is not always necessary. Our simulations with approximated interface conditions showed that the threshold of bone ingrowth assuring optimal interface strength is likely to be lower for the HA coated specimens thanks to the better bone attachment strength to HA coating. The findings of the present study may assist in optimizing the shape and depth of implant's interface and judging the efficacy of bone ingrowth depth (as measured in animal studies) on interface strength. Further development of this simulation is warranted so that it can be used to pre-clinically assess the effect of metal surface morphology on the bone-metal interface under multi-axial loading conditions.

---

## Acknowledgements

This study was partly sponsored by Eurocoating SpA (Trento, Italy) and “Provincia Autonoma di Trento” under the project called “E-Ortho”. The authors would like to thank Pierfrancesco Robotti and Emanuele Magalini (Eurocoating, Trento, Italy), who actively participated in this study and provided the CT scan of the EBM produced structures.

## Reference List

- 1 **Brentel AS, de Vasconcellos LM, Oliveira MV, Graca ML, de Vasconcellos LG, Cairo CA, Carvalho YR.** Histomorphometric analysis of pure titanium implants with porous surface versus rough surface. *J Appl Oral Sci* 2006;14(3):213-8.
- 2 **Frosch KH, Barvencik F, Viereck V, Lohmann CH, Dresing K, Breme J, Brunner E, Stürmer KM.** Growth behavior, matrix production, and gene expression of human osteoblasts in defined cylindrical titanium channels. *J Biomed Mater Res A* 1-2-2004;68(2):325-34.
- 3 **Jin QM, Takita H, Kohgo T, Atsumi K, Itoh H, Kuboki Y.** Effects of geometry of hydroxyapatite as a cell substratum in BMP-induced ectopic bone formation. *J Biomed Mater Res* 15-12-2000;52(4):491-9.
- 4 **Vasconcellos LM, Oliveira MV, Graca ML, Vasconcellos LG, Cairo CA, Carvalho YR.** Design of dental implants, influence on the osteogenesis and fixation. *J Mater Sci Mater Med* 2008;19(8):2851-7.
- 5 **Kujala S, Ryhänen J, Danilov A, Tuukkanen J.** Effect of porosity on the osteointegration and bone ingrowth of a weight-bearing nickel-titanium bone graft substitute. *Biomaterials* 2003;24(25):4691-7.
- 6 **Hulbert SF, Young FA, Mathews RS, Klawitter JJ, Talbert CD, Stelling FH.** Potential of ceramic materials as permanently implantable skeletal prostheses. *J Biomed Mater Res* 1970;4(3):433-56.
- 7 **Itälä AI, Ylänen HO, Ekholm C, Karlsson KH, Aro HT.** Pore diameter of more than 100 microm is not requisite for bone ingrowth in rabbits. *J Biomed Mater Res* 2001;58(6):679-83.
- 8 **Kienapfel H, Sprey C, Wilke A, Griss P.** Implant fixation by bone ingrowth. *J Arthroplasty* 1999;14(3):355-68.
- 9 **Hollister SJ, Lin CY, Saito E, Lin CY, Schek RD, Taboas JM, Williams JM, Partee B, Flanagan CL, Diggs A, Wilke EN, Van Lenthe GH, Muller R, Wirtz T, Das S, Feinberg SE, Krebsbach PH.** Engineering craniofacial scaffolds. *Orthod Craniofac Res* 2005;8(3):162-73.
- 10 **Zhang E, Zou C.** Porous titanium and silicon-substituted hydroxyapatite biomodification prepared by a biomimetic process: characterization and in vivo evaluation. *Acta Biomater* 2009;5(5):1732-41.
- 11 **Nguyen HQ, Deporter DA, Pilliar RM, Valiquette N, Yakubovich R.** The effect of sol-gel-formed calcium phosphate coatings on bone ingrowth and osteoconductivity of porous-surfaced Ti alloy implants. *Biomaterials* 2004;25(5):865-76.
- 12 **Wazen RM, Lefebvre LP, Baril E, Nanci A.** Initial evaluation of bone ingrowth into a novel porous titanium coating. *J Biomed Mater Res B Appl Biomater* 2010;94(1):64-71.
- 13 **Søballe K, Hansen ES, Brockstedt-Rasmussen H, Hjortdal VE, Juhl GI, Pedersen CM, Hvid I, Bünger C.** Gap healing enhanced by hydroxyapatite coating in dogs. *Clin Orthop Relat Res* 1991;(272):300-7.
- 14 **Faeda RS, Tavares HS, Sartori R, Guastaldi AC, Marcantonio E Jr.** Biological performance of chemical hydroxyapatite coating associated with implant surface modification by laser beam: biomechanical study in rabbit tibias. *J Oral Maxillofac Surg* 2009;67(8):1706-15.
- 15 **Heinl P, Müller L, Körner C, Singer RF, Müller FA.** Cellular Ti-6Al-4V structures with interconnected macro porosity for bone implants fabricated by selective electron beam melting. *Acta Biomater* 2008;4(5):1536-44.
- 16 **Li JP, Habibovic P, van den DM, Wilson CE, de W, Jr., van Blitterswijk CA, de GK.** Bone ingrowth in porous titanium implants produced by 3D fiber deposition. *Biomaterials* 2007;28(18):2810-20.
- 17 **Biemond JE, Hannink G, Jurrius A, Verdonschot N, Buma P.** In vivo assessment of bone ingrowth potential of 3-dimensional E-beam produced implant surfaces and the effect of additional treatment by acid-etching and hydroxyapatite coating. *Journal of Biomaterials Applications* 2010;
- 18 **Buser D, Nydegger T, Oxland T, Cochran DL, Schenk RK, Hirt HP, Snétivy D, Nolte LP.** Interface shear strength of titanium implants with a sandblasted and acid-etched surface: a biomechanical study in the maxilla of miniature pigs. *J Biomed Mater Res* 1999;45(2):75-83.
- 19 **Bobyn JD, Stackpool GJ, Hacking SA, Tanzer M, Krygier JJ.** Characteristics of bone ingrowth and interface mechanics of a new porous tantalum biomaterial. *J Bone Joint Surg Br* 1999;81(5):907-14.
- 20 **Majumdar S, Kothari M, Augat P, Newitt DC, Link TM, Lin JC, Lang T, Lu Y, Genant HK.** High-resolution magnetic resonance imaging: three-dimensional trabecular bone architecture and biomechanical properties. *Bone* 1998;22(5):445-54.

- 
- 21 **Waanders D, Janssen D, Mann KA, Verdonshot N.** The mechanical effects of different levels of cement penetration at the cement-bone interface. *J Biomech* 19-4-2010;43(6):1167-75.
  - 22 **Rho JY, Ashman RB, Turner CH.** Young's modulus of trabecular and cortical bone material: ultrasonic and microtensile measurements. *J Biomech* 1993;26(2):111-9.
  - 23 **Stolk J, Verdonshot N, Murphy BP, Prendergast PJ, Huiskes R.** Finite element simulation of anisotropic damage accumulation and creep in acrylic bone cement. *Eng Fract Mech* 2004;71:513-28.
  - 24 **Keyak JH, Kaneko TS, Tehranzadeh J, Skinner HB.** Predicting proximal femoral strength using structural engineering models. *Clin Orthop Relat Res* 2005;(437):219-28.
  - 25 **Rancourt D, Shirazi-Adl A, Drouin G, Paiement G.** Friction properties of the interface between porous-surfaced metals and tibial cancellous bone. *J Biomed Mater Res* 1990;24(11):1503-19.
  - 26 **Janssen D, Mann KA, Verdonshot N.** Micro-mechanical modeling of the cement-bone interface: the effect of friction, morphology and material properties on the micromechanical response. *J Biomech* 14-11-2008;41(15):3158-63.
  - 27 **Lin H, Xu H, Zhang X, de GK.** Tensile tests of interface between bone and plasma-sprayed HA coating-titanium implant. *J Biomed Mater Res* 1998;43(2):113-22.
  - 28 **Pröbster L, Voigt C, Fuhrmann G, Gross UM.** Tensile and Torsional Shear-Strength of the Bone Implant Interface of Titanium Implants in the Rabbit. *Journal of Materials Science-Materials in Medicine* 1994;5(6-7):314-9.



## ***The effect of bone ingrowth depth on the tensile and shear strength of implant-bone interface***

***Comparison between a geometrically ordered  
and random EBM and laser produced structure***



## Abstract

*Techniques, such as electron beam melting (EBM) and direct metal laser sintering (LASER), allow to manufacture complex porous metal surfaces. However, the effect of surface parameters on interface strength cannot be easily predicted. Therefore, new structures need to be tested using histology or mechanical tests. These mechanical tests can be partly mimicked using finite element method (FEM).*

*The goal of the present FEM study was to analyze whether the strength of a metal-bone interface will differ when the metal surface structure is geometrically ordered or random (produced with the LASER and EBM techniques). We also quantified the magnitude of histomorphometric parameters and correlated these to interface strength.*

*Interface strength was sensitive to the degree of surface order, being greater for the ordered structures. Histomorphometric parameters positively correlated with interface strength, but only up to 750 $\mu$ m of bone ingrowth depth. Theoretical prediction of interface strength based on the magnitude of histomorphometric parameters as used in this study was proven not possible.*

---

## Introduction

The survival of cementless implants depends on bone ingrowth into the metal interface structure. There are multiple factors which have an effect on bone ingrowth. For instance, there are biological processes like cell migration and adhesion, which are stimulated by osteoconductive coatings <sup>1-4</sup>. There are also multiple morphology-related factors, such as pore size <sup>5</sup>, porosity <sup>6-8</sup>, and surface roughness <sup>9,10</sup>. These morphological parameters are mainly a result of the chosen surface topography and manufacturing technique.

There are multiple techniques which allow manufacturing metal surfaces with any desired surface characteristic. The electron beam melting (EBM)<sup>11</sup> and direct metal laser sintering <sup>12,13</sup> techniques are both based on rapid prototyping from metal powder in a layer by layer manner. During the prototyping each layer of a CAD defined geometry is melted by electron beam or laser exposure. Both techniques allow obtaining complex interface structures of any desired shape and porosity up to a certain level of porosity. One of the main differences is surface detail, defined by the accuracy of the process (diameter of beam focus), much higher for laser. Furthermore, EBM technology is more energy efficient than laser technology <sup>11</sup>.

New surface structures are often tested in animal experiments, because the effects of changes in pore size and porosity on bone ingrowth cannot be easily predicted. Commonly, a histology study is performed <sup>14</sup> providing information on maximum ingrowth depth, direct implant-bone contact length and bone ingrown volume. Interface shear strength of new structures is often measured in a push out test <sup>8</sup>. In the study by Oh et al. <sup>15</sup> the magnitude of ultimate interface strength was attributed to bone-implant contact length at varied time points. Also in other studies the results of mechanical tests on bone-implant interfaces were reflected in histomorphometric results <sup>16,17</sup>. It can therefore be assumed that deeper bone ingrowth or greater implant-bone contact assure greater interface strength. However, this assumption may not be correct along the whole ingrowth depth range. As shown in our previous study <sup>18</sup>, there seems to be a threshold beyond which further increase in bone ingrowth depth does not necessarily enhance interface strength. Naturally, the magnitude of this threshold may differ between different porous structures, due to differences in their morphology.

The goal of the present finite element (FE) study was to compare the theoretical mechanical response of an interface with a geometrically ordered and a random surface structure produced using the LASER and EBM technique. The geometrically ordered structure consisted of a repetitive wave shape, while the other consisted of randomly spread pieces.

We created FEM micro-models of the two LASER and two EBM-produced structures. Our interests focused on differences in metal-bone interface strength between geometrically ordered and random interfaces produced with both techniques. We also analyzed

the effect of metal-bone interlock, volume of ingrown bone, metal-bone contact area and ingrowth depth on interface strength. The following questions were addressed:

- 1 Can we expect a difference in interface strength yielded by geometrically ordered and random interfaces?
- 2 Is the effect of reduced bone ingrowth depth the same on interface tensile and shear strength?
- 3 Can the mechanical strength of a porous interface be explained by interface morphology parameters so that the theoretical strength can be estimated while designing these structures?

## Materials and Methods

Both manufacturing processes (LASER, EBM) were given the same computer-aided design (CAD) although adapted to the resolution input. Because the resolution of the EBM process in our study was smaller, the input shape had to be approximately 1.4 times greater when compared with the input for the laser technique. Two laser and two EBM-produced interface structures (ordered and random) were provided by the manufacturer (EUROCOATING Spa, Italy) (Fig.1). They were  $\mu$ CT scanned ((SkyScan micro-CT model 1072, Kontich, Belgium), pixel size of  $11.3\mu\text{m}$ ), and this data was subsequently used to create FEM micro-models ( $5\times 5\times 5\text{mm}$ ) (Fig. 2). Each model consisted of a solid metal layer ( $\sim 1.5\text{mm}$ , bottom), a metal-bone interface layer ( $\sim 2\text{mm}$ , middle) and a solid bone layer ( $\sim 1.5\text{mm}$ , top) (Fig. 2).

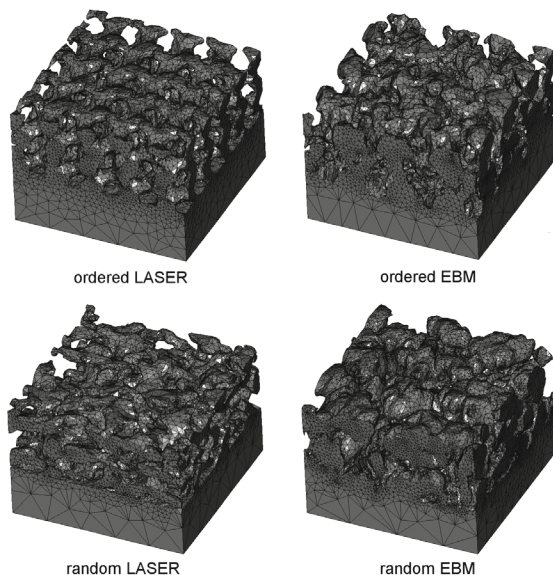


*Fig. 1 Two interface structures (ordered and random) produced using two technologies (EBM and LASER).*

The bone structure was modeled by solidly filling the cavities in the surface structure. The models were 3D meshed with four-noded tetrahedral elements using MIMICS 14.0 (Materialise, Belgium). The metal structures consisted of ~145,000 solid tetrahedral elements and the bone structures of ~121,000 elements.

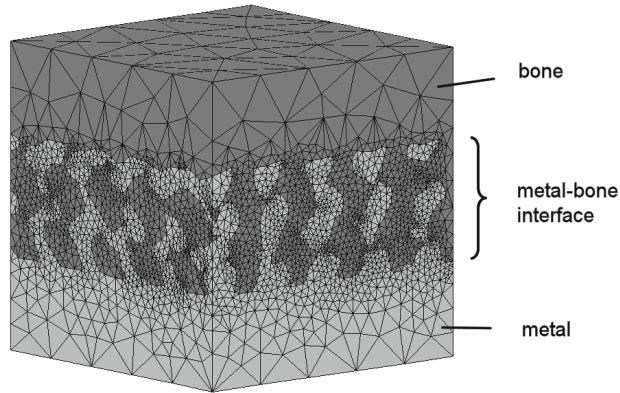


*Fig. 2 FE micro models consisted of top bone layer, metal-bone interface layer and bottom metal layer.*

We used the model with maximal ingrowth depth (2mm) to subsequently generate models with reduced ingrowth depths. The models with reduced ingrowth depths were generated by removing the elements below a defined level 19. In total, four cases were modeled: a complete ingrowth (~2mm), and 750 $\mu$ m, 500 $\mu$ m, 250 $\mu$ m of ingrowth depth. In total we created 16 unique FEM micro models (4 ingrowth depths, 2 structures, and 2 manufacturing techniques). Both bone and metal were modeled isotropic, with a Young's modulus of 6.8GPa and 105GPa for the bone and the metal structure, respectively. A frictional contact was assumed between bone and metal structure ( $\mu=0.3$ )<sup>20</sup>.

To measure interface strength under tension and shear, the models were loaded until failure. To simulate this process the top part of the model was fixed (bone), while the metal part was displaced with an incremental displacement of 2 $\mu$ m, while monitoring the reaction force of the bottom nodes of metal model. We simulated damage to the bone and metal using a modified in-house failure algorithm<sup>21</sup>. Only static failure was allowed to occur<sup>19</sup>. A crack could occur perpendicular to the principal stress direction when the stress of bone or metal exceeded their ultimate strength. The ultimate tensile bone strength was set to 47.5 MPa and was calculated from the equation proposed by Keyak et al.<sup>22</sup>. The ultimate tensile strength of the TiAlV alloy structure was set to 900MPa. Cracks could occur in any of the principal directions (three per element). A crack occurrence was simulated by setting the Young's modulus perpendicular to the principal stress direction to 0.1MPa, while leaving the stiffness in the other directions intact.

In order to test the effect of surface morphology on interface tensile strength we quantified two typical histology parameters: ingrowth volume and metal-bone contact area. With real animal experiments, histology measurements are preformed on 2D samples. Given that

we had a 3D model of all samples, we were able to measure the total bone volume and total bone-metal contact area.

We also computed the interface area of metal which is likely to contribute to the interface strength (creates an interlock with bone when displaced under tension) (Fig. 3). In short, the interlocking contact area was normalized to the loading direction, thereby determining the fraction of the contact area that could contribute to the interface strength. This weighted contribution was calculated for each model and correlated with the corresponding tensile strength.

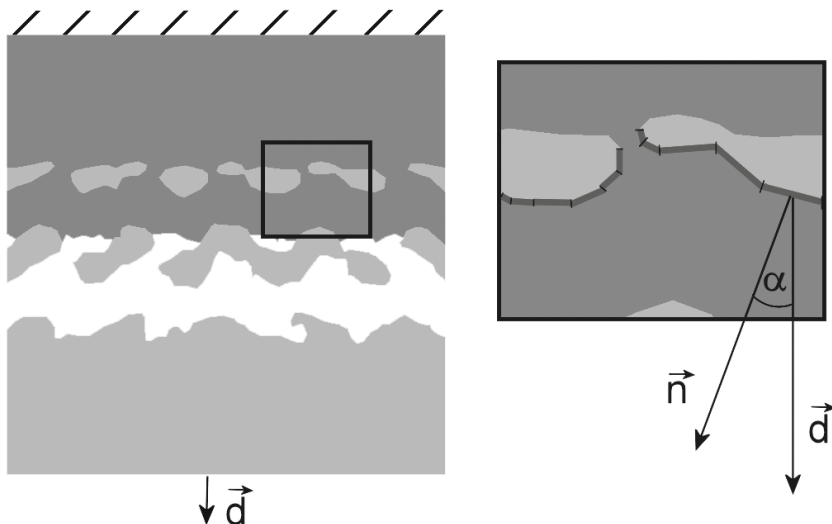


*Fig. 3 The weighted area of metal-bone interlock was equal to the summation of weighted contributions of all metal faces in direct contact with bone. It was assumed that a metal face would contribute to interface strength when its normal vector has the same direction as the tensile displacement vector. If the angle  $\alpha$  between the normal vector  $n$  of a metal face and the displacement vector  $d$  was between  $0$  and  $\pi/2$ , then the weighted contribution of this face would be equal to  $\cos(\alpha)$  multiplied by the face area. Hence, in case  $\alpha=0$  the contribution would be maximal, while in case  $\alpha = \pi/2$  a face would not contribute to interface strength.*

## Results

### Metal-bone interface strength

Under tension and tension the *ordered* structures were stronger than the *random* structures when compared within the same production technique (Fig. 4). The *ordered LASER* structure was the strongest in tension while the *ordered EBM* the strongest in shear.

All structures were slightly stronger in shear than in tension (Fig.4). Reduced bone ingrowth depth had a greater effect on interface strength in tension than in shear. In tension,

decreasing bone ingrowth depth caused a gradual decrease of tensile interface strength. Under shear, there was almost no effect of reduced bone ingrowth depth on interface strength, especially when bone ingrowth depth exceeded 500 $\mu\text{m}$ . Tensile strength of the samples with 250 $\mu\text{m}$  bone ingrowth was considerably lower, while in shear this reduction was considerably smaller.

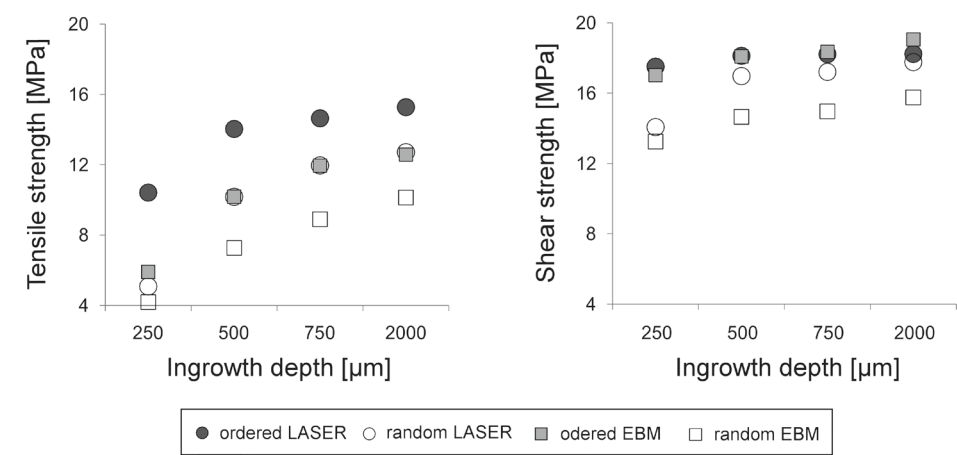


*Fig. 4 Theoretical tensile and shear strength of metal-bone interfaces with varying ingrowth depth.*

### Stresses in the bone

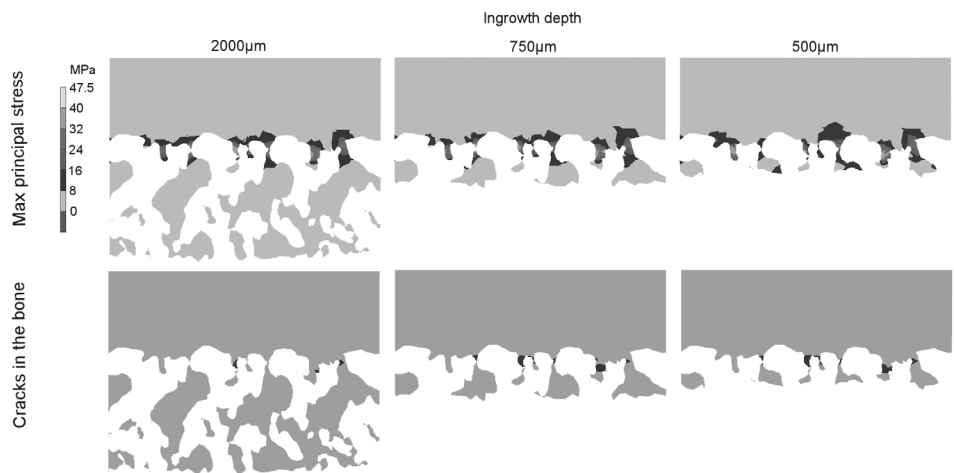


*Fig. 5 Maximum principal stress distribution in models of varied ingrowth depth in tension under the same loading conditions. The magnitude of stress increased with decreasing bone ingrowth depth.*

The maximal principal stress was increasing with decreasing bone ingrowth depth (Fig. 5). Bone in areas of deep ingrowth was not subjected to high stresses. Bone areas with high stress were corresponding between the models. Even though bone ingrowth depth varied, crack formation patterns were similar between the models (Fig. 5).

### Interface morphology vs. interface tensile strength

Up to the level of 750 $\mu$ m ingrowth, there was a correlation between each morphology parameter tested in the present study and interface tensile strength. An increase in magnitudes of ingrowth volume, contact area or weighted area of metal-bone interlock resulted in an increase of interface strength (Fig. 6). For the models with maximum ingrowth, no further increase in interface tensile strength occurred even though the magnitudes of each morphology parameter was considerably greater than in the models with 750 $\mu$ m bone ingrowth.

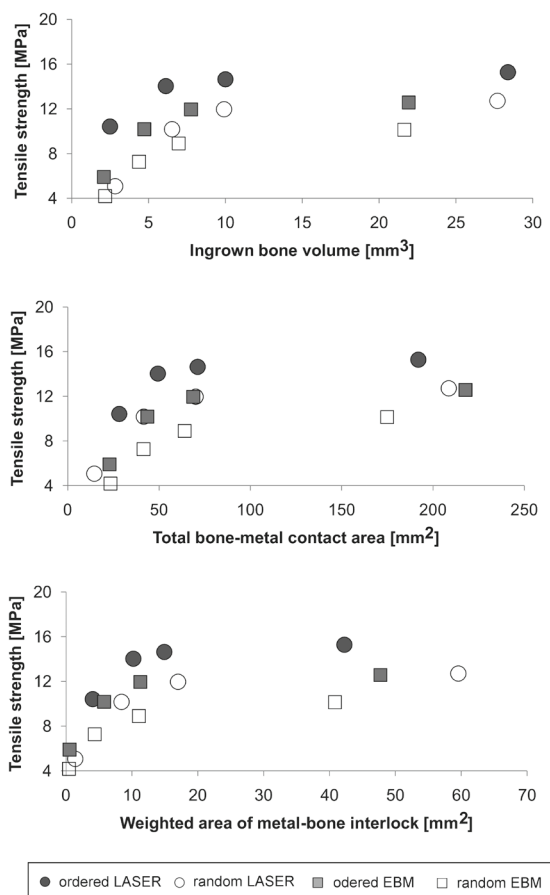


Fig. 6 Relationship between morphology parameters and theoretical tensile strength of metal-bone interfaces with simulated varied ingrowth depths.

---

For each of the morphological parameters, there appears to be a maximal value above which the particular parameter does not cause an increase of tensile strength (Fig. 6). For instance, the magnitudes of ingrown bone volume for the structures produced with the same technology were almost identical and still the *ordered* structures yielded greater interface strength. Furthermore, the *random LASER* produced interface had the greatest metal-bone interlock area but it did not result in the greatest interface tensile strength.

## Discussion

In the present FE study a geometrically ordered and a random interface produced using *EBM* and *LASER* techniques were compared in terms of interface tensile and shear strength. Furthermore, the effect of interface morphological parameters was studied.

We analyzed one geometrically ordered and one random interface structures produced with two different techniques. For both production techniques the ordered structures yielded greater tensile and shear strength than the random structures.

The effect of reduced bone ingrowth depth on interface tensile strength and shear strength was different. Tensile strength was reduced when bone ingrowth depth decreased, while shear strength was barely affected. The effect of reduced bone ingrowth depth on interface shear strength was negligible especially for samples with ingrowth depth greater than 500 $\mu\text{m}$ . Bone ingrowth depth of only 250 $\mu\text{m}$  resulted in relatively low interface tensile strength.

Finally, we wanted to answer the question whether the mechanical strength of a porous interface can be theoretically predicted by interface morphology parameters. Our results showed that, a relationship between bone volume in the porous metal structure and bone-metal contact area, and the interface strength existed only up to the level of 750 $\mu\text{m}$  bone ingrowth. Up to that level, an increase in the magnitude of morphology parameter resulted in enhancement of interface strength. Out of all morphology parameters tested in the current study, the metal-bone interlock appeared to be the best correlated with the interface tensile strength. However, for each of the parameters there was a threshold beyond which the interface strength did not increase, making it difficult to predict the mechanical strength of an interface based on morphology.

Results of the current study confirm our previous findings concerning the existence of a bone ingrowth threshold beyond which further increase in bone-ingrowth depth does not result in an increase of interface strength. It appears that this threshold can depend on how detailed the structure actually is, with a finer design requiring less interface depth, while coarse designs may need more interface depth to achieve an efficient interlock between metal and bone. Furthermore, the present study showed that bone in the deeper parts of the interface is not subjected to high stresses, and therefore does not considerably contribute to interface strength. This finding explains why the pattern of interface failure does not differ between interfaces with varied ingrowth depths.



Current FE models were built from linear tetrahedrons suitable for the node-to-surface contact algorithm adopted for modeling frictional contact (MSC.Marc). The chosen element size allowed us to accurately model complexity of each surface and at the same time assured a reasonable computational time. It needs to be mentioned that in our failure algorithm larger elements require greater energy to fail than the small ones. However, the effect of chosen element size on failure pattern for models with reduced bone ingrowth depth can be considered negligible given that the meshes had a similar element size distribution. One of the weaknesses of the present study is the fact that no fatigue but an instant damage of elements was simulated. Furthermore, we neglected the morphology of an ingrown bone, but bone structure was modeled as a solid. However, in our previous study<sup>18</sup> bone was modeled both as a porous and solid structure, displaying a very good correlation between the results of both types of bone representations. This indicates that neither the failure patterns nor the effect of reduced ingrowth depth on interface strength depends on the way the bone structure is modeled, justifying the current approach. In addition, in the present study the maturation of growing bone in time was not simulated. In the physiological situation, the effect of bone maturation can be seen in the localization of interface failure (occurring either to the bone or to the coating), which strongly depends on time<sup>23</sup>. In the study by Lin et al. (1998), failure after the tensile test occurred initially (at 2 and 4 weeks) mainly at the bony tissue, at 8 weeks inside the HA, and at 16 weeks at the HA coating-metal substrate interface, indicating bone maturation and degradation of the coating. Another weakness of the present study is related to the loading cases we chose. We tested the interface strength either in shear or in tension, while such pure direction of loading is rather unlikely to occur physically.

The choice of surfaces tested in the present study was made based on tensional resistance (tests performed by the manufacturer) and porosity parameters. Both surfaces were built at the highest capability of both technologies (greater for LASER) to obtain as small as possible pores. The resulting porosity ranged between 49 and 63%, reported suitable for bone ingrowth<sup>6</sup>. The LASER produced structures had on average 10% greater porosity than the EBM produced surfaces. This discrepancy can be explained by the size of CAD input files for both techniques (1.4:1 for the EBM and LASER technique, respectively). The differences in the size of input for both production techniques, are likely to affect the interface strength; therefore, a direct comparison between production techniques was not possible. Smaller parts in the structure would result in more interlock between bone and metal, already at a small ingrowth depth simulated, while no interlock is yet achieved for the coarser structure of the same shape. The effect of the CAD input size on results is likely most pronounced in the interface tensile strength magnitudes.

Unfortunately, the interface strength computed in the present study cannot be directly compared with any experimental data. However, the strength magnitudes in the current study are in the range of those yielded by our previous FE study with a cubic enlarged EBM surface<sup>18</sup>. In that study, the ultimate tensile and shear strength reached approx. 10

---

and 15.5MPa, respectively. In the present study the strength of the *ordered EBM* structure reached 12.6 and 19MPa under tension and shear, respectively. The strength of the *random EBM* structure was smaller: 10.1 and 15.8MPa under tension and shear, respectively. Although the *ordered* and cubic enlarged structures have geometrically ordered interfaces, their interface strengths are not corresponding, likely due to the differences in pore size and available metal-bone contact area (greater for the *ordered* surface). It appears that from a mechanical perspective the *ordered* structure is superior, likely thanks to a greater interlocking area. On the other hand, the strengths of the cubic enlarged and random structures were corresponding. Given that both interfaces differ in many aspects, this result confirms that interface strength cannot be predicted by the magnitude of metal-bone contact area or bone ingrowth depth magnitude.

The current study showed differences in interface strength when metal surface structure was geometrically ordered or random. The strength of metal-bone interface with geometrically ordered structure was greater than the strength of interface with a random structure. Our study also showed that histomorphometric parameters, such as bone-metal contact area, volume of ingrown bone or area of metal-bone interlock, are correlated with interface strength but only to a certain degree of bone ingrowth depth. Up to that threshold increasing magnitude of histomorphometric parameters results in an increase of interface strength. However, based on these parameters mechanical strength of an interface cannot be defined.

## Acknowledgements

This study was partly sponsored by Eurocoating SpA (Trento, Italy) and “Provincia Autonoma di Trento” under the project called “INSPIRED”. The authors would like to thank Pierfrancesco Robotti and Emanuele Magalini (Eurocoating, Trento, Italy), who actively participated in this study.

## Reference List

- 1 **Zhang E, Zou C.** Porous titanium and silicon-substituted hydroxyapatite biomodification prepared by a biomimetic process: characterization and in vivo evaluation. *Acta Biomater* 2009;5(5):1732-41.
- 2 **Caulier H, Van Der Waerden JP, Paquay YC, Wolke JG, Kalk W, Naert I, Jansen JA.** Effect of calcium phosphate (Ca-P) coatings on trabecular bone response: a histological study. *J Biomed Mater Res* 1995;29(9):1061-9.
- 3 **Cook SD, Thomas KA, Dalton JE, Volkman TK, Whitecloud TS, III, Kay JF.** Hydroxylapatite coating of porous implants improves bone ingrowth and interface attachment strength. *J Biomed Mater Res* 1992;26(8):989-1001.
- 4 **Søballe K, Hansen ES, Brockstedt-Rasmussen H, Hjortdal VE, Juhl GI, Pedersen CM, Hvid I, Bünger C.** Gap healing enhanced by hydroxyapatite coating in dogs. *Clin Orthop Relat Res* 1991;272:300-7.
- 5 **Itälä AI, Ylänen HO, Ekholm C, Karlsson KH, Aro HT.** Pore diameter of more than 100 microm is not requisite for bone ingrowth in rabbits. *J Biomed Mater Res* 2001;58(6):679-83.
- 6 **Kujala S, Ryhänen J, Danilov A, Tuukkanen J.** Effect of porosity on the osteointegration and bone ingrowth of a weight-bearing nickel-titanium bone graft substitute. *Biomaterials* 2003;24(25):4691-7.
- 7 **Wazen RM, Lefebvre LP, Baril E, Nanci A.** Initial evaluation of bone ingrowth into a novel porous titanium coating. *J Biomed Mater Res B Appl Biomater* 2010;94(1):64-71.
- 8 **Bobyn JD, Stackpool GJ, Hacking SA, Tanzer M, Krygier JJ.** Characteristics of bone ingrowth and interface mechanics of a new porous tantalum biomaterial. *J Bone Joint Surg Br* 1999;81(5):907-14.
- 9 **Brentel AS, de Vasconcellos LM, Oliveira MV, Graca ML, de Vasconcellos LG, Cairo CA, Carvalho YR.** Histomorphometric analysis of pure titanium implants with porous surface versus rough surface. *J Appl Oral Sci* 2006;14(3):213-8.
- 10 **Vasconcellos LM, Oliveira MV, Graca ML, Vasconcellos LG, Cairo CA, Carvalho YR.** Design of dental implants, influence on the osteogenesis and fixation. *J Mater Sci Mater Med* 2008;19(8):2851-7.
- 11 **Lindhe U, Larsson M, Harrysson O.** Rapid Manufacturing with Electron Beam Melting (EBM)-A Manufacturing Revolution, Direct Metal Fabrication.18-8-2003;
- 12 **Mangano C, Piattelli A, d'Avila S, Iezzi G, Mangano F, Onuma T, Shibli JA.** Early human bone response to laser metal sintering surface topography: a histologic report. *J Oral Implantol* 2010;36(2):91-6.
- 13 **Hollander DA, von WM, Wirtz T, Sellei R, Schmidt-Rohlfing B, Paar O, Erli HJ.** Structural, mechanical and in vitro characterization of individually structured Ti-6Al-4V produced by direct laser forming. *Biomaterials* 2006;27(7):955-63.
- 14 **Biamond JE, Hannink G, Jurrius A, Verdonshot N, Buma P.** In vivo assessment of bone ingrowth potential of 3-dimensional E-beam produced implant surfaces and the effect of additional treatment by acid-etching and hydroxyapatite coating. *Journal of Biomaterials Applications* 2010;
- 15 **Oh S, Tobin E, Yang Y, Carnes DL, Jr., Ong JL.** In vivo evaluation of hydroxyapatite coatings of different crystallinities. *Int J Oral Maxillofac Implants* 2005;20(5):726-31.
- 16 **Johansson CB, Han CH, Wennerberg A, Albrektsson T.** A quantitative comparison of machined commercially pure titanium and titanium-aluminum-vanadium implants in rabbit bone. *Int J Oral Maxillofac Implants* 1998;13(3):315-21.
- 17 **Castellani C, Lindtner RA, Hausbrandt P, Tschegg E, Stanzl-Tschegg SE, Zanoni G, Beck S, Weinberg AM.** Bone-implant interface strength and osseointegration: Biodegradable magnesium alloy versus standard titanium control. *Acta Biomater* 2011;7(1):432-40.
- 18 **Tarala M, Waanders D, Diamond JE, Hannink G, Janssen D, Buma P, Verdonshot N.** The effect of bone ingrowth depth on the tensile and shear strength of the implant-bone E-beam produced interface. *under review* 2011;
- 19 **Waanders D, Janssen D, Mann KA, Verdonshot N.** The mechanical effects of different levels of cement penetration at the cement-bone interface. *J Biomech* 19-4-2010;43(6):1167-75.
- 20 **Rancourt D, Shirazi-Adl A, Drouin G, Paiement G.** Friction properties of the interface between porous-surfaced metals and tibial cancellous bone. *J Biomed Mater Res* 1990;24(11):1503-19.

- 
- 21 **Stolk J, Verdonchot N, Murphy BP, Prendergast PJ, Huiskes R.** Finite element simulation of anisotropic damage accumulation and creep in acrylic bone cement. *Eng Fract Mech* 2004;71:513-28.
  - 22 **Keyak JH, Kaneko TS, Tehranzadeh J, Skinner HB.** Predicting proximal femoral strength using structural engineering models. *Clin Orthop Relat Res* 2005;(437):219-28.
  - 23 **Lin H, Xu H, Zhang X, de GK.** Tensile tests of interface between bone and plasma-sprayed HA coating-titanium implant. *J Biomed Mater Res* 1998;43(2):113-22.



# Chapter 10

## *General discussion*

Providing good implant stability is one of the main goals of any orthopedic implant design given that aseptic loosening, which is associated with inferior stability, has been reported as the main reason for revision surgery in total hip arthroplasty (THA) <sup>1</sup>. If good stability is achieved, physiological processes occurring in the bone or at the implant-bone interface are likely to improve implant survival. Good initial mechanical stability (achieved intra-operatively) provides ideal conditions for bone ingrowth by reducing the relative implant-bone motion. Subsequently, if the implant-bone interface is stabilized by osseointegration, the implant is likely to perform well on the longer term.

Finite element analysis (FEA) has been commonly used to simulate implant stability. Detailed FEA models of THA reconstructions combined with algorithms describing physiological processes occurring at the implant-bone interface or in the bone have been used to quantify effects of interface micromotions <sup>2-4</sup> or bone remodeling <sup>5-7</sup>.

The potential of FEA in predicting stability of orthopedic implants has increased over the years. Current models include more details and, due to improved computer capacities, the computer time to solve the calculations is still within a reasonable time frame. Furthermore, due to improved finite element algorithms it has become easier to simulate more physiological interface conditions such as gaps or friction at the interface. Commonly available scanning techniques, such as  $\mu$ CT, QCT or MRI, allow for building detailed case-specific models of bones with more realistic material properties <sup>8,9</sup>. Micro-CT scans of high accuracy provide detailed information for micro models; e.g. models of cement-bone interface <sup>10</sup>, trabecular bone architecture <sup>11</sup> or tissue engineering scaffolds <sup>12,13</sup>.

While improvements in modeling of THA reconstruction were achieved as a consequence of new techniques and technologies, the improvements to FEA predictions of implant stability were mainly made thanks to data obtained in experimental studies. For instance, bone ingrowth simulations would not be possible without the specification of parameters which govern this physiological process. Animal studies allowed defining the maximum micromotions and gaps magnitudes for bone ingrowth <sup>14,15</sup>, they proved that strength of ingrown bone increases in time <sup>15</sup>, showed the effect of using a surface coating <sup>16</sup> and of bone quality <sup>17</sup>. By implementing this information in algorithms combined with FEA models one could simulate bone osseointegration. Also in this thesis we implemented experimental findings to improve and develop FEA tools to simulate implant stability by quantifying interface micromotions (**Chapter 4**) or the bone ingrowth process (**Chapter 6**). The novelty of our stability simulation was the way in which we quantified interface micromotions. The new method takes into account the elastic deformation of bone, whereas this was neglected in previous studies. Thus, implant stability prediction was more physiological. Similarly, in the bone ingrowth process simulation we implemented additional factors (e.g. gradual increasing strength of ingrown bone in time) which are present in the osseointegration process. Thus, we simulated the stabilizing effect of growing bone on implant stability. The study presenting the bone ingrowth process showed that the effect of interface conditions modeled in FE reconstruction was greater than the stabilizing effect of

ingrown bone. Therefore, in order to further improve FEA predictability of implant stability we should focus on detailed and thorough modeling of implant-bone interface. This can be performed thanks to new scanning techniques. It needs to be mentioned that there are also other factors which can be crucial for reliable bone ingrowth process simulation. Therefore, further animal studies are required to define mathematical descriptions of processes occurring at the interface.

Bone remodeling simulations used in combination with FEA are based on the hypothesis posed by Wolff in 19th century<sup>18</sup>. Wolff observed that bone tissue would respond in terms of mass and structural orientation to the magnitude and direction of imposed forces. These observations were studied later in FEA models of bone, as these enable the prediction of stresses and strains in bone. Subsequently, a mathematical description of the bone remodeling theory was implemented in FEA models and validated with animal studies. Similarly to the implant stability prediction based on magnitudes of interface micromotions, also here a detailed and accurate modeling of the interface conditions is necessary (**Chapter 3**). The fixation manner between implant and bone has a considerable effect on remodeling prediction since it alters the patterns of load transfer between implant and bone<sup>19</sup>. Therefore, when new implant designs are tested in bone remodeling prediction, exact modeling of the interface and the effect of implant coating must be implemented. This again emphasizes the importance of animal and clinical studies in improving FEA predictions.

Clinical or experimental data provides an input for algorithms to mathematically describe physiological processes in bone after THA. Subsequently, detailed FEA models combined with algorithms can help in return to overcome limitations of some experimental studies (**Chapter 2**) or they can complement findings of animal experiments (**Chapter 8** and **9**). For instance, motion sensors which are used in experimental studies are often large and therefore it is questionable whether their attachment to a reconstruction does not affect the measurement. This can be tested using an algorithm to quantify micromotions by mimicking the experimental approach and quantifying micromotions at the actual implant-bone interface. In **Chapter 2**, using a validated FEA model we proved that the manner in which commonly used micromotion measurement sensors are attached to the reconstruction do not lead to reliable micromotion predictions. FEA simulations predicting stability or bone remodeling have been used in this thesis to test the effect of changes to implant design on implant stability (**Chapter 4** and **5**). Using FEA tools offers the potential to identify bad implants; the production costs can be reduced and time consuming animal test can be limited.

Not only the implant shape but also the composition of metal surface structures applied to the implant to enhance implant-bone interface strength can be optimized before time consuming experiments and costly animal tests are performed. In this thesis, we tested the correlation between bone ingrowth depth and interface strength of structures with various shapes and porosity (**Chapter 8** and **9**). We showed that histological data of bone ingrowth depth may not be sufficient to select the best performing structure design. Only up to a certain level an increase of ingrowth depth resulted in an increase of interface strength, and



this depth depends on the architecture of the porous surface structure. This finding can be of importance for the manufactures, the depth of interface surfaces could be reduced to their efficacy level resulting in reduction of costs. The findings presented in **Chapter 8** and **9** helped understanding the effect of magnitude of histomorphometric parameters on metal-bone interface strength. Thus, along with histology data they can help judging the actual interface quality and strength for a variety of porous surface designs.

A few chapters of this thesis aimed to improve FEA tools used to predict implant stability. We proposed a new method to quantify micromotions (**Chapter 2**), a combined ingrowth and bone remodeling approach to balance incompatible design goals (**Chapter 4**) and a simulation of bone ingrowth process (**Chapter 6**). The improvements in modeling of THA reconstructions were presented in **Chapter 7**. We applied a consistent set of muscle forces derived from the musculoskeletal modeling system Anybody™ to study the effects of detailed loading on the magnitude and direction of interface micromotions throughout a walking cycle. It allowed us to test the effect of loading simplifications in FEA models on implant stability prediction. In future studies, also other activities like stair climbing, running, etc. could be simulated by using data provided by musculoskeletal models. Furthermore, a collection of muscle force data could allow for an estimation of the loading variability between patients and can be used for sensitivity studies to test the robustness of prosthetic designs.

FEA models used in this thesis should be further improved in order to increase their predictability and reliability in simulating physiological processes. For instance, we modeled bone as an isotropic tissue while bone is anisotropic. Thus, applying orthotropic material properties to bone and properly orienting them along the irregular bone anatomy<sup>20,21</sup> would improve the models<sup>8</sup>. Other improvements to our FEA models could be made to the modeling of metal-bone interface. Using CT data of a THA reconstruction to create a FEA model one is not capable of capturing exact implant-bone interface due to low scanning resolution (pixel size greater than interface gap) or artifacts, such as starburst streaking<sup>22</sup>. Therefore, it remains difficult to create a model mimicking the exact implant-bone interface (distribution and magnitudes of the gaps). In models used in this thesis we simulated interface gaps in interface areas of low bone density and we modeled the amount of gaps as found in manually reamed cavities. Naturally, it is only an estimation of the actual implant-bone interface conditions. Given that the gap size has a rather considerable effect on implant stability<sup>23</sup>; by modeling an exact implant-bone interface we could reliably predict bone ingrowth for a specific reconstruction.

Not only the models but also the algorithms we proposed to simulate certain processes could be further improved. For instance, in our bone ingrowth simulation (**Chapter 6**) we could include the effect of growth factors<sup>24</sup> and bone vascularization<sup>25</sup> on bone remodeling. The effect of age could be also included given that the amount of some growth factors decreases with age<sup>26</sup>. Furthermore, bone maturation could be simulated in a more reliable way. In our bone ingrowth process simulation we did not simulate tissue differentiation but

---

its effect on mechanical stability of the implant. However, there have been other FEA studies in which tissue differentiation at the implant-bone interface was simulated by modeling the interaction between biophysical stimuli (tissue strain and fluid velocity) and tissue phenotype<sup>27,28</sup>. In those models the gap tissue had biphasic properties (solid and fluid). Tissue strain and fluid velocity distributions were calculated in an FEA model. Subsequently, based on their magnitudes tissue phenotype properties were updated. To improve bone ingrowth simulation presented in **Chapter 6** we could include the effect of biophysical stimuli as done in aforementioned studies. However, more experimental studies are needed to quantify the magnitudes of input parameters, such as permeability of varied tissue phenotypes. Currently, given the approximated thresholds of some parameters in both ingrowth simulations, by merging them, one would likely introduce further uncertainties.

In summary, to improve the predictive power of FEA simulations we should focus on implementing the results of recent and future experimental studies in algorithms so that physiological processes can be reliably simulated. We believe that future improvements to FEA predictions of implant stability will be possible thanks to new developments in measurement techniques and methodologies. Likely, the improvements will be seen in even more detailed modeling and data which will allow mimicking physiological conditions in a more personalized manner enabling pre-clinical testing of cementless implants in a more reliable and robust manner.

## Reference List

- 1 **Ulrich SD, Seyler TM, Bennett D, Delanois RE, Saleh KJ, Thongtrangan I, Kuskowski M, Cheng EY, Sharkey PF, Parvizi J, Stiehl JB, Mont MA.** Total hip arthroplasties: what are the reasons for revision? *Int Orthop* 2008;32(5):597-604.
- 2 **Caouette C, Yahia LH, Bureau MN.** Reduced stress shielding with limited micromotions using a carbon fibre composite biomimetic hip stem: a finite element model. *Proc Inst Mech Eng H* 2011;225(9):907-19.
- 3 **Pettersen SH, Wik TS, Skallerud B.** Subject specific finite element analysis of implant stability for a cementless femoral stem. *Clin Biomech (Bristol, Avon)* 2009;24(6):480-7.
- 4 **Fernandes PR, Folgado J, Ruben RB.** Shape optimization of a cementless hip stem for a minimum of interface stress and displacement. *Comput Methods Biomech Biomed Engin* 2004;7(1):51-61.
- 5 **Huiskes R, Weinans H, Van Rietbergen B.** The relationship between stress shielding and bone resorption around total hip stems and the effects of flexible materials. *Clin Orthop Relat Res* 1992;(274):124-34.
- 6 **Weinans H, Huiskes R, Van Rietbergen B, Sumner DR, Turner TM, Galante JO.** Adaptive bone remodeling around bonded noncemented total hip arthroplasty: a comparison between animal experiments and computer simulation. *J Orthop Res* 1993;11(4):500-13.
- 7 **Lin CL, Lin YH, Chang SH.** Multi-factorial analysis of variables influencing the bone loss of an implant placed in the maxilla: prediction using FEA and SED bone remodeling algorithm. *J Biomech* 3-3-2010;43(4):644-51.
- 8 **Trabelsi N, Yosibash Z.** Patient-specific finite-element analyses of the proximal femur with orthotropic material properties validated by experiments. *J Biomech Eng* 2011;133(6):061001.
- 9 **Rajapakse CS, Magland JF, Wald MJ, Liu XS, Zhang XH, Guo XE, Wehrli FW.** Computational biomechanics of the distal tibia from high-resolution MR and micro-CT images. *Bone* 2010;47(3):556-63.
- 10 **Waanders D, Janssen D, Miller MA, Mann KA, Verdonchot N.** Fatigue creep damage at the cement-bone interface: an experimental and a micro-mechanical finite element study. *J Biomech* 13-11-2009;42(15):2513-9.
- 11 **Van Rietbergen B, Majumdar S, Pistoia W, Newitt DC, Kothari M, Laib A, Ruegsegger P.** Assessment of cancellous bone mechanical properties from micro-FE models based on micro-CT, pQCT and MR images. *Technol Health Care* 1998;6(5-6):413-20.
- 12 **Lacroix D, Chateau A, Ginebra MP, Planell JA.** Micro-finite element models of bone tissue-engineering scaffolds. *Biomaterials* 2006;27(30):5326-34.
- 13 **Lacroix D, Planell JA, Prendergast PJ.** Computer-aided design and finite-element modelling of biomaterial scaffolds for bone tissue engineering. *Philos Transact A Math Phys Eng Sci* 28-5-2009;367(1895):1993-2009.
- 14 **Jasty M, Bragdon C, Burke D, O'Connor D, Lowenstein J, Harris WH.** In vivo skeletal responses to porous-surfaced implants subjected to small induced motions. *J Bone Joint Surg Am* 1997;79(5):707-14.
- 15 **Dalton JE, Cook SD, Thomas KA, Kay JF.** The effect of operative fit and hydroxyapatite coating on the mechanical and biological response to porous implants. *J Bone Joint Surg Am* 1995;77(1):97-110.
- 16 **Hara T, Hayashi K, Nakashima Y, Kanemaru T, Iwamoto Y.** The effect of hydroxyapatite coating on the bonding of bone to titanium implants in the femora of ovariectomised rats. *J Bone Joint Surg Br* 1999;81(4):705-9.
- 17 **Fini M, Giavaresi G, Rimondini L, Giardino R.** Titanium alloy osseointegration in cancellous and cortical bone of ovariectomized animals: histomorphometric and bone hardness measurements. *Int J Oral Maxillofac Implants* 2002;17(1):28-37.
- 18 **Wolff J.** Das Gesetz der Transformation der Knochen. Translated as The Law of Bone Remodeling (Maquet, P.; Furlong, R.) . *Springer-Verlag* 1986;
- 19 **Weinans H, Huiskes R, Grootenboer HJ.** Effects of fit and bonding characteristics of femoral stems on adaptive bone remodeling. *J Biomech Eng* 1994;116(4):393-400.
- 20 **Yosibash Z, Tal D, Trabelsi N.** Predicting the yield of the proximal femur using high-order finite-element analysis with inhomogeneous orthotropic material properties. *Philos Transact A Math Phys Eng Sci* 13-6-2010;368(1920):2707-23.

- 
- 21 **San Antonio T, Ciaccia M, Müller-Karger C, Casanova E.** Orientation of orthotropic material properties in a femur FE model: A method based on the principal stresses directions. *Med Eng Phys* 16-11-2011;
  - 22 **Zannoni C, Viceconti M, Pierotti L, Cappello A.** Analysis of titanium induced CT artifacts in the development of biomechanical finite element models. *Med Eng Phys* 1998;20(9):653-9.
  - 23 **Viceconti M, Brusi G, Pancanti A, Cristofolini L.** Primary stability of an anatomical cementless hip stem: a statistical analysis. *J Biomech* 2006;39(7):1169-79.
  - 24 **Baylink DJ, Finkelman RD, Mohan S.** Growth factors to stimulate bone formation. *J Bone Miner Res* 1993;8 Suppl 2:S565-S572.
  - 25 **Barou O, Mekraldi S, Vico L, Boivin G, Alexandre C, Lafage-Proust MH.** Relationships between trabecular bone remodeling and bone vascularization: a quantitative study. *Bone* 2002;30(4):604-12.
  - 26 **Nicolas V, Prewett A, Bettica P, Mohan S, Finkelman RD, Baylink DJ, Farley JR.** Age-related decreases in insulin-like growth factor-I and transforming growth factor-beta in femoral cortical bone from both men and women: implications for bone loss with aging. *J Clin Endocrinol Metab* 1994;78(5):1011-6.
  - 27 **Huiskes R, Van Driel WD, Prendergast PJ, Søballe K.** A biomechanical regulatory model for periprosthetic fibrous-tissue differentiation. *J Mater Sci Mater Med* 1997;8(12):785-8.
  - 28 **Prendergast PJ, Huiskes R, Søballe K.** ESB Research Award 1996. Biophysical stimuli on cells during tissue differentiation at implant interfaces. *J Biomech* 1997;30(6):539-48.



# Chapter **11**

---

## *Summary*

This thesis aimed to develop and improve upon FEA simulations which predict stability of cementless implants. A good understanding of bone ingrowth and bone remodeling processes was essential to achieve our goal. In **Chapters 2** and **3** we assessed the correspondence between FEA predictions and the experimental and clinical results. Subsequently, we studied the effect of surgical and implant-related parameters on implant stability (**Chapter 4** and **5**). In the following chapters, by proposing innovative FEA algorithms, we focused on the improvement of FEA tools used currently to judge implant stability. We proposed a simulation of bone ingrowth progression enriched by findings of animal studies (**Chapter 6**) and, a pioneering simulation to quantify interface micromotions throughout a complete activity of normal walking (**Chapter 7**). Finally, we focused on micro-mechanics of implant-bone interface (**Chapter 8** and **9**). We tested whether a theoretical prediction of interface strength for porous metal surface structures based on the magnitudes of bone ingrowth parameters is possible.

In this chapter, the findings of aforementioned studies will be summarized and their relevance towards the goal of this thesis, the development and improvement of FEA simulations to improve survival of cementless implants, will be assessed.

## The relation between FEA and clinical and experimental research

### Experimental versus FEA implant-bone micromotions (Chapter 2)

Any measurement method has its limitations. In experimental *in-vitro* set-ups, implant stability is generally tested under a simplified loading configuration<sup>1</sup>, and the measurement sensors and rigs are in some cases quite large,<sup>1-4</sup> which limits the validity of the measurement system due to deformations of the frame, bone and prosthetic system. On the other hand, FEA tools allow measurements in any desired location but are subject to many assumptions<sup>5</sup>. When an FEA model is properly validated the results are considered reliable. In **Chapter 2**, using a validated FEA model and micromotion measurement algorithm, the correlation between the experimental and computational quantification of interface micromotions was studied. The hypothesis that implant-bone micromotions measured in *in-vitro* studies using sensors attached to the bone surface differ considerably from micromotions when measured at the actual interface, was confirmed. No correlation between measurements at the actual interface and in the experimental manner was found. This indicated that, primarily, the effect of bone elastic deformation is not negligible, implying that sensors should be mounted precisely at the measurement location.

This finding brings a new insight into the understanding of experimental micromotion measurement sensors, making one aware of their limitations. The method in which measurement sensors are attached can considerably affect the measurement. An incorrect *in-vitro* assessment of interface micromotions may lead to an incorrect pre-clinical prediction of implant stability.

---

## Periprosthetic bone remodeling: Clinical versus FEA prediction (Chapter 3)

Implant design is an important factor influencing the stability and survival of cementless implants<sup>3,5</sup>. Over the years the shape, length, composition and interface treatments of implants have undergone modifications and improvements in order to meet patient needs. For instance, younger patients with a long life expectancy require an implant which will perform well during their highly active life. Older patients need implants which will be stable in bones which are often of poor quality. Currently, the market offers prosthetic implants of many variations in length, shape and composition. Often implants characterized by an already good survival rate are being further “improved” using innovative techniques. In **Chapter 3** we tested whether the effect of design improvements of an already well-performing implant can be predicted in an FEA remodeling study. Initially, the FEA remodeling predictions did not show the exact patterns of bone remodeling as the clinical data. The FEA and clinical results showed only a fair correlation, likely due to differences in interface conditions and those simulated in the FEA model. When the implant-bone interface conditions were adapted to the clinical observations, the FEA and clinical remodeling results were in much better agreement.

Although the adaptive remodeling theory applied in this study has proven its sensitivity to implant shape changes, modeling the effects of multiple design variations in one simulation can become very precarious as often the relative effects and time-constants are not known. Hence, some design-effect parameters need to be estimated which reduce the predictive capacity of the FEA models. In these circumstances we propose to perform sensitivity analyses in order to unravel the independent and combined effects of the design parameters.

## Surgical and implant-related parameters to improve implant stability

### Balancing incompatible implant design goals (Chapter 4)

Besides its shape, also the material composition of an implant is known to have an effect on implant performance<sup>6</sup>. While stiffer implants may be more optimal from a stability point of view, the composite ones are suggested to cause less bone resorption. Given that implant stiffness has a conflicting effect on interface micromotions and bone remodeling<sup>7,8</sup>, it is of a great interest to find a balance between these two aspects. In **Chapter 4** we presented a methodology which combined subsequent ingrowth and remodeling simulation to face a problem of incompatible design goals when designing an implant<sup>9</sup>. The study showed that information on micromotions alone may not be sufficient to discriminate between different implant compositions. A combined analysis of micromotions and bone remodeling allowed



for judgment of the long term performance of various implant compositions, and for selection of the best design between those analyzed in this thesis.

The methodology presented in **Chapter 4** has a great capability to improve the pre-clinical prediction of implant survival. By combining common FEA algorithms, one can considerably increase the FEA predictability of implant performance. A combined analysis of two physiological processes, which depend on multiple factors, is difficult since the relative time frames of the different processes are unknown and commonly estimated based on the available clinical data. To feed these multi-process FE simulations, the relative (time) constants should be established by clinical (or animal) studies in order to generate a reliable and robust simulation.

### **Balancing implant stability and risk of intra-operative bone damage (Chapter 5)**

Implant survival can be increased by good mechanical stability achieved intra-operatively. A high initial mechanical stability will reduce interface micromotions, thus, it will enhance bone ingrowth. However, an excessive impaction force may cause bone damage<sup>10,11</sup>. In **Chapter 5** of this thesis, we analyzed the risk of bone damage caused by an intra-operative impaction force in bones of variable quality. The results showed that a balance between good initial implant stability and a low risk of intra-operative bone damage would be to impact the prosthesis with strong but not excessive force in bones of good and medium quality. To prevent intra-operative bone damage and allow for secondary fixation by bone ingrowth, a gentle impaction force and a longer low load bearing period would be advised in bones of poor quality.

When validated, the simulation proposed in **Chapter 5** could be used to predict the risk of intra-operative bone damage for THA reconstruction of known bone quality. It would allow the surgeon adjusting the magnitude of impaction force so that the optimal intra-operative stability is reached without the risk of bone damage.

## **Towards a more realistic simulation of ingrowth and micromotions predictions**

### **Bone ingrowth simulation (Chapter 6)**

In **Chapter 6** we proposed a novel algorithm to simulate bone ingrowth to improve reliability of FEA predictions. The main difference with previous simulations<sup>12-15</sup> was the fact that for the first time bone ingrowth was simulated as a process. We built on the previous FEA bone ingrowth simulations and proposed one, which includes the effect of gradual bone maturation in time<sup>16</sup> and the effect of bone quality on osseointegration<sup>17,18</sup>. The effect of time was shown in the gradual increase of local implant-bone interface strength.

---

Furthermore, all parameters governing the bone ingrowth process in our simulation were derived from results of animal studies<sup>16,19,20</sup>. The results showed the sensitivity of our new algorithm to the bone quality and initial implant-bone contact area. The simulation allowed differentiation in simulating the ingrowth process (gradual changes in implant-bone interface strength) which was not possible in the previous FEA approaches.

The simulation proposed in **Chapter 6** can be used as a tool to predict implant stability after THA. It could indicate conditions, for instance, the bone quality threshold in which the THA reconstruction will obtain good stability thanks to osseointegration. Ideally, clinical studies should be used to verify and validate the proposed simulation.

### **The effect of more realistic loading configuration on micromotions (Chapter 7)**

In **Chapter 7** we proposed a pioneering FEA approach to quantify the magnitude and direction of interface micromotions using an FEA model with a consistent set of muscle forces. While in previous FEA studies local micromotion was commonly defined as a relative implant-bone motion between two time points, it could now be defined throughout an activity of normal walking. In contrast with the previous studies<sup>5</sup>, now a full set of muscle forces, derived from a consistent musculoskeletal model was used. The new approach of micromotion measurements was used to test the effect of commonly applied FEA boundary conditions and loading configurations on the magnitude of interface micromotions. The full set of muscle forces and time dependent loading configuration provided detailed information on micromotions (direction and magnitude) throughout an activity. Surprisingly, the commonly used diaphysis constraint and loading when maximal hip reaction forces occur provided a good estimation of the distribution of micromotions during walking, but not of their magnitude and direction. Micromotions direction and magnitude were not affected by the simplified constraints set, whereas simplifications of the loading set did have an effect.

The results of this study are significant for all FEA simulations testing implant stability. More realistic loading configurations derived with musculoskeletal modeling systems allows for detailed analysis of micromotions magnitude and direction. Such detailed information can be of great importance when predicting areas of bone ingrowth, bone remodeling, implant stability and long term survival.

## Detailed implant-bone interface micro-mechanics

### Theoretical prediction of interface strength (Chapter 8-9)

Nowadays, new production technologies (e-beam and laser-beam)<sup>21,22</sup> have led to a new generation of porous implant surface structures which are meant to enhance bone ingrowth. Optimizing porosity, structure thickness, pore-shape and geometrical order of a surface structure can lead to enhancement of metal-bone interface strength (better implant stability). The process of introducing new implant surface structures is time consuming, expensive and it often requires pre-clinical animal studies<sup>23,24</sup>. In **Chapters 8 and 9** we made an attempt to assist in this process by enhancing the interpretation of histological measurements of ingrown structures, relative to strength estimates. Using finite element methods we set out to predict interface strength by assessing a relationship between bone ingrowth parameters and implant-bone interface strength. Bone ingrowth depth and interface strength appeared to be proportional, but only to a certain degree of bone ingrowth depth (**Chapter 8**). Beyond that level no further increase in interface strength occurred. The exact strength of a bone-porous surface interface could not be predicted based on the magnitude of the metal-bone contact area, the area of metal-bone interlock or the bone ingrown volume (**Chapter 9**). However, up to a certain level, those histomorphometric parameters and interface tensile strength were proportional. The study described in **Chapter 9** tested also the effect of geometrical order of interface structure on interface strength. Geometrically ordered structures created a stronger interface with bone than the structures of random design.

The results presented in **Chapters 8 and 9** are meaningful for the goal of this study, improvement of implant survival. They show an attempt to predict performance of new surface structures and to reduce the need of animal tests. The magnitude of histomorphometric parameters was correlated with interface tensile strength. Thus, this information could be used for quicker and a more economic distinction between good and bad surface designs (in terms of interface strength). The results are also significant for the production of porous surfaces. Given that deep bone ingrowth does not enhance interface strength beyond a certain ingrowth depth, the depth of a porous surface could be reduced to that particular level. The benefit of it would be shown in the reduction of production costs and more design space for cementless implants.

---

## Reference List

- 1 **Bühler DW, Berlemann U, Lippuner K, Jaeger P, Nolte LP.** Three-dimensional primary stability of cementless femoral stems. *Clin Biomech (Bristol, Avon)* 1997;12(2):75-86.
- 2 **Berzins A, Sumner DR, Andriacchi TP, Galante JO.** Stem curvature and load angle influence the initial relative bone-implant motion of cementless femoral stems. *J Orthop Res* 1993;11(5):758-69.
- 3 **Westphal FM, Bishop N, Honl M, Hille E, Püschel K, Morlock MM.** Migration and cyclic motion of a new short-stemmed hip prosthesis--a biomechanical in vitro study. *Clin Biomech (Bristol, Avon)* 2006;21(8):834-40.
- 4 **Chareancholvanich K, Bourgeault CA, Schmidt AH, Gustilo RB, Lew WD.** In vitro stability of cemented and cementless femoral stems with compaction. *Clin Orthop Relat Res* 2002;(394):290-302.
- 5 **Viceconti M, Brusi G, Pancanti A, Cristofolini L.** Primary stability of an anatomical cementless hip stem: a statistical analysis. *J Biomech* 2006;39(7):1169-79.
- 6 **Kärrholm J, Anderberg C, Snorrason F, Thanner J, Langeland N, Malchau H, Herberts P.** Evaluation of a femoral stem with reduced stiffness. A randomized study with use of radiostereometry and bone densitometry. *J Bone Joint Surg Am* 2002;84-A(9):1651-8.
- 7 **Otani T, Whiteside LA, White SE, McCarthy DS.** Effects of femoral component material properties on cementless fixation in total hip arthroplasty. A comparison study between carbon composite, titanium alloy, and stainless steel. *J Arthroplasty* 1993;8(1):67-74.
- 8 **Bobyn JD, Glassman AH, Goto H, Krygier JJ, Miller JE, Brooks CE.** The effect of stem stiffness on femoral bone resorption after canine porous-coated total hip arthroplasty. *Clin Orthop Relat Res* 1990;(261):196-213.
- 9 **Huiskes R.** Failed innovation in total hip replacement. Diagnosis and proposals for a cure. *Acta Orthop Scand* 1993;64(6):699-716.
- 10 **Toni A, Ciaroni D, Sudanese A, Femino F, Marraro MD, Bueno Lozano AL, Giunti A.** Incidence of intraoperative femoral fracture. Straight-stemmed versus anatomic cementless total hip arthroplasty. *Acta Orthop Belg* 1994;60(1):43-54.
- 11 **Lindahl H.** Epidemiology of periprosthetic femur fracture around a total hip arthroplasty. *Injury* 2007;38(6):651-4.
- 12 **Fernandes PR, Folgado J, Jacobs C, Pellegrini V.** A contact model with ingrowth control for bone remodelling around cementless stems. *J Biomech* 2002;35(2):167-76.
- 13 **Folgado J, Fernandes PR, Jacobs CR, Pellegrini VD, Jr.** Influence of femoral stem geometry, material and extent of porous coating on bone ingrowth and atrophy in cementless total hip arthroplasty: an iterative finite element model. *Comput Methods Biomech Biomed Engin* 2009;12(2):135-45.
- 14 **Spears IR, Pfeleiderer M, Schneider E, Hille E, Bergmann G, Morlock MM.** Interfacial conditions between a press-fit acetabular cup and bone during daily activities: implications for achieving bone in-growth. *J Biomech* 2000;33(11):1471-7.
- 15 **Andreykiv A, Prendergast PJ, van KF, Swieszkowski W, Rosing PM.** Bone ingrowth simulation for a concept glenoid component design. *J Biomech* 2005;38(5):1023-33.
- 16 **Bobyn JD, Stackpool GJ, Hacking SA, Tanzer M, Krygier JJ.** Characteristics of bone ingrowth and interface mechanics of a new porous tantalum biomaterial. *J Bone Joint Surg Br* 1999;81(5):907-14.
- 17 **Fini M, Giavaresi G, Rimondini L, Giardino R.** Titanium alloy osseointegration in cancellous and cortical bone of ovariectomized animals: histomorphometric and bone hardness measurements. *Int J Oral Maxillofac Implants* 2002;17(1):28-37.
- 18 **Shih LY, Shih HN, Chen TH.** The effects of sex and estrogen therapy on bone ingrowth into porous coated implant. *Journal of Orthopaedic Research* 2003;21(6):1033-40.
- 19 **Jasty M, Bragdon C, Bürke D, O'Connor D, Lowenstein J, Harris WH.** In vivo skeletal responses to porous-surfaced implants subjected to small induced motions. *J Bone Joint Surg Am* 1997;79(5):707-14.
- 20 **Dalton JE, Cook SD, Thomas KA, Kay JF.** The effect of operative fit and hydroxyapatite coating on the mechanical and biological response to porous implants. *J Bone Joint Surg Am* 1995;77(1):97-110.

- 21 **Lindhe U, Larsson M, Harrysson O.** Rapid Manufacturing with Electron Beam Melting (EBM)-A Manufacturing Revolution, Direct Metal Fabrication.18-8-2003;
- 22 **Shibli JA, Mangano C, d'Avila S, Piattelli A, Pecora GE, Mangano F, Onuma T, Cardoso LA, Ferrari DS, Aguiar KC, Iezzi G.** Influence of direct laser fabrication implant topography on type IV bone: a histomorphometric study in humans. *J Biomed Mater Res A* 2010;93(2):607-14.
- 23 **Biemond JE, Hannink G, Jurrius A, Verdonschot N, Buma P.** In vivo assessment of bone ingrowth potential of 3-dimensional E-beam produced implant surfaces and the effect of additional treatment by acid-etching and hydroxyapatite coating. *Journal of Biomaterials Applications* 2010;
- 24 **Buser D, Nydegger T, Oxland T, Cochran DL, Schenk RK, Hirt HP, Snétivy D, Nolte LP.** Interface shear strength of titanium implants with a sandblasted and acid-etched surface: a biomechanical study in the maxilla of miniature pigs. *J Biomed Mater Res* 1999;45(2):75-83.





# Chapter **12**

---

## *Samenvatting*



Het doel van dit proefschrift was om eindige elementen methode (EEM) simulaties te ontwikkelen en te verbeteren welke de stabiliteit van cementloze implantaten kunnen voorspellen. Om dit doel te bereiken is het essentieel om over een goede kennis van botingroei en botremodellering te beschikken. In de **Hoofdstukken 2 en 3** beoordeelden we de overeenkomsten tussen EEM voorspellingen en de experimentele en klinische bevindingen. Vervolgens hebben we het effect van chirurgische en implantaat gerelateerde parameters op de stabiliteit van het implantaat bestudeerd (**Hoofdstuk 4 en 5**). In de daaropvolgende hoofdstukken richtten we ons, door middel van innovatieve EEM algoritmes, op het verbeteren van de huidige EEM instrumenten die gebruikt worden om de implantaat stabiliteit te beoordelen. Op basis van data uit dierexperimenten ontwikkelden we een simulatie die het verloop van botingroei aantoonde (**Hoofdstuk 6**) en ontwikkelden we een uniek model om de microbewegingen op de implantaat-bot verbinding te simuleren, die optreden tijdens een complete loopcyclus (**Hoofdstuk 7**). Als laatste hebben we ons gericht op de micromechanica van de implantaat-bot verbinding (**Hoofdstuk 8 en 9**). We onderzochten of het theoretisch mogelijk is om de sterke van de verbinding met verschillende dieptes van botingroei te testen voor innovatieve coatings.

In dit hoofdstuk zullen de bevindingen van bovengenoemde studies samengevat worden en hun relevantie voor wat betreft het doel van dit proefschrift, het ontwikkelen en verbeteren van EEM simulaties welke de levensduur van cementloze implantaten kunnen verbeteren, zal beoordeeld worden.

## **De vergelijking tussen EEM en klinisch en experimenteel onderzoek**

### **Experimentele en EEM-gesimuleerde microbewegingen op de implantaat-bot verbinding (Hoofdstuk 2)**

Iedere meetmethode heeft zijn specifieke beperkingen. In experimentele opstellingen wordt de stabiliteit van een implantaat doorgaans getest onder gesimplificeerde belastingen.<sup>1</sup> Daarnaast zijn de meetsensoren en bijbehorende constructies in sommige gevallen erg groot,<sup>1-4</sup> waardoor het aantal meetpunten beperkt is en problemen ontstaan met de bevestiging van de sensoren. In EEM simulaties kan echter op ieder willekeurig punt een meting verricht worden, hoewel er verschillende aannames gedaan worden in de modellen, die de resultaten beïnvloeden.<sup>5</sup> Het is daarom belangrijk om een EEM model adequaat te valideren. In **Hoofdstuk 2** hebben we een vergelijking gemaakt van microbewegingen op de implantaat-bot verbinding zoals experimenteel gemeten, en zoals voorspeld door een algoritme gebaseerd op een gevalideerd EEM model. De hypothese, dat de experimenteel gemeten microbewegingen sterk afhankelijk zijn van de locatie waar de sensoren worden bevestigd ten opzichte van het meetpunt, werd door deze studie bevestigd. De experimentele meetresultaten correleerde niet met de EEM voorspellingen, wat aangeeft dat de

---

elastische vervorming van het bot niet verwaarloosd kan worden tijdens experimentele metingen. Dit houdt in dat de sensoren zo dicht mogelijk op de implantaat-bot verbinding geplaatst dienen te worden om de daadwerkelijke microbewegingen te meten.

Deze nieuwe informatie is van belang bij het interpreteren van experimentele resultaten, aangezien een incorrecte experimentele meetmethode in de pre-klinische fase kan leiden tot een verkeerde voorspelling van de stabiliteit van een ongecementeerd heupimplantaat.

### **Botremodellering: EEM voorspellingen ten opzichte van klinische resultaten (Hoofdstuk 3)**

Het ontwerp van een implantaat is van groot belang bij de stabiliteit en de overleving van een ongecementeerde heupprothese<sup>3,5</sup>. Gedurende de jaren zijn de vorm, lengte, materiaal en oppervlakte van de implantaten aangepast en verbeterd om aan de specifieke eisen van de patiënt te kunnen voldoen. Zo zullen implantaten voor relatief jonge patiënten, met nog een heel leven voor zich, compatibel moeten zijn met een actieve levensstijl, terwijl oudere patiënten vooral implantaten zullen krijgen die stabiliteit moeten kunnen geven in botten van lage kwaliteit. De huidige markt biedt prothesen aan die verschillen in vorm, lengte en materiaal. Implantaten die al een goede overleving hebben worden vaak ‘verbeterd’ met gebruik van de nieuwste technieken. In **Hoofdstuk 3** hebben we bekeken of we met behulp van EEM konden voorspellen wat het effect zou zijn van een aanpassing in het ontwerp van een reeds succesvolle prothese. In eerste instantie lieten de voorspellingen van de EEM niet hetzelfde beeld zien als het botremodelleringspatroon dat klinisch gevonden werd. Er was slechts een beperkte correlatie tussen de simulaties en het klinische beeld, waarschijnlijk door verschillen op de bot-implantaat verbinding. Nadat de bot-implantaat interface was aangepast waren de resultaten van de simulaties in betere overeenstemming met de klinische resultaten.

Ondanks het bewijs dat de gebruikte remodelleringstheorie sensitief is voor implantaatvormverandering blijft het simuleren van meerdere ontwerpvarianties in één analyse moeilijk, aangezien relatieve effecten en tijdsconstanten onbekend zijn. Daarom moeten sommige ontwerpparameters worden geschat wat de voorspellende waarde van de modellen zal verminderen. We stellen daarom voor om sensitiviteitsanalyses uit te voeren om zo onafhankelijke en gecombineerde effecten van ontwerpparameters beter te kunnen begrijpen.

## **Chirurgische en implantaatontwerp gerelateerde parameters en hun effect op stabiliteit**

### **Het balanceren van tegenstrijdige ontwerpdoelen (Hoofdstuk 4)**

Behalve de morfologie hebben ook de materiaaleigenschappen een effect op het func-

tioneren van implantaten<sup>6</sup>. Zo geven stijvere implantaten meer stabiliteit, terwijl minder stijve composietimplantaten minder botresorptie veroorzaken. Omdat de stijfheid van een implantaat een tegenstrijdig effect heeft op microbewegingen op de implantaat-bot verbinding aan de ene kant, en op botremodelling aan de andere kant<sup>7,8</sup>, is het van groot belang om deze twee aspecten juist tegen elkaar af te wegen. In **Hoofdstuk 4** hebben we een methode ontwikkeld die zowel ingroei als botremodelling simuleert, om zo een oplossing te vinden voor de tegenstrijdige doelen die bestaan bij het ontwerpen van een implantaat<sup>9</sup>. De resultaten van deze studie lieten zien dat informatie over microbewegingen alleen onvoldoende is om een onderscheid te kunnen maken tussen de verschillende composietimplantaten. Een analyse die zowel microbewegingen als botremodelling simuleerde gaf wel voldoende informatie om het functioneren van de verschillende composietimplantaten op lange termijn te beoordelen/vergelijken, en zo het optimale ontwerp te kiezen uit de implantaten zoals bestudeerd in dit proefschrift.

De methoden zoals gepresenteerd in **Hoofdstuk 4** bieden zeer goede perspectieven om de preklinische voorspellingen van het functioneren van implantaten te verbeteren. Door veelgebruikte EEM algoritmes te combineren kan de voorspelkracht van EEM ten aanzien van implantaat functionaliteit aanzienlijk verbeterd worden. Echter, deze analyse is zeer complex omdat ze twee fysiologische processen combineert die beide afhankelijk zijn van vele factoren. De relatieve timing van deze verschillende processen is onbekend, en wordt gewoonlijk gebaseerd op beschikbare klinische data. Om deze beide complexe processen op een robuuste en betrouwbare manier te kunnen simuleren met EEM, moeten de relatieve (tijds-) constanten daarom bepaald worden aan de hand van klinische of dierstudies.

### **Het balanceren van mechanische stabiliteit en het risico op intra-operatieve botscheuren (Hoofdstuk 5)**

De levensduur van een implantaat kan worden vergroot door al tijdens de operatie een goede mechanische stabiliteit te bereiken. Een hoge initiële mechanische stabiliteit zal de microbewegingen van het implantaat ten opzichte van het bot verlagen, waardoor betere botingroei mogelijk is. Door gebruik van een te grote impactiekracht kan het bot echter beschadigen<sup>10,11</sup>.

In **Hoofdstuk 5** van dit proefschrift analyseerden we het risico op beschadiging van het bot veroorzaakt door het toepassen van een variabele intra-operatieve impactiekracht op botten met verschillende kwaliteit. De resultaten lieten zien dat, voor botten van goede en matige kwaliteit, met een ferme klap een goede balans tussen de initiële stabiliteit van het implantaat en een laag risico op intra-operatieve botschade bereikt wordt. Om deze botbeschadiging te voorkomen en secundaire fixatie door botingroei mogelijk te maken, worden bij botten met een slechte kwaliteit een gematigde impactiekracht en een langere ontlastingsperiode geadviseerd.

Na validatie kan de simulatie zoals gepresenteerd in **Hoofdstuk 5** gebruikt worden om

---

het risico op intra-operatieve botbeschadiging bij THA reconstructies te bepalen, wanneer de botkwaliteit van de patiënt bekend is. Op deze manier kan de orthopedisch chirurg de grootte van de impactiekracht zodanig aanpassen, dat een optimale intra-operatieve stabiliteit van het implantaat bereikt wordt zonder daarbij het risico te lopen dat het bot beschadigd raakt.

## **De ontwikkeling van een realistische simulatie van botingroei en microbewegingen**

### **Simulatie van botingroei (Hoofdstuk 6)**

In **Hoofdstuk 6** is een verbeterde EEM simulatie voor botingroei geïntroduceerd. Het grote verschil met andere simulaties waarbij botingroei meer statisch werd benaderd <sup>12-15</sup>, is dat met het nieuwe algoritme botingroei als een proces kan worden gesimuleerd waarbij ook de veranderende eigenschappen van bot (bot maturatie <sup>16</sup> en het effect van botkwaliteit op osseointegratie <sup>17,18</sup>) kon worden meegenomen. Tijdseffecten tijdens het ingroeiproces werden geïmplementeerd als een toename van de sterkte van de implantaat-bot interface. Alle parameters betrokken bij het ingroeiproces werden geschat op basis van dierexperimentele studies <sup>16,19,20</sup>. De resultaten toonden aan dat de nieuwe simulatie gevoelig is voor initiële botkwaliteit en de grootte van het implantaat-bot contactgebied. De simulatie een gradueel verloop zien van het ingroeiproces (toenemende sterkte van de implantaat-bot interface sterkte), dat eerder niet kon worden gesimuleerd.

De simulatie zoals beschreven in **Hoofdstuk 6** kan worden gebruikt als een middel om de stabiliteit van een implantaat te bepalen. Met een dergelijke simulatie zou men bijvoorbeeld de gevoeligheid van patiëntspecifieke factoren (botkwaliteit, vorm van de endostale caviteit en verwachte fit, belastbaarheid) kunnen analyseren op de ingroeikansen van het implantaat. Uiteraard zouden dergelijke simulaties verder met klinische studies moeten worden onderbouwd.

### **Het effect van een realistische belasting op microbewegingen op de implantaat-bot verbinding (Hoofdstuk 7)**

In **Hoofdstuk 7** hebben we een nieuwe manier ontwikkeld om de grootte en richting van microbewegingen op de implantaat-bot verbinding te simuleren. Hiervoor hebben we gebruik gemaakt van een geschaalde set spierkrachten. In eerdere EEM studies werden microbewegingen gedefinieerd als het relatieve verschil tussen de verplaatsing van het bot en het implantaat op twee verschillende discrete tijdstippen (belast vs. onbelast). In de nieuwe simulatie worden de microbewegingen echter gemeten gedurende een hele loopcyclus. In tegenstelling tot eerdere studies, <sup>5</sup> is ook gebruik gemaakt van een volledige set van spierkrachten. Deze nieuwe aanpak is getest ten opzichte van de gebruikelijke simulatiemeth-

odes, waarbij de resulterende microbewegingen zijn vergeleken. Daarnaast is gekeken naar het effect van verschillende manieren van inklemming van het femur tijdens de simulatie.

De volledige set spierkrachten en de simulatie van een volledige loopcyclus gaf gedetailleerde informatie over het verloop van de microbewegingen (grootte en richting) tijdens de cyclus. Hoewel de grootte van de microbewegingen niet werd beïnvloed door de manier van het aanbrengen van de krachten (instantaan of continu), had dit wel een effect op de richting. Een fixatie van een model ter hoogte van de diafyse, zoals doorgaans gebruikt wordt bij dergelijk simulaties, gaf een goede representatie van de fixatie van het femur.

De resultaten van deze studie geven aan dat een meer gedetailleerde beschrijving van de spierkrachten het patroon van microbewegingen op de implantaat-bot verbinding beïnvloedt. Deze informatie is van belang voor het voorspellen van regio's van botingroei, botremodellering en de lange termijn stabiliteit van ongecementeerde implantaten.

## Gedetailleerde micro-mechanica van de implantaat-bot interface

### Theoretische voorspelling van de sterkte van de implantaat-bot interface (Hoofdstuk 8-9)

Nieuwe productietechnieken, zoals E-beam en selective laser melting <sup>21,22</sup>, hebben geleid tot een nieuwe generatie van implantaten met open oppervlaktestructuren die bedoeld zijn om de botingroei te bevorderen. Het optimaliseren van de porositeit, de grootte en vorm van de poriën en de dikte en geometrie van deze oppervlaktestructuren kan leiden tot een verbetering van de sterkte van de implantaat-bot verbinding (en daarmee een betere stabiliteit van het implantaat). Het testen van nieuwe oppervlaktestructuren op implantaten is tijdrovend en kostbaar en dient vaak gepaard te gaan met preklinische dierstudies <sup>23,24</sup>.

In **Hoofdstukken 8 en 9** hebben we geprobeerd dit proces te vergemakkelijken door de interpretatie van histologische metingen aan oppervlaktestructuren te relateren aan mechanische schattingen van de sterkte van de interface. Door gebruik te maken van EEM hebben we getracht de sterkte van de implantaat-bot verbinding te voorspellen door de relatie tussen botingroeiparameters en de sterkte te bepalen. De botingroeidiepte en de sterkte bleken evenredig, maar echter maar tot een bepaald niveau (**Hoofdstuk 8**). Voorbij dit niveau trad er geen verdere toename van de sterkte van de verbinding op. De exacte sterkte van een verbinding van bot en poreus metaal kon niet worden voorspeld op basis van de grootte van het implantaat-bot contactoppervlak, het oppervlakte van de implantaat-bot interlock en/of het volume ingegroeid bot (**Hoofdstuk 9**). Tot op een zeker niveau waren de histomorfometrische parameters evenredig met de treksterkte van de interface. In het onderzoek beschreven in **Hoofdstuk 9** werd tevens het effect van de geometrie van de interfacestructuur op de interfacesterkte getest. Oppervlaktestructuren met een ge-

---

ometrisch geordend oppervlak vormden een sterkere interface dan structuren met een willekeurig georiënteerd oppervlak.

De resultaten gepresenteerd in **Hoofdstukken 8 en 9** zijn van belang voor het doel van dit onderzoek, het verbeteren van de overleving van implantaten/prothesen. Er werd getracht het gedrag van nieuwe oppervlaktestructuren te voorspellen en het aantal dierproeven te verminderen. De histomorfometrische parameters bleken tot een bepaal niveau te correleren met de treksterkte van de interface. Deze informatie zou gebruikt kunnen worden om sneller een onderscheid te maken tussen goede, minder goede en slechte oppervlaktedesigns (in termen van verbindingsterkte). De resultaten zijn tevens van belang voor de productie van poreuze oppervlaktestructuren. Het gegeven dat de botingroei voorbij een bepaald niveau geen invloed meer heeft op de sterkte zou betekenen dat de diepte van een poreuze coating geoptimaliseerd zou kunnen worden. Dit zou een vermindering van de productiekosten en meer ruimte voor het design van ongecementeerde implantaten op kunnen leveren.

## Reference List

- 1 **Buhler DW, Berlemann U, Lippuner K, Jaeger P, Nolte LP.** Three-dimensional primary stability of cementless femoral stems. *Clin Biomech (Bristol, Avon)* 1997;12(2):75-86.
- 2 **Berzins A, Sumner DR, Andriacchi TP, Galante JO.** Stem curvature and load angle influence the initial relative bone-implant motion of cementless femoral stems. *J Orthop Res* 1993;11(5):758-69.
- 3 **Westphal FM, Bishop N, Honl M, Hille E, Püschel K, Morlock MM.** Migration and cyclic motion of a new short-stemmed hip prosthesis--a biomechanical in vitro study. *Clin Biomech (Bristol, Avon)* 2006;21(8):834-40.
- 4 **Chareancholvanich K, Bourgeault CA, Schmidt AH, Gustilo RB, Lew WD.** In vitro stability of cemented and cementless femoral stems with compaction. *Clin Orthop Relat Res* 2002;(394):290-302.
- 5 **Viceconti M, Brusi G, Pancanti A, Cristofolini L.** Primary stability of an anatomical cementless hip stem: a statistical analysis. *J Biomech* 2006;39(7):1169-79.
- 6 **Kärrholm J, Anderberg C, Snorrason F, Thanner J, Langeland N, Malchau H, Herberts P.** Evaluation of a femoral stem with reduced stiffness. A randomized study with use of radiostereometry and bone densitometry. *J Bone Joint Surg Am* 2002;84-A(9):1651-8.
- 7 **Otani T, Whiteside LA, White SE, McCarthy DS.** Effects of femoral component material properties on cementless fixation in total hip arthroplasty. A comparison study between carbon composite, titanium alloy, and stainless steel. *J Arthroplasty* 1993;8(1):67-74.
- 8 **Bobyn JD, Glassman AH, Goto H, Krygier JJ, Miller JE, Brooks CE.** The effect of stem stiffness on femoral bone resorption after canine porous-coated total hip arthroplasty. *Clin Orthop Relat Res* 1990;(261):196-213.
- 9 **Huiskes R.** Failed innovation in total hip replacement. Diagnosis and proposals for a cure. *Acta Orthop Scand* 1993;64(6):699-716.
- 10 **Toni A, Ciaroni D, Sudanese A, Femino F, Marraro MD, Bueno Lozano AL, Giunti A.** Incidence of intraoperative femoral fracture. Straight-stemmed versus anatomic cementless total hip arthroplasty. *Acta Orthop Belg* 1994;60(1):43-54.
- 11 **Lindahl H.** Epidemiology of periprosthetic femur fracture around a total hip arthroplasty. *Injury* 2007;38(6):651-4.
- 12 **Fernandes PR, Folgado J, Jacobs C, Pellegrini V.** A contact model with ingrowth control for bone remodelling around cementless stems. *J Biomech* 2002;35(2):167-76.
- 13 **Folgado J, Fernandes PR, Jacobs CR, Pellegrini VD, Jr.** Influence of femoral stem geometry, material and extent of porous coating on bone ingrowth and atrophy in cementless total hip arthroplasty: an iterative finite element model. *Comput Methods Biomech Biomed Engin* 2009;12(2):135-45.
- 14 **Spears IR, Pfeleiderer M, Schneider E, Hille E, Bergmann G, Morlock MM.** Interfacial conditions between a press-fit acetabular cup and bone during daily activities: implications for achieving bone in-growth. *J Biomech* 2000;33(11):1471-7.
- 15 **Andreykiv A, Prendergast PJ, van KF, Swieszkowski W, Rosing PM.** Bone ingrowth simulation for a concept glenoid component design. *J Biomech* 2005;38(5):1023-33.
- 16 **Bobyn JD, Stackpool GJ, Hacking SA, Tanzer M, Krygier JJ.** Characteristics of bone ingrowth and interface mechanics of a new porous tantalum biomaterial. *J Bone Joint Surg Br* 1999;81(5):907-14.
- 17 **Fini M, Giavaresi G, Rimondini L, Giardino R.** Titanium alloy osseointegration in cancellous and cortical bone of ovariectomized animals: histomorphometric and bone hardness measurements. *Int J Oral Maxillofac Implants* 2002;17(1):28-37.
- 18 **Shih LY, Shih HN, Chen TH.** The effects of sex and estrogen therapy on bone ingrowth into porous coated implant. *Journal of Orthopaedic Research* 2003;21(6):1033-40.
- 19 **Jasty M, Bragdon C, Bürke D, O'Connor D, Lowenstein J, Harris WH.** In vivo skeletal responses to porous-surfaced implants subjected to small induced motions. *J Bone Joint Surg Am* 1997;79(5):707-14.
- 20 **Dalton JE, Cook SD, Thomas KA, Kay JF.** The effect of operative fit and hydroxyapatite coating on the mechanical and biological response to porous implants. *J Bone Joint Surg Am* 1995;77(1):97-110.

- 
- 21 **Lindhe U, Larsson M, Harrysson O.** Rapid Manufacturing with Electron Beam Melting (EBM)-A Manufacturing Revolution, Direct Metal Fabrication.18-8-2003;
  - 22 **Shibli JA, Mangano C, d'Avila S, Piattelli A, Pecora GE, Mangano F, Onuma T, Cardoso LA, Ferrari DS, Aguiar KC, Iezzi G.** Influence of direct laser fabrication implant topography on type IV bone: a histomorphometric study in humans. *J Biomed Mater Res A* 2010;93(2):607-14.
  - 23 **Biemond JE, Hannink G, Jurrius A, Verdonschot N, Buma P.** In vivo assessment of bone ingrowth potential of 3-dimensional E-beam produced implant surfaces and the effect of additional treatment by acid-etching and hydroxyapatite coating. *Journal of Biomaterials Applications* 2010;
  - 24 **Buser D, Nydegger T, Oxland T, Cochran DL, Schenk RK, Hirt HP, Snétivy D, Nolte LP.** Interface shear strength of titanium implants with a sandblasted and acid-etched surface: a biomechanical study in the maxilla of miniature pigs. *J Biomed Mater Res* 1999;45(2):75-83.





---

## Acknowledgements

It would not have been possible to write this doctoral thesis without the help and support of the kind and generous people around me. In a new place it takes a while until you create your world. In Nijmegen, thanks to the wonderful people I met, it did not take that long until I felt at home. Thank you all!

At the ORL, I met many knowledgeable people and experienced a unique working environment. Therefore, first of all, I would like to thank **Nico and Pieter**, for the opportunity they gave me and the faith they had in me. I learnt so much from you, both on the professional and personal level. Many thanks!

Dear **Nico**, my promoter, it was a great pleasure and honor to be working with you. This thesis would not have been possible without your critical insights and enthusiastic support. Thank you very much for being patient and understanding with me, for your time and guidance. Work is important, but for you it also mattered how I was doing over the years. Thank you, I really appreciate that.

Many thanks to my copromoter! **Dennis**, without your support, patience and guidance I would have never completed this work. Thank you very much for all your corrections to my academic writing (we both know you had a lot of work because of me), your stimulating comments and all the time you dedicated to our projects. I was really lucky to have you as my supervisor.

Special thanks to all my colleagues and friends at the ORL. I learnt a lot from you during the research meetings and probably even more during the lunch breaks. I was really honored when you came all the way to Poland, to my home town, to celebrate my wedding. It was really special! **Anne, Astrid, Eric, Ervin, Esther, Daan, Dennis, Gerjon, Hendi, Huub, Ineke, Jorrit, Leon, Liesbeth, Loes, Miranda, Nico, Pieter, Pieter H, Paweł, René, Sanaz, Willem and Wojtek**, thank you for all the wonderful memories!

**Ineke**, thank you for your unlimited kindness, hospitality and generosity. I am really grateful for all you have done to make my life easy during my stay in the Netherlands.

**Willem**, thank you very much for your always positive and cheerful approach and for your great help especially during my first project.

My special thanks to **René van der Venne**, thanks to his work and the programs he built I was able to perform the simulations and analyze the data. My deepest condolences to his family and friends for their loss.

My working days would not have been the same without my friends and officemates **Liesbeth, Daan, Anne and Ervin**. Thank you for your smile, sense of humor, happiness and good advices. I could always count on you when I had either a research or every-day-life question. Many thanks for your friendship!

**Liesbeth**, thank you for all the wonderful and unforgettable memories from the work days, our dinners and trips. Thank you for your help and support. I am really lucky to have you as a friend!

**Daan**, my best man and most of all a great friend. I really miss our Monday dinners, movie watching and talks. Thanks to you I learnt a lot about the Netherlands, and ... about its classic horror movies like 'Amsterdamned' and 'De Lift' :) Thank you for your trust and your support whenever I need it.

This thesis would not have been the same without the work of four master students I had a pleasure to work with, and without the collaboration with dr. René ten Broeke. **Bas, Deko, Marc and Sam**, many thanks for your excellent and hard work which considerably added to various chapters of this thesis. **René**, thank you for giving me the opportunity to work with you, for your enthusiasm, hard work and time you dedicated to our paper.

My experience in Nijmegen was fulfilled thanks to the interesting and creative people I met also outside of work.

I was very lucky to meet **Babsi and Karol**. Even though we did not know each other at all when we began to share a house, we easily found ourselves in the new situation and in a short time we became friends. Thank you both for being there for me!

**Babsi**, thank you for your friendship and your presence. I miss our talks, romantic comedy evenings and your wonderful cooking. I was very fortunate to have you around. Thanks to you, our house was a great place to come back to after a day of work.

Special thanks to my 'international' friends: **Adriana, Alfi, Andrew, Eva, Eugene, Georgeta, Gleb, Irene, Jasper, Lucian, Olha, Peer and Silvia**. Thank you for your initiatives, radiating happiness and all the fun! I hope we will always stay in touch even though we all in different countries now.

Many thanks to my **friends from the Italian and Dutch courses**. Grazie per la vostra allegria, amicizia e gentilezza, per le lezioni sempre vivaci, coinvolgenti ed interessanti. Bedankt voor jullie vriendschap, onze lessen met taart proeven, de interessante cursus, initiatieven en gastvrijheid!

---

Dear **father Joop and all the friends from in the student's church**, I was really lucky to be a part of such wonderful and cheerful group. Thank you for your happiness, support and all initiatives.

Grazie agli **amici di Milano** e alla loro gentilezza, ospitalità, amicizia ed allegria mi sono innamorata dell'Italia. Grazie di tutto! **Paolo**, grazie mille per l'aiuto con la copertina di questa tesi. E' venuta benissimo!

**Gosiu i Pawle**, dziękuję za waszą przyjaźń, otwartość i wsparcie zwłaszcza w ostatnich miesiącach mojego pobytu w Nijmegen. Wielkie dzięki za waszą gościnność kiedy jestem w Nijmegen, za waszą troskę i zaufanie.

Gorące podziękowania dla **Eweliny, Magdy i Grześka**. Cieszę się że po tylu latach od ukończenia szkoły podstawowej nadal trzymamy się razem i że zawsze znajdujemy czas na to żeby się spotkać przy piwie.

Wreszcie gorące podziękowania dla moich najbliższych, mojej **wspaniałej Rodziny**, bez której wsparcia i miłości nic nie byłoby możliwe. W tym największe i szczególne podziękowania należą się moim **Rodzicom. Mamo i Tato**, wasza ciężka praca daje mi przykład, a ogromne wsparcie dodawało i dodaje sił. Dziękuję Wam Kochani!

**Michele**, senza di te non ne sarebbe valsa la pena. Grazie del tuo amore, la pazienza e il tuo sorriso che illumina le mie giornate. Grazie che ci sei.

I would like to thank the sponsors of my thesis:

**Radboud University Nijmegen**

**Radboud University Nijmegen**



**Stichting Anna Fonds | NOREF**

Anna  
Fonds

**RMS Foundation, Bettlach, Switzerland**



Testing • Research • Consulting

[www.rms-foundation.ch](http://www.rms-foundation.ch)

---



---

## Curriculum Vitae

**Maria Tarala** was born on October 11, 1982, in Rzeszów (Poland). She attended primary and secondary school in Nowa Wieś and high school in Rzeszów. In 2001, she moved to Wrocław where she studied Biomedical Engineering at Wrocław University of Technology. During her studies she chose two specializations: the Electromedical Apparatus and Biomechanics (under the supervision of prof. Romuald Będziński). In the final year of her master studies, she joined the Erasmus Programme and did her master's research at Bristol University (Bristol, UK) under the supervision of prof. Mike Adams. She graduated from Wrocław University of Technology in June 2006 by defending her thesis titled 'Mechanical compatibility of human intervertebral discs and vertebrae'. To gain work experience Maria joined another European programme for students (Leonardo da Vinci programme). It allowed her to do an internship at the Orthopaedic Research Laboratory (Nijmegen, The Netherlands) under the supervision of prof. Nico Verdonchot. After six months of internship Maria was offered a PhD and an EC project manager position. Her PhD research focused on cementless implants in total hip arthroplasty and the results of her work are presented in this thesis. Since July 2011 Maria lives in Milan (Italy) with her husband Michele Pischetola.

### List of publications

**Skrzypiec D, Tarala M, Pollintine P, Dolan P, Adams MA.** *When are intervertebral discs stronger than their adjacent vertebrae?* Spine (Phila Pa 1976). 2007 Oct 15;32(22):2455-61.

**Tarala M, Janssen D, Telka A, Waanders D, Verdonchot N.** *Experimental versus computational analysis of micromotions at the implant-bone interface.* Proc Inst Mech Eng H. 2011 Jan;225(1):8-15.

**Tarala M, Janssen D, Verdonchot N.** *Balancing incompatible endoprosthetic design goals: a combined ingrowth and bone remodeling simulation.* Med Eng Phys. 2011 Apr;33(3):374-80.

**Tarala M, Waanders D, Biemond JE, Hannink G, Janssen D, Buma P, Verdonchot N.** *The effect of bone ingrowth depth on the tensile and shear strength of the implant-bone e-beam produced interface.* J Mater Sci Mater Med. 2011 Oct;22(10):2339-46.

**van der Ploeg B, Tarala M, Homminga J, Janssen D, Buma P, Verdonchot N.** *Toward a more realistic prediction of peri-prosthetic micromotions.* J Orthop Res. 2012 Jul;30(7):1147-54.













